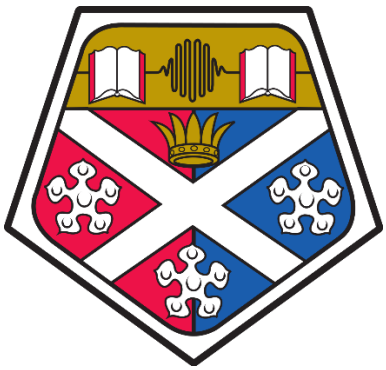

University of Strathclyde

Department of Electronic and Electrical Engineering

Design and Analysis of Secure Offshore Wind Farms

by

James Gordon Tait

B.Eng. (*First class honours*), M.Sc. (*Distinction*)

A thesis presented in fulfilment of the requirements for the degree of Doctor of Philosophy

2023

Copyright

Acknowledgements

I would like to express my sincerest and deepest gratitude to my supervisor Dr. Khaled Ahmed who led, encouraged and supervised me significantly.

I would like to express a special tribute to Dr. Shuren Wang for his vital support, encouragement, and guidance throughout my PhD.

I would like to express my appreciation to Dr. Grain Adam, the Power Electronics Drives & Energy Conversion (PEDEC) research group, everyone in the CDT for Smart Grids and Future Power Networks for assistance, useful discussion, and an encouraging atmosphere and EPSRC for funding of the CDT program.

A special thanks to my wife Katie and daughter Sophie who had to put up with me through completing my PhD. I would like to give a special thankyou to my family for their support and encouragement.

Thanks to everyone who helped me to get through such a fruitful and memorable journey.

Abstract

This thesis investigates methods and system architectures which improve system security of offshore wind farms. This is demonstrated through enhancing dc collector network fault resiliency which also remain reliable throughout ac network disturbances.

Initially key techniques applied to alleviate the effects of power imbalance during ac network faults for permanent magnet synchronous generator (PMSG) based wind energy conversion systems (WECSs), are comparatively analysed based on performance, economic and practical metrics. Based on a qualitative review of technically viable designs, this study presents quantitative substantiation with time-domain simulations. At wind turbine level, the assessment findings suggest potential financial and practical barriers that may exist regarding the implementation of the LVFRT solutions especially with energy storage-based techniques. However, the flexibility, benefits and increasing feasibility regarding energy storage systems may make them a preferred option for LVFRT of critical WECSs, particularly used in a coordinated manner with other lower cost techniques.

Expanding to system level this research proposes an enhanced system for series-connected offshore wind farm (SC-OWF) with enhanced fault resilience to internal collector faults, where comprehensive circuit configuration and protection strategies are articulated. A grouping scheme and substation are adopted to realise prompt fault bypass/isolation and protection functions in the event of offshore collector faults. Additionally, an onshore fault-tolerant modular multilevel converter with a modified dc-system-oriented control is employed to enable smooth and secure operation under steady-state and fault conditions. The SC-OWF presented system is quantitatively substantiated by time-domain simulations. The results consolidate the feasibility of the proposed configuration by demonstrating enhanced resiliency to dc collector faults and remaining post ac network disturbances via adoption of the proposed coordinated control system and bypass station configuration. However, due to current technical and practical limitations regarding component and cable ratings.

To address challenges with windfarm sizing limitations a modular-series-parallel topology with reduced weight and volume requirements is proposed. A comprehensive circuit configuration and protection strategies are presented, which aim to minimise

the detrimental effects caused by dc cable faults to ensure system security in a cost-effective manner. The system architecture employs a grouping scheme, where each group consists of a string of series connected wind energy converter systems (WECS) interfaced to a uni-directional high gain dc/dc converter with parallel connection at the high voltage dc (HVDC) transmission point. The system configuration allows the containment off collector faults with in each of the groups, allowing secure system operation via control and balancing systems, with power quality achieved through an adaptive phase-shift control function on the dc output of the offshore converter station. The proposed wind farm system is quantitatively substantiated by time-domain simulations where two dc fault cases are considered. The results consolidate the feasibility of the proposed configuration and control, indicating fault resilience of the MSPC-OWF system without requirement for dc circuit breakers (DCCBs). Furthermore, a weight/size assessment demonstrates weight and volume reductions in comparison to HVDC converter stations interfaced to ac collector networks.

List of Abbreviations

BESS	Battery energy storage system
CAPEX	Capital expenditure
CC	Coordinated control technique
CSC	Current source converter
DOM	Dc offset modifier
DCCB	DC circuit breaker
DFIG	Doubly fed induction generators
DIS	Disconnectors
DR	Dumping resistor
DSRF	Double synchronous reference frame
ESS	Energy storage system
FB	Full bridge
FB-MMC	Full-bridge modular multilevel converter
FB-SM	Full bridge submodule
HB	Half-bridge
HB-MMC	Half-bridge modular multilevel converter
HVDC	High-voltage dc
IG	Induction generators
LVDC	Low-voltage dc
LVFRT	Low voltage fault ride through
MF	Medium frequency
MFT	Medium-frequency transformer
MMC	Modular multilevel converter
MTDC	Multi-terminal dc
MV	Medium voltage
MVDC	Medium-voltage dc
OPEX	Operational expenditure
OTC	Optimum torque control
OWF	Offshore wind farm
PCC	Point of common coupling
PC-OWF	Parallel-connected offshore wind farm
PDIS	Parallel disconnector
PLL	Phase locked loop
PMSG	Permanent magnet synchronous generator
PIR	Proportional-integral-resonant
PWM	Pulse width modulation
SCES	Supercapacitor energy storage
SC-OWF	Series-connected offshore wind farm
SCR	Short circuit ratio
SDIS	Series disconnector
SM	Submodule

SMES	Superconductive magnetic energy storage
SO	System operator
SPC-OWF	Series-parallel-connected offshore wind farm
VSC	Voltage source converter
WECS	Wind energy conversion system
WG	Wind energy conversion system group

List of Symbols

λ	Tip-speed ratio
ρ	Air density
β	Pitch angle
Ω_{ms}	Shaft angular velocity
A	Swept area
C	Capacitance
C_p	Wind turbine power coefficient
E	Energy
F	Viscous rotor friction coefficient
I	DC current
i	AC current
i_d	D-axis current
i_q	Q-axis current
J	Inertia
L_d	Stator d-axis inductance
L_q	Stator q-axis inductance
P	Active power
p	Pole pairs
P_m	Mechanical power
Q	Reactive power
R	Resistance
R_b	Blade radius
S	Apparent power
T	Torque
t	Time (secs)
u_w	Wind speed
V	DC voltage
v	AC voltage
v_d	D-axis voltage
v_q	Q-axis voltage
ω	Angular velocity

Table of Contents

Chapter 1

Introduction

1.1 Background

As a means of combatting the effects of climate change governments globally have set targets, though roadmaps, in achieving net carbon zero through the decarbonisation of key sectors Differing from the wider GB network, (England and Wales, on a roadmap to a 2030 target [1]) road map Scotland aims to be net-carbon zero by 2032 [2]. With focus on the electricity sector, the plans state further exploitation of the abundant wind energy resource further from shore and expand energy exportation to the wider UK nations and Europe, aiding in their decarbonisation efforts [2]. A key focus is the use of emerging technologies, such as floating wind, to aid in the projected 8-11 GW [3] of installed wind capacity by 2030 in Scotland, with global installed capacity projected at 70 GW [4]. This thesis investigates the means in which offshore wind energy is collected offshore and transported back from shore over the long distances required and addressing technical challenges around the system security and system costs by reducing system infrastructure. In general, power system security refers to the level of risk in its survivability and robustness to imminent disturbances without interruption of customer service [5]. The term secure throughout this thesis is used to relate to an offshore collector network's ability to survive internal network and external network disturbances.

The thesis focuses on permanent magnet synchronous generator (PMSG) based WECS technology, widely utilised, especially in the offshore wind sector. Initially this thesis investigates their reliability during ac network faults. Reliability is a probabilistic term of the satisfactory power and load balance ability to withstand disturbances [6], and is used in the context of the thesis for WECS units' ability to ride though faults on the network in which it is interfaced. It can be ascertained from industry offerings that PMSG is the dominant technology for wind power delivery, with doubly fed induction generators (DFIGs) being offered at lower power output levels [7]. Also, the controllability of the PMSG equipped with fully rated converters is improved [8].

Starting with Squirrel cage induction generators (SGIGs), typically fixed speed generators, rely on a strong ac grid, and during network faults require reactive compensation due to the collapse of the stator voltage [9]. Technology progressed to DFIGs which have improved controllability over SGIGs, however, they are sensitive to unbalanced faults, where additional ac connected, hardware (partially rated power converter) is required to manage circulating rotor currents caused by the imbalance between rotor and stator magnetic flux [10] due to their synchronous coupling to ac network. As PMSGs are synchronously decoupled from the network by adopted voltage source converters (VSCs), PMSG-based WECSs do not inherently respond to ac network faults, thus allowing the system to maintain with normal operational limits (i.e., rotor speed and torque), and/or provide the required reactive current [11] For grid connected turbines, ac system faults cause the most severe conditions, inflicting high levels of stress on WECSs and therefore should be addressed sufficiently. Low voltage fault ride through (LVFRT) requirements, set by grid codes, state that WECSs must remain galvanically connected and transiently stable during ac network faults, with defined periods of time and levels of voltage (for example, voltage level of 0 – 0.15 pu and duration of 140 ms – 200 ms in [12]). Additionally, WECSs are typically required to deliver reactive power to the network during fault and post-fault, to ensure operation security, aid in voltage restoration, and minimise risk of voltage collapse [13]. The amount of reactive power delivery varies between grid codes; however, it is typically stated that WECSs should deliver the maximum reactive power without compromising the converter limits [14]. Grid codes stipulate what the WECS must withstand; they do not offer instruction on how this is achieved, and it can be assured that strong grid assumptions are made and only apply to the ac point of common coupling (PCC) and do not consider internal wind farm networks.

Considering OWFs near to shore (<50 km from shore) utilise conventional means of grid interface, were a group of WECSs are parallel connected to an ac collector voltage at MV level (33 kV or 66 kV) at 50/60 Hz and interfaced to the grid system via MV/HV transformer. Generally, offshore wind farms (OWFs) located at distances beyond 50–80 km from shore benefit from high-voltage dc (HVDC) technology for bulk transmission, due to technical and commercial constraints associated with conventional ac transmission [15]. Which may be the predominant means of bulk

power transmission especially in proposals for far from shore OWFs. To enable HVDC deployment, OWFs typically employ conventional ac collector medium voltage (MV) levels), with each string parallel-connected to a centralised offshore converter station, as shown in Fig. 1.1 [16].

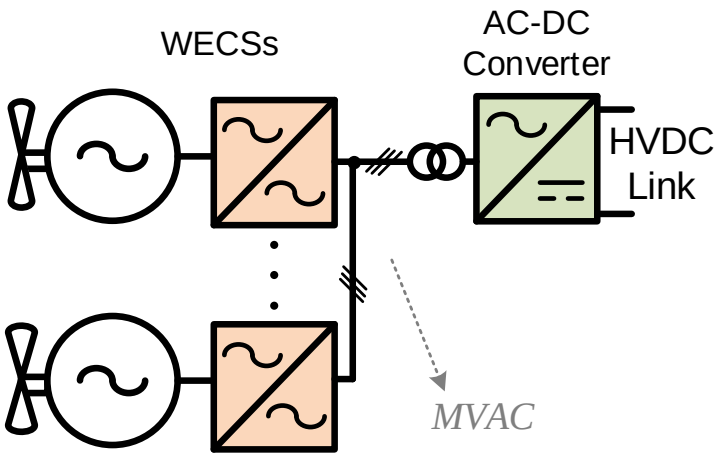

Fig. 1.1. Conventional OWF with centralised MMC station.

However, the utilisation of modular multilevel converters (MMCs) leads to high weight and size requirements on the offshore platforms [17]. For example, the estimated topside weight is approximately 12,000 tons for the current DorWin and BorWin offshore 900 MW converter stations [18]. Therefore, the application of dc collection systems is potentially advantageous in terms of weight and size requirements on the offshore converter station platforms [19]. Another OWF scheme, based on ac collector networks, facilitates diode rectifier units, as illustrated in Fig. 1.2 [23]. Although the rectifier design is simplified the eight requirements from filtration require a large platform footprint.. However, the feasibility for practical applications of such schemes is still questionable, mainly due to the challenges of the ac system control, and stability with many connected wind turbines [21].

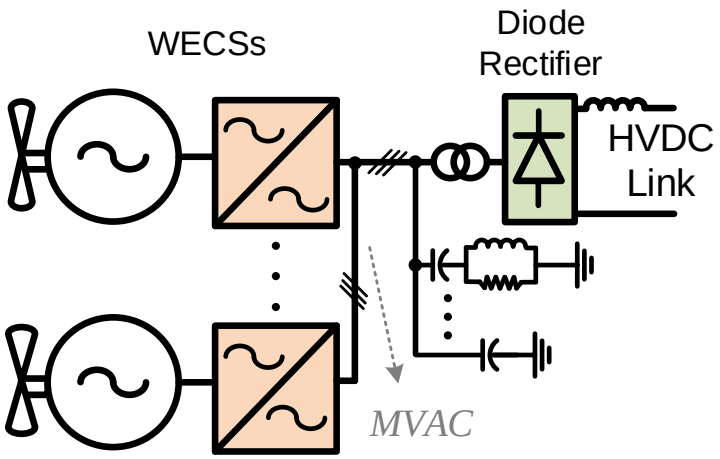

Fig. 1.2. Diode rectifier unit based OWF.

As a means of mitigating large converter stations, which attribute to high capital expenditure (CAPEX) and operational expenditure (OPEX), OWFs facilitating dc collector networks are becoming popular in literature. The two key challenges with these configurations are that all current studies focus on the operational aspects of the OWF and do not consider fault resiliency. The second challenge concerns dc/dc converter technology. Different current/voltage source based converter topologies have been considered for interfacing WECSs with the HVDC-link, including uncontrolled diode rectifiers [22] and pulse width modulation (PWM) based converters [23]–[26]. In addition, high-ratio dc/dc conversion employing medium-frequency transformer (MFT) technologies and robust diodes are implemented to achieve successful trade-offs between high wind turbine level controllability, high operation efficiency, galvanic isolation, reduced mass, etc., for offshore system implementation [27]–[29]. Existing literature published by other researchers don't address energy imbalance at turbine or system level to address fault resiliency risks (defined as the ability to limit the extend, severity or system degradation during a contingency period [6]), even though known threats exist in the systems.

1.2 Motivation and Objectives

The key motivation of this research is to improve overall system security ac or dc network faults in offshore wind farm networks. Initially, the security and management of energy imbalance, caused by system faults, are addressed at wind turbine level to determine a suitable method that meets a tradeoff between performance and cost.

Resiliency, particularly concerning cascading faults has not yet been researched in offshore wind farms implementing dc collectors. Therefore, this thesis proposes a modified series-connected wind farm concept facilitating an offshore bypass station to aid in the safe isolation of series connected network wind turbines in a dc collector network in addition a control architecture to ensure safe operation though a novel balancing scheme suitable for handling energy imbalance during ac and dc network faults. Additionally, offshore wind farms utilising multi-terminal dc arrangements generally involve multiple conversion stages and require dc circuit breakers. Therefore, an offshore wind farm topology is proposed, which employs unit-directional lightweight converter stations each consisting of secure series connected strings of wind turbines to directly form distribution level voltage. The output of which can be paralleled at high voltage dc level and secured against dc network faults.

The main research objectives can be summarized as follows:

- Assess the suitability of current techniques used to address energy imbalance during network contingency periods for wind energy conversion systems.
- Assess energy storage options for wind energy conversion systems for low voltage fault ride through.
- Assess fault resiliency challenges in series-connected offshore wind farms implementing dc collector systems.
- Assess fault resiliency challenges in parallel-connected offshore wind farms implementing dc collector systems.
- Propose a novel system level architecture and control system allowing safe operation and security against internal dc and external ac network faults.
- Propose a system level architecture and control system for a lightweight offshore converter station suitable for multi-terminal dc operation.

1.3 Thesis Structure

This thesis has been organized into six chapters.

Chapter 1 introduces the background of system security and fault resilience issues concerning offshore wind farms. In addition, the research motivations and objectives are outlined.

Chapter 2 provides a brief review of low voltage fault ride through techniques to mitigate electrical and mechanical stress in wind energy conversion systems at wind turbine level. In addition, a review of fault resiliency and offshore network configuration for high voltage dc offshore wind farms implementing dc collector networks is presented.

Chapter 3 presents a comparative analysis of four common low voltage fault ride through techniques proposed in literature. These include a conventional method, a software-based method and two energy storage systems-based methods. The methods are assessed in terms of performance, commercial and practical metrics using quantitative substantiation and time-domain simulations.

Chapter 4 presents a fault-resilient offshore wind farm based on series connection of wind energy conversion units with lightweight offshore bypass station. The chapter highlights the benefits over existing conventional systems in literature with increased system security during contingency periods. The proposal is substantiated using time-domain simulation verification. In addition, a qualitative assessment is provided to justify the lightweight offshore bypass station.

Chapter 5 proposes a lightweight offshore converter station suitable for multi-terminal dc applications. In addition, the dc collector network is formed of multiple small groups of series connected wind energy conversion units to mitigate additional conversion stages between voltage levels. The proposed system is verified using time-domain simulations and a qualitative assessment relating to mass and size for the proposed converter.

Chapter 6 presents the general conclusions of the presented thesis. In addition, the research contributions are stated, and future research suggestions presented.

References

[1] The Environment Agency, “The environment agency: reaching net zero by 2030.”

[2] Scottish Government, “Update to the climate change plan,” Edinburgh, 2020.

[3] Scottish Government, “Offshore wind policy statement,” Edinburgh, 202AD.

[4] Carbon Trust, “Floating wind joint industry project R&D findings delivered to support 70GW by 2040,” 2020. https://www.carbontrust.com/news-and-insights/news/floating-wind-joint-industry-project-rd-findings-delivered-to-support-70gw-by-2040 (accessed May 23, 2023).

[5] P. Kundur, J. Paserba, and S. Vitet, “Overview on definition and classification of power system stability,” in *CIGRE/IEEE PES International Symposium Quality and Security of Electric Power Delivery Systems, 2003. CIGRE/PES 2003.*, IEEE, 2003, pp. 1–4. doi: 10.1109/QSEPDS.2003.159786.

[6] CIGRE, “Defining power system resilience,” Sep. 30, 2019. https://www.cigre.org/article/GB/news/the_latest_news/defining-power-system-resilience (accessed May 23, 2023).

[7] Siemens Gamesa, “Onshire Expertise Your Trusted Partner.” https://www.siemensgamesa.com/en-int/products-and-services/onshore (accessed Mar. 07, 2022).

[8] Y. L. Hu, Y. K. Wu, C. K. Chen, C. H. Wang, W. T. Chen, and L. il Cho, “A Review of the Low-Voltage Ride-Through Capability of Wind Power Generators,” in *Energy Procedia*, 2017. doi: 10.1016/j.egypro.2017.11.046.

[9] A. M. Rauf, V. Khadkikar, and M. S. El Moursi, “A new fault ride-through (FRT) topology for induction generator based wind energy conversion systems,” *IEEE Transactions on Power Delivery*, vol. 34, no. 3, pp. 1129–1137, Jun. 2019, doi: 10.1109/TPWRD.2019.2894378.

[10] H. Xu, Y. Zhang, Z. Li, R. Zhao, and J. Hu, “Reactive current constraints and coordinated control of DFIG’s RSC and GSC during asymmetric grid condition,” *IEEE Access*, vol. 8, pp. 184339–184349, 2020, doi: 10.1109/ACCESS.2020.3029227.

[11] J. F. C. and R. F. C. Watson, R., and Watson, J.F. Conroy and R., “Low-voltage ride-through of a full converter wind turbine with permanent magnet generator,” *IET Renewable Power Generation*, vol. 3, no. 1, pp. 182–189, 2007, doi: 10.1049/iet-rpg.

[12] O. P. Mahela, N. Gupta, M. Khosravy, and N. Patel, “Comprehensive overview of low voltage ride through methods of grid integrated wind generator,” *IEEE Access*, vol. 7, pp. 99299–99326, 2019, doi: 10.1109/ACCESS.2019.2930413.

[13] S. W. Ali *et al.*, “Offshore Wind Farm-Grid Integration: A Review on Infrastructure, Challenges, and Grid Solutions,” *IEEE Access*, vol. 9. Institute of Electrical and Electronics Engineers Inc., pp. 102811–102827, 2021. doi: 10.1109/ACCESS.2021.3098705.

[14] European Network of Transmission System Operators for Electricity (ENTSO-E), “Requirements for grid connection applicable to all generators,” *ENTSOE Standards*, no. October, p. 86, 2013.

[15] E. Apostolaki-Iosifidou, R. Mccormack, W. Kempton, P. Mccoy, and D. Ozkan, “Transmission design and analysis for large-scale offshore wind energy development,” *IEEE Power and Energy Technology Systems Journal*, vol. 6, no. 1, pp. 22–31, Feb. 2019, doi: 10.1109/jpets.2019.2898688.

[16] P. Lakshmanan, R. Sun, and J. Liang, “Electrical collection systems for offshore wind farms: A review,” *CSEE Journal of Power and Energy Systems*, vol. 7, no. 5. Institute of Electrical and Electronics Engineers Inc., pp. 1078–1092, Sep. 01, 2021. doi: 10.17775/CSEEJPES.2020.05050.

[17] S. Hardy, K. van Brusselen, S. Hendrix, and D. van Hertem, “Techno-economic analysis of HVAC, HVDC and OFAC offshore wind power connections.,” *2019 IEEE Milan PowerTech*, 2019.

[18] Dragados Offshore, “Dolwin 4 & Borwin 4 HVDC grid connection projects,” 2022. Accessed: Oct. 27, 2022. [Online]. Available: https://www.dragadosoffshore.com/HTML/index.php/information-materials.html

[19] F. An, B. Zhao, B. Cui, and R. Bai, “Multi-functional DC collector for future all-DC offshore wind power system: Concept, scheme, and implement,” *IEEE Transactions on Industrial Electronics*, vol. 69, no. 8, pp. 8134–8145, Aug. 2022, doi: 10.1109/TIE.2021.3109539.

[20] R. Blasco-Gimenez, S. Ano-Villalba, J. Rodriguez-D’Derlee, F. Morant, and S. Bernal, “Distributed voltage and frequency control of off-shore wind farms connected with a diode

based HVDC link," in *IECON 2010 - 36th Annual Conference on IEEE Industrial Electronics Society*, IEEE, Nov. 2010, pp. 2994–2999. doi: 10.1109/IECON.2010.5674956.

[21] L. Yu, R. Li, L. Xu, and G. P. Adam, "Analysis and control of offshore wind farms connected with diode rectifier-based HVDC system," *IEEE Transactions on Power Delivery*, vol. 35, no. 4, pp. 2049–2059, Aug. 2020, doi: 10.1109/TPWRD.2019.2960405.

[22] R. J. Thomas, A. G. Phadke, and C. Pottle, "Operational characteristics of a large wind-farm utility system with a controllable ac/dc/acinterface," *IEEE Transactions on Power Systems* , vol. 3, no. 1, pp. 220–225, 1988, doi: 10.1109/59.43202.

[23] M. Popat, B. Wu, F. Liu, and N. Zargari, "Coordinated control of cascaded current-source converter based offshore wind farm," *IEEE Trans Sustain Energy*, vol. 3, no. 3, pp. 557–565, 2012, doi: 10.1109/TSTE.2012.2191986.

[24] E. Veilleux and P. W. Lehn, "Interconnection of direct-drive wind turbines using a series-connected dc grid," *IEEE Trans Sustain Energy*, vol. 5, no. 1, pp. 139–147, Jan. 2014, doi: 10.1109/TSTE.2013.2276616.

[25] P. Hu, R. Yin, B. Wei, Y. Luo, and F. Blaabjerg, "Modular isolated llc dc/dcConversion system for offshore wind farm collection and integration," *IEEE J Emerg Sel Top Power Electron*, vol. 9, no. 6, pp. 6713–6725, Dec. 2021, doi: 10.1109/JESTPE.2021.3062677.

[26] L. Li, B. Li, Z. Wang, M. Yang, and D. Xu, "Monopolar symmetrical dc-dc converter for all dc offshore wind farms," *IEEE Trans Power Electron*, vol. 37, no. 4, pp. 4275–4287, Apr. 2022, doi: 10.1109/TPEL.2021.3125095.

[27] Y. Xia, K. H. Ahmed, and B. W. Williams, "A pwm current source-based DC transmission system for multiple wind turbine interfacing," *IEEE J Emerg Sel Top Power Electron*, vol. 2, no. 4, pp. 784–796, 2014.

[28] Q. Wei, B. Wu, D. Xu, and N. R. Zargari, "Further study on a PWM current-source-converter-based wind energy conversion system considering the DC-link voltage," *IEEE Trans Power Electron*, vol. 34, no. 6, pp. 5378–5387, Jun. 2019, doi: 10.1109/TPEL.2018.2866045.

[29] M. Guan, "A series-connected offshore wind farm based on modular dual-active-bridge (DAB) isolated DC–DC converter," *IEEE Transactions on Energy Conversion*, vol. 34, no. 3, pp. 1422–1431, May 2019, doi: 10.1109/tec.2019.2918200.

Chapter 2

Review of Fault Resilience and Security for Offshore Wind Farms

The effects of ac networks faults on offshore wind farms (OWFs) configured in ac collector networks are a well-researched topic with well-defined grid codes. Firstly, this chapter will provide a review of the technologies used to comply with low voltage fault ride through requirements (LVFRT), for wind energy conversion systems (WECS) connected to ac networks. Secondly, due to their rise in growing popularity with other researchers, OWFs employing dc collector networks will be reviewed, with a focus on their fault management methodologies. The chapter will present a review of three common (in research) topologies, namely, parallel-connected, series-connected, and series-parallel type architectures. The review aims to identify the system performance during dc network faults.

2.1 Low Voltage Fault Ride Through Requirements

This section provides a summary of LVFRT requirements, as specified in grid codes and a selection of techniques presented by other researchers in literature to meet said requirements.

In summary, grid code state requirements state that the connected generating unit must remain connected, stable, and provide reactive power to the synchronous network during ac network faults [1], [2]. To articulate these stipulations, grid codes specify the resultant fault voltage levels (v_{fault}) with respect to steady state grid voltage (v_{nom}), fault duration (t_{clear}) recovery voltages (v_{rec}) and recovery times (t_{rec}) and present them in form of an LVFRT curve (simplified version shown in Fig. 2.1), with the beginning of the fault duration starting at t_{fault} [3]. The generating unit is only permitted to disconnect if the network conditions fall below the LVFRT curve. The severity of fault that generating units must withstand is dependent on their power export capability, with larger plants (groups of generating unit) subject to more onerous grid codes [4].

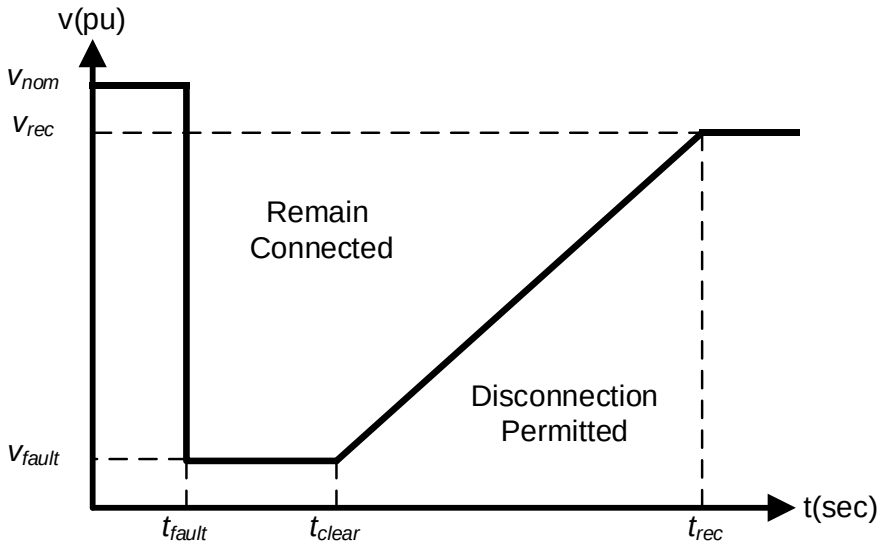

Fig. 2.1 . Typical low voltage fault ride through curve

For WECS units connected to the ac network, voltage sags caused by ac network faults, prevent the normal active power transfer from the generator into the network [5]. Fig. 2.2 shows a WECS equipped with permanent magnet synchronous generator (PMSG), two-level back-to-back converter connected to the ac network via power transformer and no LVFRT measures implemented. On the occurrence of an ac network fault, the ac grid voltage (v_g) will depress, impeding the power export capability of the grid-side converter, shown as P_g [6]. As a result, the dc link capacitor voltage (V_{dc}) will sharply increase, power transfer from the grid-side converter, P_{gsc} will reduce causing acceleration of the wind turbine rotor (ω_r) as the input and output powers are imbalanced [7]. If unmanaged this will lead to high levels of stresses on electro-mechanical systems and potentially lead to system shutdowns and non-compliant with grid code requirements [8].

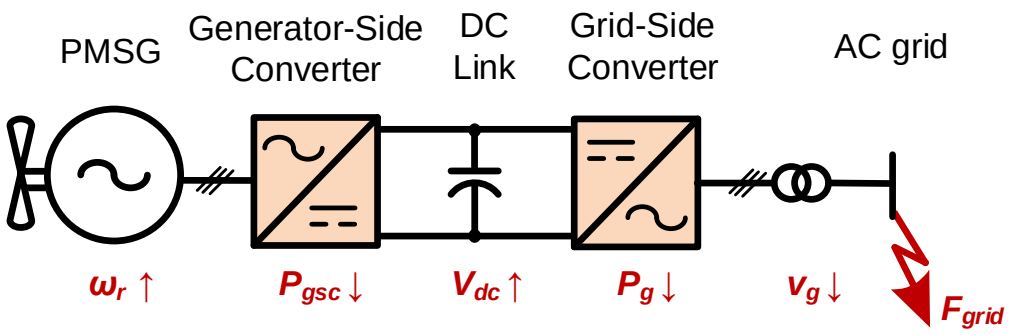

Fig. 2.2 . Schematic diagram of ac network fault on WECS.

Several techniques have been proposed in the literature to mitigate the negative effects on the WECS and comply with grid codes during network faults. Real power containment methods are employed to maintain or limit the power flow into the dc-link from the generator side converter during an ac fault to keep the dc-link voltage within operating range [9]. Blade pitch controllers have been proposed for reducing the rotor speed, thus power flow into the dc-link. However, the slow dynamics of pitch controllers prevent adequate power regulation within the millisecond time scales usually required [10]. Although, the power converter's fast dynamics can block the power flow into the system, this practice inflicts mechanical stress on the PMSG through rapid de-loading [5], [10].

The technique proposed in [11] and [12] de-loads the PMSG by implementing a multiplication factor to the generator control reference (i_q). In [11] the multiplication factor is based on a look-up table which reduces based on the dc-link voltage with respect to setpoint. In [12] the de-loading factor is proportional to the ac network voltage magnitude. During an ac network fault, the system with coordinated control (CC) de-loads the PMSG which may result in rotor speed increase and torque reduction, with the aim of containing dc-link voltage rise. This system negates hardware requirements, therefore is an attractive option. However, the key drawback is that the dynamics of the mechanical systems and the sudden change of voltage may cause overvoltage on the stator terminals along with rotor overspeed, which may not be fully highlighted by the small-scale machine-based experiment in [11].

Parallel connected with the dc-link, the commonly used dumping resistor (DR) can provide protection to the dc-link capacitor from overvoltage and is commonly well coordinated with other LVFRT techniques. The DR can be implementation through a self-commutated semiconductor switch. Featuring relatively low hardware cost and control complexity (via hysteresis control or PI controller method), the DR method is easily implemented and widely used [10]. The significant drawbacks of the DR are the heat dissipation and wasted energy during the activation periods [13].

To avoid energy dissipation during LVFRT and mitigate additional complex equipment connected to the dc terminals of the WECS, energy storage system (ESS) based methods have been proposed as attractive solutions for power smoothing to improve output power quality, smooth undesired transients and provide post-fault

support especially for weak ac grids, where power oscillations occur [14]. Many variations of ESS have been considered in literature. For example, flywheel energy storage has been proposed at wind farm level, which provides excellent support by releasing power into the networks during deep voltage sags [15]. However, its high cost, large footprint and complicated implementation make this method limited to certain schemes [5]. Commonly, static ESS elements installable at converter level can be connected into the dc-link and be operated for LVFRT. By employing this method, WECSs can actively maintain the dc-link voltage during faults and have desirable grid code compliance. Battery energy storage systems (BESSs) have a lower self-discharge rate than that of other comparable storage systems [16], but present practical challenges for wind energy applications due to chemical elements [5]. Although, the state of existing superconducting magnetic-based energy storage (SMES) technologies still requires improvement, they are attracting more attention for practical implementation in bulk power systems where the high performance is expected during extreme cases such as system faults [17]– [19].Supercapacitor-based energy storage systems have been seen as a promising alternative. Although self-discharge issues and high capital cost exist [20], supercapacitors have high power density in terms of both size and weight, which are particularly suitable for short-term high-power applications [21].

2.2 Faults in Offshore Wind Farms with DC Collector Networks

Generally, OWFs located at distances beyond 50–80 km from shore benefit from high-voltage dc (HVDC) technology for bulk transmission, due to technical and commercial constraints associated with conventional ac transmission [22]. This section looks at three configurations of OWF employing dc collector networks and assesses their behaviour during fault conditions.

2.2.1 Parallel-Connected Offshore Wind Farms

In terms of dc collector system based OWFs, a straightforward construction method, like the conventional ac-system based OWFs, is the parallel connection of multiple dc WECSs to form a parallel-connected offshore wind farm (PC-OWF), as illustrated in Fig. 2.3.

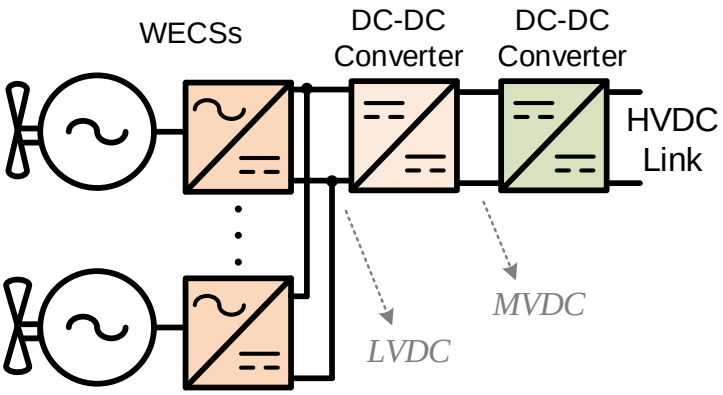

Fig. 2.3 . Parallel-Connected OWF (PC-OWF).

Thus, high gain dc-dc converters are required to step the voltage up, from low-voltage dc (LVDC) level of the WECS (for example, less than 10 kV), to medium-voltage dc (MVDC) level, and then to HVDC for bulk power transmission (up to hundreds kV) [23], [24]. Predominantly, a two-stage arrangement is needed to achieve such low-medium-high dc voltage conversion [25]– [28]. Different converter topologies are applicable. For instance, a unidirectional conversion with the input stage consisting of a half-bridge (HB) MMC and the output stage achieved by a diode bridge can be used [29], [30]. Although, improvement of such a topology is feasible in terms of output performance and operation modes, the high step-up ratio and galvanic isolation functionalities are achieved, with the deployed low-frequency phase-shifted transformer. The merits of such a scheme include high controllability over the WECSs and across all dc stages, and sensible isolation and protection setup. However, the multiple power electronic stages will involve significant weight and size requirements, high operation losses, and significant capital cost.

2.2.2 Series-Connected Offshore Wind Farms

The propositions to eliminate the requirement for the offshore power electronic converter station are popular, mainly achieved via the direct construction of HVDC transmission level voltage through series connection of WECSs [31], as shown in Fig. 2.4.

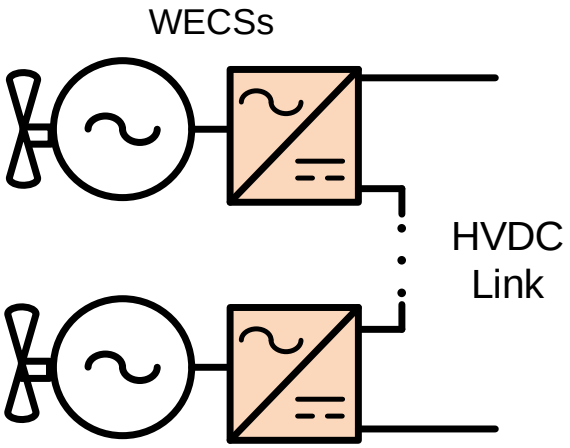

Fig. 2.4. Series-Connected OWF (SC-OWF).

The series-connected offshore wind farm (SC-OWF) concept, featuring the elimination of bulky offshore platforms, constructs the HVDC voltage with the WECS converter based on either voltage source converters (VSCs) [31]– [36] or current source converters (CSCs) [37]–[39]. For SC-OWF systems which operate with a constant (e.g., 1 pu) dc-link voltage, an onshore HB-MMC can be employed [40]; whereas inter-WECS voltage balancing is necessary to prevent the WECS terminal overvoltage, which is usually achieved by wind turbine power curtailment [40], [41] or energy storage [42]. The power curtailment method (via power converter control scheme) shows feasibility of curtailing output power by short terms but does not consider the effects of rotor over speed and requires an interface with the pitch controller [42]. For SC-OWF systems with a constant HVDC link current (a current-source based dc system), inter-WECS balancing may require more advanced onshore converter stations, which are capable of large range of dc-terminal voltage, such as full-bridge (FB) MMCs. Another key issue of the SC-OWF is the poor fault-tolerant capability for dc collector/cable fault ride-through if significant topological improvements are not implemented [41], [43], [44]. For the SC-OWF, the whole WECS string is easily affected by short and open circuit faults, via cascading effect, the consequence of which is a full power loss [41], severely effecting the resiliency off the dc network and reliability though loss of supply to the ac network.

Operational characteristics and requirements of the overall SC-OWF differ from its parallel-connected counterpart. As a means of balancing voltages of the WECSs in series connection, extra circuits may be adopted to either exchange energy between

units [31] or employing energy storage [42], which increases costs on power converters. However, the motivation of deploying the additional circuitry is system balancing, not to enhance system resiliency against system-wide faults. Coordinated operation between the offshore WECSs and the onshore half-bridge modular multilevel converter (HB-MMC) station (operating in constant dc-link voltage control mode) can also be used to avoid WECS overvoltage issues via communications link [40]. In [41], the voltage sharing between offshore WECSs can be addressed by the HB-MMC, which operates in a dc-link current control mode. However, the effectiveness is limited by the dc-terminal voltage range of HB-MMCs under low wind power (thereby dc-link voltage) conditions, and therefore a backup function is usually required to regain dc-link voltage control, leading to non-linear control and operation. Other MMC types with larger dc-terminal voltage ranges, such as the full-bridge MMC (FB-MMC), can be used to facilitate the dc-link current control in the SC-OWF applications [33].

MMCs with dc fault isolation or ride-through capability (such as FB-MMC [33], hybrid MMC [45], and T-type MMC [46]) can be used to protect the onshore system against severe dc-side/offshore faults. Yet, due to topological characteristics, SC-OWFs high fault vulnerability increases the overall system's reliability risk. A salient merit of conventional SC-OWFs is eliminating the requirement for offshore infrastructure [40], however the system security of this configuration is compromised when subject to offshore cable faults (short and open circuits). Offshore grounding faults are studied in [43], where the cascading effect of such faults is highlighted, and a fault-clearance method based on coordinated operation of a specific WECS dc/dc converter and protective switches is given, however, only short-circuit to ground faults are considered in this study. Although, dumping resistors (DRs) are deployed within the WECSs to provide wind turbine level protection, any collector cable rupture (open circuit) fault will completely cease the system power transmission [41], leaving the system vulnerable to long periods of zero power production. Also, the coordinated regulation of offshore and onshore subsystems in various fault scenarios is not yet determined. Conclusively, wide research gaps clearly exist for SC-OWF applications, predominantly with the consideration of overall system resiliency against different

onshore and offshore faults. Key challenges with SC-OWF systems are identified as low reliability, voltage variations due to wind fluctuations and fault management [47].

2.2.3 Series-Parallel-Connected Offshore Wind Farms

A series-parallel-connected offshore wind farm (SPC-OWF) shown in Fig. 2.5 could provide system redundancy and improve fault ride-through capability compared to the SC-OWF. Similarly, to reach to the same power rating, multiple WECS groups (WGs), with each consisting of series connected WECSs, are connected to one HVDC link. Therefore, the offshore converter platform is mitigated [40], [42], [48]. However, significant challenges would arise in terms of balancing different WGs and WECSs within the system [31].

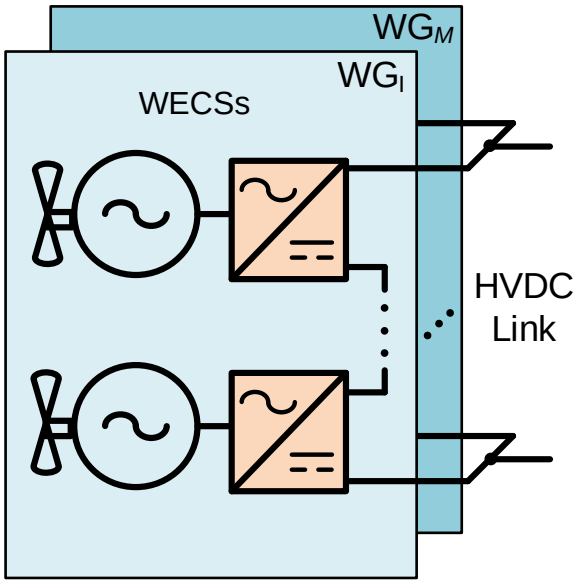

Fig. 2.5. Series-Parallel-Connected OWF (SPC-OWF).

In general, the dc circuit breakers (DCCBs) are proposed to be used to quickly isolate the fault in PC-OWFs and SPC-OWFs [42]; however, the high cost of current DCCBs would be the main barrier. Moreover, although the SC-OWF and SPC-OWF can theoretically eliminate the requirement of offshore converter stations, the feasibility is limited in practical terms given the high voltage offset issue of inter-string WECS components inherent to series connected voltage sources[34]. Both schemes will pose high requirement for the galvanic isolation of the WECS converters (which interfaces the wind turbine and HVDC link). For example, the topmost WECS in a string is

required to withstand the full HVDC link voltage (in hundreds of kV), which makes manufacturing prohibitively difficult.

2.3 Summary

This first section of this chapter presented a review of low voltage fault ride through requirements stipulated by grid codes and means of meeting those requirements. It highlighted that the technique had to be capable of dissipating or storing the energy imbalance present at the WECS caused by ac network faults. Although many methods are presented by other researchers in literature, the performance and cost of the proposed methods have not been investigated and compared.

The second section of this chapter presented a review of offshore windfarms employing dc collector networks. For the parallel-connected offshore the architecture allows for separation of the connected units during faults but introduces additional conversion stages, increasing losses and complexity of the network. The series-connected offshore wind farm proposes aims to minimise offshore converter stations by directly constructing high voltage direct current voltage through series-connection of wind energy conversion system unit. Although this is a promising concept, there has been no consideration in previous research for a system wide fault analysis as there is the potential for cascading faults which could pose a threat to system security and power export. For voltage-controlled series-connected networks balancing issues exist in other research proposals, where curtailment or energy storage are the predominant solutions, however these solutions require accepting potentially large power disruptions or the costly installation of energy storage devices. Series-parallel connected systems aim to improve on the redundancy of series-connected network and allow potential for expansion. However balancing issues exist as the system must operate in voltage control mode and are open to the same vulnerabilities regarding faults on the ac and dc network as series-connected systems with the inclusion of isolation equipment.

References

[1] C. Sourkounis and P. Tourou, "Grid code requirements for wind power integration in Europe," *Conference Papers in Energy*, vol. 2013, pp. 1–9, 2013, doi: 10.1155/2013/437674.

[2] F. Kalverkamp, B. Schowe-Von Der Brelie, T. D. Nguyen, T. Mertens, and M. Meuser, "Comparative analysis of european grid codes and compliance standards for distributed power generation plants with respect to future requirements of ENTSO-E and CENELEC," *International ETG Congress 2015; Die Energiewende - Blueprints for the New Energy Age*, pp. 605–610, 2015.

[3] European Network of Transmission System Operators for Electricity (ENTSO-E), "Requirements for grid connection applicable to all generators," *ENTSOE Standards*, no. October, p. 86, 2013.

[4] National Grid Electricity System Operator Limited, "The Grid code | National Grid," no. 5, pp. 1–998, 2019.

[5] R. A. Ibrahim, M. S. Hamad, Y. G. Dessouky, and B. W. Williams, "A review on recent low voltage ride-through solutions for PMSG wind turbine," *SPEEDAM 2012 - 21st International Symposium on Power Electronics, Electrical Drives, Automation and Motion*, pp. 265–270, 2012, doi: 10.1109/SPEEDAM.2012.6264594.

[6] E. Buraimoh and I. E. Davidson, "Comparative analysis of the fault ride-through capabilities of the VSG methods of microgrid inverter control under faults," *Proceedings - 2019 Southern African Universities Power Engineering Conference/Robotics and Mechatronics/Pattern Recognition Association of South Africa, SAUPEC/RobMech/PRASA 2019*, pp. 400–405, 2019, doi: 10.1109/RoboMech.2019.8704754.

[7] Z. Zheng, Q. Xie, C. Huang, X. Xiao, and C. Li, "Superconducting technology based fault ride through strategy for PMSG-based wind turbine generator: A comprehensive review," *IEEE Transactions on Applied Superconductivity*, vol. 31, no. 8, Nov. 2021, doi: 10.1109/TASC.2021.3101767.

[8] A. Moawwad, M. S. el Moursi, and W. Xiao, "Advanced Fault Ride-Through Management Scheme for VSC-HVDC Connecting Offshore Wind Farms," *IEEE Transactions on Power Systems*, vol. 31, no. 6, pp. 4923–4934, 2016, doi: 10.1109/TPWRS.2016.2535389.

[9] O. P. Mahela, N. Gupta, M. Khosravy, and N. Patel, "Comprehensive overview of low voltage ride through methods of grid integrated wind generator," *IEEE Access*, vol. 7, pp. 99299–99326, 2019, doi: 10.1109/ACCESS.2019.2930413.

[10] J. F. C. and R. F. C. Watson, R., and Watson, J.F. Conroy and R., "Low-voltage ride-through of a full converter wind turbine with permanent magnet generator," *IET Renewable Power Generation*, vol. 3, no. 1, pp. 182–189, 2007, doi: 10.1049/iet-rpg.

[11] R. Basak, G. Bhuvaneswari, and R. R. Pillai, "Low-Voltage Ride-Through of a Synchronous Generator-Based Variable Speed Grid-Interfaced Wind Energy Conversion System," in *IEEE Transactions on Industry Applications*, Institute of Electrical and Electronics Engineers Inc., Jan. 2020, pp. 752–762. doi: 10.1109/TIA.2019.2946125.

[12] G. P. Adam, K. H. Ahmed, S. J. Finney, and B. W. Williams, "AC fault ride-through capability of a VSC-HVDC transmission systems," *2010 IEEE Energy Conversion Congress and Exposition, ECCE 2010 - Proceedings*, pp. 3739–3745, 2010, doi: 10.1109/ECCE.2010.5617786.

[13] Y. L. Hu, Y. K. Wu, C. K. Chen, C. H. Wang, W. T. Chen, and L. il Cho, "A Review of the Low-Voltage Ride-Through Capability of Wind Power Generators," in *Energy Procedia*, 2017. doi: 10.1016/j.egypro.2017.11.046.

[14] S. D. Ahmed, F. S. M. Al-Ismail, M. Shafiullah, F. A. Al-Sulaiman, and I. M. El-Amin, "Grid Integration Challenges of Wind Energy: A Review," *IEEE Access*, vol. 8, no. type 1, pp. 10857–10878, 2020, doi: 10.1109/ACCESS.2020.2964896.

[15] F. Islam, A. Al-Durra, and S. M. Muyeen, "Smoothing of wind farm output by prediction and supervisory-control-unit- based FESS," *IEEE Trans Sustain Energy*, vol. 4, no. 4, pp. 925–933, 2013, doi: 10.1109/TSTE.2013.2256944.

[16] O. P. Mahela, N. Gupta, M. Khosravy, and N. Patel, "Comprehensive overview of low voltage ride through methods of grid integrated wind generator," *IEEE Access*, vol. 7, pp. 99299–99326, 2019, doi: 10.1109/ACCESS.2019.2930413.

[17] Seung-Tak Kim, Byung-Kwan Kang, Sun-Ho Bae, and Jung-Wook Park, "Application of SMES and Grid Code Compliance to Wind/Photovoltaic Generation System," *IEEE*

Transactions on Applied Superconductivity, vol. 23, no. 3, p. 5000804, 2012, doi: 10.1109/tasc.2012.2232962.

[18] C. Huang, X. Y. Xiao, Z. Zheng, and Y. Wang, "Cooperative Control of SFCL and SMES for Protecting PMSG-Based WTGs under Grid Faults," *IEEE Transactions on Applied Superconductivity*, vol. 29, no. 2, Mar. 2019, doi: 10.1109/TASC.2019.2891908.

[19] H. S. Salama and I. Vokony, "Voltage and Frequency Control of Balanced / Unbalanced Distribution System Using the SMES System in the Presence of Wind Energy," pp. 205–224, 2021.

[20] C. K. Das, O. Bass, G. Kothapalli, T. S. Mahmoud, and D. Habibi, "Overview of energy storage systems in distribution networks: Placement, sizing, operation, and power quality," *Renewable and Sustainable Energy Reviews*, vol. 91, no. November 2016, pp. 1205–1230, 2018, doi: 10.1016/j.rser.2018.03.068.

[21] C. Abbey and G. Joos, "Supercapacitor energy storage for wind energy applications," *IEEE Trans Ind Appl*, vol. 43, no. 3, pp. 769–776, 2007, doi: 10.1109/TIA.2007.895768.

[22] E. Apostolaki-Iosifidou, R. Mccormack, W. Kempton, P. Mccoy, and D. Ozkan, "Transmission design and analysis for large-scale offshore wind energy development," *IEEE Power and Energy Technology Systems Journal*, vol. 6, no. 1, pp. 22–31, Feb. 2019, doi: 10.1109/jpets.2019.2898688.

[23] A. Madariaga, J. L. Martín, I. Zamora, I. Martínez de Alegría, and S. Ceballos, "Technological trends in electric topologies for offshore wind power plants," *Renewable and Sustainable Energy Reviews*, vol. 24, pp. 32–44, Aug. 2013, doi: 10.1016/j.rser.2013.03.039.

[24] A. Follo, O. Saborío-Romano, E. Tedeschi, and N. A. Cutululis, "Challenges in all-DC offshore wind power plants," *Energies (Basel)*, vol. 14, no. 19, p. 6057, Sep. 2021, doi: 10.3390/en14196057.

[25] H. Liu, M. S. A. Dahidah, J. Yu, R. T. Naayagi, and M. Armstrong, "Design and control of unidirectional DC-DC modular multilevel converter for offshore DC collection point: Theoretical analysis and experimental validation," *IEEE Trans Power Electron*, vol. 34, no. 6, pp. 5191–5208, Jun. 2019, doi: 10.1109/TPEL.2018.2866787.

[26] L. Li, B. Li, Z. Wang, M. Yang, and D. Xu, "Monopolar symmetrical DC-DC converter for all DC offshore wind farms," *IEEE Trans Power Electron*, vol. 37, no. 4, pp. 4275–4287, Apr. 2022, doi: 10.1109/TPEL.2021.3125095.

[27] X. Zhang and T. C. Green, "The modular multilevel converter for high step-up ratio DC-DC conversion," *IEEE Transactions on Industrial Electronics*, vol. 62, no. 8, pp. 4925–4936, Aug. 2015, doi: 10.1109/TIE.2015.2393846.

[28] F. An, B. Zhao, B. Cui, and R. Bai, "Multi-functional DC collector for future all-DC offshore wind power system: Concept, scheme, and implement," *IEEE Transactions on Industrial Electronics*, vol. 69, no. 8, pp. 8134–8145, Aug. 2022, doi: 10.1109/TIE.2021.3109539.

[29] H. Liu, M. S. A. Dahidah, J. Yu, R. T. Naayagi, and M. Armstrong, "Design and control of unidirectional DC-DC modular multilevel converter for offshore DC collection point: theoretical analysis and experimental validation," *IEEE Trans Power Electron*, vol. 34, no. 6, pp. 5191–5208, Jun. 2019, doi: 10.1109/TPEL.2018.2866787.

[30] H. Liu, M. Dahidah, R. T. Naayagi, M. Armstrong, and J. Yu, "A novel modular multilevel step-up DC/DC converter for offshore systems," in *IEEE International Symposium on Industrial Electronics*, Institute of Electrical and Electronics Engineers Inc., Aug. 2017, pp. 576–581. doi: 10.1109/ISIE.2017.8001310.

[31] F. Rong, G. Wu, X. Li, S. Huang, and B. Zhou, "All-DC offshore wind farm with series-connected wind turbines to overcome unequal wind speeds," *IEEE Trans Power Electron*, vol. 34, no. 2, pp. 1370–1381, Feb. 2019, doi: 10.1109/TPEL.2018.2834965.

[32] A. O. Almeida, I. F. Lopes, P. M. Almeida, M. A. Tomim, J. A. Passos Filho, and P. G. Barbosa, "Series-DC connection of offshore wind generating units: Modeling, control and galvanic isolation.," *Electric Power Systems Research*, vol. 195, Jun. 2021, doi: 10.1016/j.epsr.2021.107149.

[33] G. Guo *et al.*, "Series-connected-based offshore wind farms with full-bridge modular multilevel converter as grid- and generator-side converters," *IEEE Transactions on Industrial Electronics*, vol. 67, no. 4, pp. 2798–2809, Apr. 2020, doi: 10.1109/TIE.2019.2912777.

[34] G. Guo *et al.*, "HB and FB MMC based onshore converter in series-connected offshore wind farm," *IEEE Trans Power Electron*, vol. 35, no. 3, pp. 2646–2658, Mar. 2020, doi: 10.1109/TPEL.2019.2929689.

[35] Z. Li, Q. Song, R. Zeng, B. Zhao, J. Meng, and Z. Deng, “A DC grid access solution based on series-connected distributed full-bridge submodule-based MMCs,” 2019.

[36] M. Guan, “A series-connected offshore wind farm based on modular dual-active-bridge (DAB) isolated DC-DC converter,” *IEEE Transactions on Energy Conversion*, vol. 34, no. 3, pp. 1422–1431, May 2019, doi: 10.1109/tec.2019.2918200.

[37] M. Popat, B. Wu, F. Liu, and N. Zargari, “Coordinated control of cascaded current-source converter based offshore wind farm,” *IEEE Trans Sustain Energy*, vol. 3, no. 3, pp. 557–565, 2012, doi: 10.1109/TSTE.2012.2191986.

[38] Q. Wei, B. Wu, D. Xu, and N. R. Zargari, “Further study on a PWM current-source-converter-based wind energy conversion system considering the DC-link voltage,” *IEEE Trans Power Electron*, vol. 34, no. 6, pp. 5378–5387, Jun. 2019, doi: 10.1109/TPEL.2018.2866045.

[39] Q. Wei, B. Wu, D. Xu, and N. R. Zargari, “A medium-frequency transformer-based wind energy conversion system used for current-source converter-based offshore wind farm,” *IEEE Trans Power Electron*, vol. 32, no. 1, pp. 248–259, Jan. 2017, doi: 10.1109/TPEL.2016.2524635.

[40] H. Zhang, F. Gruson, D. M. F. Rodriguez, and C. Saudemont, “Overvoltage limitation method of an offshore wind farm with DC series-parallel collection grid,” *IEEE Trans Sustain Energy*, vol. 10, no. 1, pp. 204–213, Jan. 2019, doi: 10.1109/TSTE.2018.2829929.

[41] A. O. Almeida, M. A. Tomim, P. M. Almeida, and P. G. Barbosa, “A control strategy for an offshore wind farm with the generating units connected in series with a VSC-HVDC transmission link,” *Electric Power Systems Research*, vol. 180, Mar. 2020, doi: 10.1016/j.epsr.2019.106121.

[42] H. J. Bahirat and B. A. Mork, “Operation of DC series-parallel connected offshore wind farm,” *IEEE Trans Sustain Energy*, vol. 10, no. 2, pp. 596–603, Apr. 2019, doi: 10.1109/TSTE.2018.2839712.

[43] G. Guo, K. Zha, J. Zhang, Z. Wang, F. Zhang, and J. Cao, “Grounding fault in series-connection-based offshore wind farms: Fault clearance,” *IEEE Trans Power Electron*, vol. 35, no. 9, pp. 9357–9367, Sep. 2020, doi: 10.1109/TPEL.2020.2971640.

[44] J. Tait, S. Wang, and K. H. Ahmed, “An Enhanced Series-Connected Offshore Wind Farm (SC-OWF) System Considering Fault Resiliency,” *IEEE Transactions on Power Delivery*, pp. 1–11, 2022, doi: 10.1109/TPWRD.2022.3219373.

[45] R. Zeng, L. Xu, L. Yao, and B. W. Williams, “Design and operation of a hybrid modular multilevel converter,” *IEEE Trans Power Electron*, vol. 30, no. 3, pp. 1137–1146, 2015, doi: 10.1109/TPEL.2014.2320822.

[46] S. Wang, A. M. Massoud, and B. W. Williams, “A t-type modular multilevel converter,” *IEEE J Emerg Sel Top Power Electron*, vol. 9, no. 1, pp. 843–857, 2021, doi: 10.1109/JESTPE.2019.2953007.

[47] P. Lakshmanan, R. Sun, and J. Liang, “Electrical collection systems for offshore wind farms: A review,” *CSEE Journal of Power and Energy Systems*, vol. 7, no. 5. Institute of Electrical and Electronics Engineers Inc., pp. 1078–1092, Sep. 01, 2021. doi: 10.17775/CSEEJPES.2020.05050.

[48] P. Lakshmanan, J. Guo, and J. Liang, “Energy curtailment of DC series-parallel connected offshore wind farms,” in *IET Renewable Power Generation*, Institution of Engineering and Technology, Apr. 2018, pp. 576–584. doi: 10.1049/iet-rpg.2017.0457.

Chapter 3

Comparative Assessment of Four Low Voltage Fault Ride Through Techniques for Wind Energy Conversion Systems

This chapter presents a comparative assessment of four low voltage fault ride through (LVFRT) techniques that alleviate the effects of power imbalance during ac network faults for voltage source converter (VSC)-based wind energy conversion systems (WECSs). The techniques appraised include a software-based coordinated control (CC) technique, commercially available dumping resistor (DR) technique, and two energy storage techniques, namely, superconductive magnetic energy storage (SMES) and supercapacitor energy storage (SCES). The techniques presented within this chapter are technically viable solutions for alleviating impacts of ac network faults on the WECS. The techniques have previously been assessed, by other researchers, by performance-based metrics, whereas this chapter aims to form a more comprehensive assessment by expanding the scope from the performance-based comparison to include economic considerations and practical limitations. Based on qualitative review of technically viable designs, this chapter presents quantitative substantiation with time-domain simulations of symmetrical and asymmetrical ac network faults. The comparative assessment is formulated based on assessing key performance metrics including grid code compliance, electrical and mechanical stress reduction, LVFRT response speed, hardware implementation, system efficiency and investment reduction.

3.1 Wind Energy Conversion System Configuration, Modelling and Control

The overall system, illustrated in Fig. 3.1(a) with each stage of the studied WECS. The PMSG stator is interfaced via an IGBT based generator side VSC, which is controlled by the generator side controller and the control is shown in Fig. 3.1(b). The dc output of the generator side converter VSC is connected to the dc-link with the power flow indicated by P_{in}. The energy storage system (ESS)/ DR block indicates the location where the DR, SMES or SCES will be interfaced, with charging/dissipation power represented by P_s. The dc-link capacitor is represented by C_{DC} with power flow into the

capacitor designated by P_l. The output power from the dc-link is designated by P_{out}, with the grid side converter control structure detailed in Fig.3.1(c). The ac output of the grid side converter is connected to the PCC via power transformer.

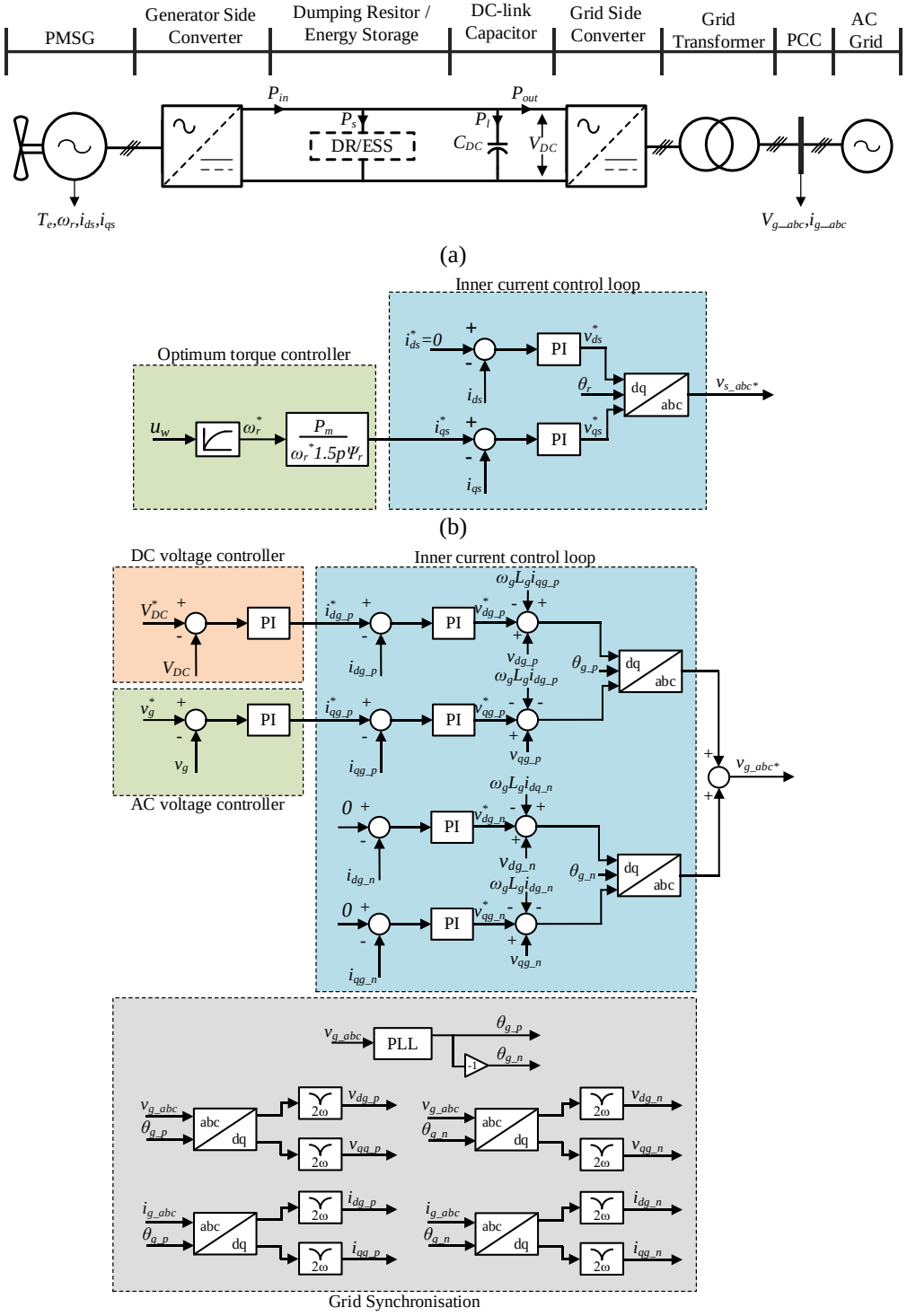

Fig. 3.1. Grid connected WECS. (a) system configuration. (b) generator side converter control block diagram. (c) grid side converter control block diagram.

The wind turbine aerodynamic model utilised is based on (3.1) to (3.4) [1], where P_m is the mechanical output power from the turbine, C_p represents the turbine power coefficient, λ is the tip speed ratio, β is the pitch angle, ρ is the air density, A is the swept area of the turbine, u_w is the wind speed, R_b is the blade radius, Ω_{ms} denotes the rotor speed, and $C_{1\text{-}6}$ are turbine coefficients.

$$P_m = C_p(\lambda,\beta)\frac{\rho A}{2}u_w^{\,3} \tag{3.1}$$

$$C_p(\lambda,\beta) = C_1\left(\frac{C_2}{\lambda_i} - C_3\beta - C_4\right)e^{\left(-\frac{C_5}{\lambda_i}\right)} + C_6\lambda_i \tag{3.2}$$

$$\frac{1}{\lambda_i} = \frac{1}{\lambda + 0.08\beta} - \frac{0.035}{\beta^3 + 1} \tag{3.3}$$

$$\lambda = \frac{R_b\Omega_{ms}}{u_w} \tag{3.4}$$

The PMSG can be modelled by (3.5) to (3.8) [2], where the d-axis and q-axis stator voltages and stator currents are represented by v_{ds}, v_{qs}, i_{ds} and i_{qs}, constants R_s, L_d and L_q represent the stator resistance and inductance of the d and q axis respectively, T_m represents the mechanical torque, T_e represents electrical torque, p represents number of pole pairs; ω_r is the rotor speed, J is the inertia, and F is viscous rotor friction coefficient.

$$\frac{d}{dt}i_{ds} = \frac{1}{L_{ds}}v_{ds} - \frac{R_s}{L_{ds}}i_{ds} + \frac{L_{qs}}{L_{ds}}p\omega_r i_{qs} \tag{3.5}$$

$$\frac{d}{dt}i_{qs} = \frac{1}{L_{qs}}v_{qs} - \frac{R_s}{L_{qs}}i_q - \frac{L_d}{L_{qs}}p\omega_r i_{ds} - \frac{\psi_r p\omega_r}{L_{qs}} \tag{3.6}$$

$$T_e = 1.5p[\psi i_{qs} + (L_{ds} - L_{qs})i_{ds}i_{qs}] \tag{3.7}$$

$$\frac{d}{dt}\omega_r = \frac{1}{J}(T_e - F\omega_r - T_m) \tag{3.8}$$

3.2 Generator-side Converter Control

The generator side converter ensures the delivery of the optimized power from the wind turbine to the dc-link using a maximum point power tracking system [3]. During an ac network fault, the generator side converter will continue to allow power flow into its dc side, which is as per design of the optimal torque control (OTC) structure. The major drawback to this method is that a power imbalance attributed to an ac network fault will result in continuous charging of the dc link capacitor (C_{DC}). Fig.3.1(b) depicts the control scheme, which employs an inner loop current controller with the *d*-axis current regulated to zero as per [4]. The *q*-axis current reference is derived from the OTC.

Synchronisation is achieved through use of the electrical angular velocity (ω_e) derived from the shaft angular velocity (ω_m) and the pole pairs (p) as per (3.9) [5].

$$\omega_e = \omega_m p \tag{3.9}$$

The control strategy of the generator side controller can be expressed as per (3.10) and (3.11) for the d-axis and q axis voltages respectively [5].

$$v_{ds} = -\left(R_s i_{ds} + L_{ds}\frac{di_{ds}}{dt}\right) \tag{3.10}$$

$$v_{qs} = -\left(R_s i_{qs} + L_{qs}\frac{di_{qs}}{dt}\right) \tag{3.11}$$

The *dq*-axis voltages, current and inductance are represented by v_{ds}, v_{qs}, i_{ds}, i_{qs}, L_{ds} and L_{qs} with the stator resistance represented by R_s. It should be noted that no compensation terms are utilised in this control scheme derived from [4]. The bracketed terms can be represented through a PI controller which can be used to regulate the current, represented in (3.12), with K_{pi}(s) represent the general term for the PI controller with K_p and K_i being the proportional and integral gains [6].

$$K_{pi}(s) = \frac{\left(K_p s + K_i\right)}{s} \tag{3.12}$$

No compensation terms are utilised, thus the controller terms for the inner loop current control can be expressed as (3.13) and (3.14) for the *dq*-axis converter voltage references respectively.

$$v_{ds}^{*} = K_{pi\_ils}(s)(i_{ds}^{*} - i_{ds}) \tag{3.13}$$

$$v_{qs}^{*} = K_{pi\_ils}(s)(i_{qs}^{*} - i_{qs}) \tag{3.14}$$

Tuning can be achieved by the internal model control technique used in [6] and refined during simulations.

3.2.1 DC-link Capacitor sizing

The dc-link voltage is commonly regulated by the grid side converter [7]. As can be seen in Fig. 3.1(a), the ac network faults create a mismatch between the power flowing into the dc-link (P_{in}) and delivered into the ac grid (P_{out}) which may lead to overvoltage [8] due to excess energy. This causes extra stresses and potentially catastrophic failure to the power switches in the power electronic converter or the capacitor if not well managed [9]. The rate in which the overvoltage occurs is dependent on the mismatched power (P_l) and the size of the dc-link capacitance. For a two-level VSC, the equivalent capacitance (C_{DC}) can be calculated by (3.15), where S_b is the converter rated apparent power, V_{DC_rated} is rated dc-link voltage and τ is a time constant, selected as 5 ms, which is deemed to have a small enough voltage ripple and is capable of handling small transients present in steady state operation [10].

$$C_{DC} = \frac{\tau S_b}{0.5V_{DC\_rated}^2} \tag{3.15}$$

3.2.2 Grid-side Converter Control

The grid side converter aims to inject wind power into the ac network. The PI inner loop current controller operates in the synchronous reference (*d*-*q*), shown in and employs a double synchronous reference frame phase locked loop (DSRF-PLL), used for both positive and negative sequence current regulation [11], as shown in Fig. 3.1(c). The Phase Locked Loop (PLL) implemented uses the classic methods of feedback of *q*-axis voltage feedback via PI controller and additional integration to obtain grid reference angle (θ_g) [11] represented in (3.16) as $K_{pll}(s)$. The signal is split to obtain a positive (θ_{g_p}) and negative (θ_{g_n}) angle references used to for the Clarke transforms to obtain the *dq*-frame voltage and current references in which are filtered through a notch filter, tuned to 2ω, allowing decouple positive and negative sequence *dq*-axis voltage and current

references for the control system [11]. Tuning can be achieved by the methods used in [6] for the purpose of the works conducted in this thesis strong grid assumption has been assumed and tuning has been achieved using the autotune feature in Matlab/Simulink for simplicity.

$$K_{pll}(s) = \frac{\left(K_{p\_pll}s + K_{i\_pll}\right)}{s} \tag{3.16}$$

A conventional vector control strategy with decoupling terms has been applied, consisting of an inner current control loop represented by the control strategy, expressed as (3.17) and (3.18). The *dq*-axis voltage and current are represented by v_{ds}, v_{qs}, i_{ds} and i_{qs}. The grid filter resistance and inductance are represented by R_g, L_g and the grid angular velocity by ω_g [5].

$$v_{dg} = \left(R_g i_{dg} + L_g \frac{di_{dg}}{dt}\right) - \omega_g L_g i_{qg} + v_{ds} \tag{3.17}$$

$$v_{qg} = \left(R_g i_{qg} + L_g \frac{di_{qg}}{dt}\right) + \omega_g L_g i_{dg} + v_{qs} \tag{3.18}$$

The bracketed terms can be represented by PI controller where the others treated as compensation terms. As such the inner loop current controllers can be expressed as (3.19) and (3.20) with K_{p_ildg} and K_{p_ilqg} and the tuning stagey stated in 3.2 [6]. Although generic equations are shown, the same controller structure and tuning is applied for both positive and negative sequence controllers, with the negative sequence controller regulating to zero to suppress negative sequence currents.

$$v_{ds}^{*} = K_{pi\_ildg}(s)(i_{dg}^{*} - i_{dg}) - \omega_g L_g i_{qg} + v_{ds} \tag{3.19}$$

$$v_{qs}^{*} = K_{pi\_ilqg}(s)(i_{qg}^{*} - i_{qg}) + \omega_g L_g i_{dg} + v_{qs} \tag{3.20}$$

The outer loop controllers, typically tuned slower than the inner loop current control, has been configured to independently regulate the dc-link voltage (V_{dc}) through injection of d-axis current into the grid and inject/absorb q-axis current based on the ac voltage (v_g) [5]. The controllers are represented by K_{pi_VDC} (3.19) and K_{pi_vg} (3.20) respectively. The outer loop controllers are only applicable to the positive sequence current controller.

$$i_{ds}^{*} = K_{pi\_VDC}(s)(V_{DC}^{*} - V_{DC}) \tag{3.19}$$

$$i_{qs}^{*} = K_{pi\_vg}(s)(v_g^{*} - v_g) \tag{3.20}$$

The positive sequence controller is equipped with an outer loop which regulates the dc-link voltage (V_{DC}) and defines reference current of the *d*-axis inner current controller. Also, the outer loop of the *q*-axis facilitates an ac voltage (v_g) control and defines the reference of the *q*-axis inner current controller.

The WECS is required to ride through ac network faults, where detailed specifications are defined by each system operator (SO) (such as National Grid ESO [7], ENTSO-E [36], and IEEE [37]). If the system falls out of the stipulated profile, then the generating unit is permitted to disconnect from the ac network [15]. The grid side converter plays a significant role for such fault ride through, whereas the overall WECS must be under tight control to ensure safe operation.

3.2.3 Low Voltage Fault Ride Through Energy Storage Systems Requirements

ESS solutions are usually proposed for power smoothing or other long-term applications [16]. To utilise ESSs for LVFRT applications, it is imperative that the ESS employed has sufficient power and energy capacity. In general, the parameters include a voltage threshold (v_{trig}), set to activate LVFRT measures; a recovery voltage (v_{rec}), which the generating unit must withstand for a longer-term period; and a retention voltage, equating to the resultant terminal voltage during the fault (v_{fault}) in which the generator must remain connected. The ac network fault clearance time (t_{clear}) specifies the time in which the ac network fault must be cleared in, and the system must withstand, on clearance of the fault the recovery time (t_{rec}). If the system parameters fall out with set parameters, then the generating unit is permitted to disconnect from the ac network. To ascertain the energy requirements (E_{LVFRT}) of ESSs during an ac fault, Eq. (2.14) can be used for basic ESS sizing [17].

$$E_{LVFRT} = P_b\left[\left(v_{trig} - v_{fault}\right)t_{clear} + 0.5(t_{rec} - t_{clear})\left(v_{trig} - v_{fault}\right)\right] \tag{3.14}$$

3.3 Four Low Voltage Fault Ride Through Techniques for Wind Energy Conversion Systems

This section discusses four techniques for LVFRT to be integrated into a WECS system, which is akin to the system detailed in section 3.1 including basic design considerations and general technological characteristics.

3.3.1 Coordinated Control

The basis of the CC technique employed was based on works presented in [18] and [17]. To implement the CC into the WECS, a de-loading reference (limited from 0 – 1 pu) taken from grid reference voltage measurement (v_{g_pu}) is implemented. The v_{g_pu} reference, via multiplication therefore scales the q-axis current reference (i_{qs}^{*}) when implemented in the generator side control scheme's outer loop control, shown in Fig. 3.2. By implementing in this manner, the power export from the WECS can be scaled dependant v_g.

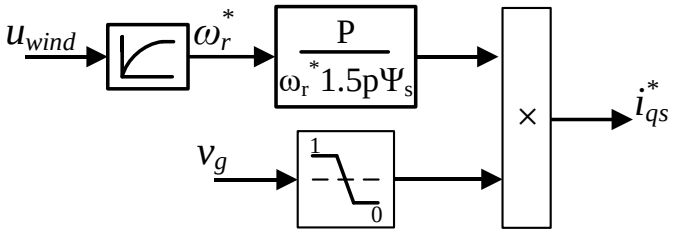

Fig. 3.2. Block diagram of generator side control system.

3.3.2 Dumping Resistor

The dumping resistor is implemented into the dc-link of the WECS as per [8] and is shown in Fig. 3.3. The IGBT switch (Q_1) is controlled via PI controller based on a fixed set point, based on a threshold of dc-link overvoltage. On exceeding the overvoltage threshold, the DR (R_{DR}) will be activated. The DR (R_{DR}) must be sized at the full active power rating of the converter (P_b), where (3.15) provides a method to calculate the resistance, while I_{DC_fault} is the maximum allowable current of the resistor bank.

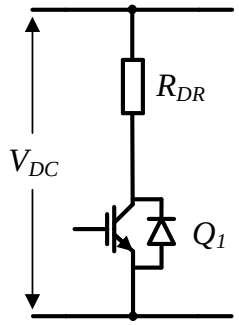

Fig. 3.3. Schematic diagram of dumping resistor

$$R_{DR} = \frac{P_b}{I^2_{DC\_fault}} \tag{3.15}$$

3.3.3 Superconducting Magnetic Energy Storage

The SMES can be implemented based on the circuit as shown in Fig.3.4, where a two-quadrant chopper circuit facilitates bi-directional current capability of the SMES, with three modes of operation. Charging operation is achieved by operating both IGBT switches (Q_1 and Q_2). They are switched on allowing power flow into the SMES. Discharging mode of operation is achieved when both IGBT switches are in the off position permitting power flow via forward bias state of the diodes (D_1 and D_2). Stand-by mode of operation is achieved when only one of the IGBT's are on and the other is off (e.g., $Q_1 = 1$ and $Q_2 = 0$ or $Q_1 = 0$ and $Q_2 = 1$). During ac network faults, the excess energy in the dc-link can be stored in the SMES to provide superior response for the WECS. The coil inductance can be estimated based on (3.16) [20], where the E_{LVFRT}, calculated from (3.15) is the energy to be stored (in an extreme case based on the fault duration and excess power into the dc-link P_l), and I_{DC_SMES} is SMES rated current.

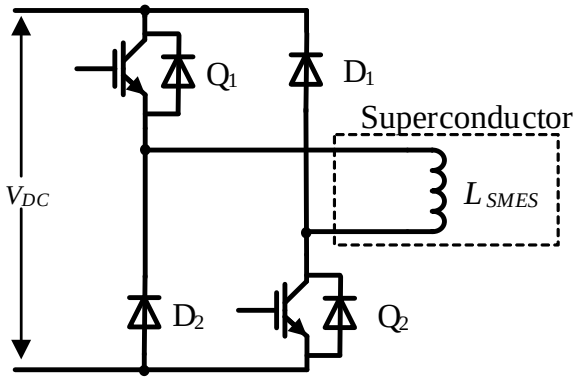

Fig. 3.4. Schematic diagram of superconducting magnetic energy storage system

$$L_{SMES} = \frac{2E_{LVFRT}}{I_{DC\_SMES}^2} \tag{2.16}$$

Superconductive material for energy storage has high efficiency, fast-responding speed, and high-power density [21]. However, major drawbacks of SMES are the high capital costs and operation requirements of cryogenic cooling, which incurs additional losses and requires specialist maintenance [22].

3.3.4 Supercapacitor Energy Storage

Featuring high power density for low (ms) to medium (s) time scales [23], supercapacitors can be equipped in the dc-link and operated as energy storage in such LVFRT applications [24]. Fig.3.5 shows the configuration with a bi-directional chopper interfacing the supercapacitor (C_{SCES}) and the dc-link. Ref. [17] provides guidance for sizing the supercapacitor based on the fault energy (E_{LVFRT}, calculated from (3.15)). Simply, assuming the allowable minimum and maximum supercapacitor voltages are 0.2 pu and 0.8 pu of the rated dc-link voltage respectively, with an initial charge voltage ($V_{DC\_initial}$) of 0.3 pu, the capacitance is estimated by (3.17). The design which considers initial charge voltage, internal resistance, current/power ratings, etc. is required, as articulated in [25].

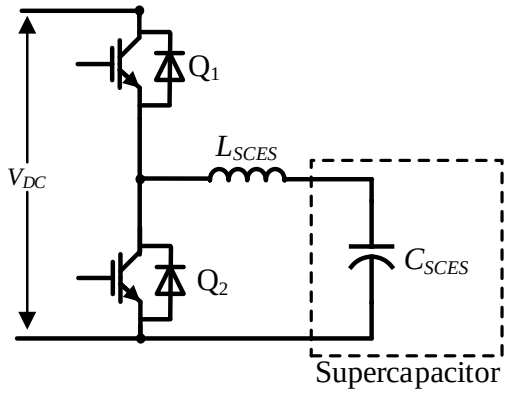

Fig. 3.5. Schematic diagram of supercapacitor energy storage system

$$C_{sc} = \frac{2E_{LVFRT}}{(V_{SCES\_rated} - V_{SCES\_initial})^2} \tag{3.17}$$

Supercapacitors have generally high-power density, relatively long-life span, and low maintenance requirements in comparison to ESS such as batteries or SMES. However, the current drawbacks with SCES are the high capital costs (components and management systems) and self-discharge effect.

3.4 Time-domain Simulation Evaluation

This section details the WECS system from section 3.2 for the simulation study and presents the system performance with each LVFRT technique presented in section 3. System modelling is based on the parameters listed in Table 3.1, which defines the medium voltage collector network, line parameters, PMSG, the two-level back-to-back VSC, including grid side converter filters, etc. Two ac network fault cases, namely, three-phase to ground and single-phase to ground faults, are used to assess the LVFRT techniques. The wind speed is set to be 12 m/s, resulting in 1 pu torque and rotor speed (ω_r). For the grid side converter, dc-link voltage reference (V_{DC}*) is set to be 1 pu and the reactive power reference (v_g^*) is set to 1 pu, considering the grid support requirements [26]. Converter current limitation mechanism is adopted to limit the current amplitude to 1.2 pu. For simplicity the PLL employed in Simulink specialised power system is set to automatically tune. PI gains for inner and outer loop controller have been applied though parameter estimation and iterative trialling of parameters.

Table 3.1. System parameters

Description	Value	Units
PCC voltage (ph-ph)	25	kV
Grid frequency	50	Hz
Grid short circuit ratio (SCR)	10	-
Transformer primary voltage (ph-ph)	25	kV
Transformer secondary voltage (ph-ph)	0.69	kV
Transformer resistance	0.01	pu
Transformer leakage	0.2	pu
Transformer power rating	2.24	MVA
PMSG mechanical power (P_m)	2	MW
PMSG torque (T)	848.826	kNm
PMSG rotor speed (ω_r)	2.36	rad/s
PMSG stator resistance (R_s)	0.82	mΩ
PMSG dq-axis synchronous inductance (L_{dq})	1.57	mH
PMSG rotor flux (ψ)	5.8	Wb
PMSG no. of pole pairs (p)	26	-
PMSG turbine inertia (J)	50	Kgm^2
DC-link voltage (V_{DC})	1250	V
DC-link capacitor (C_{DC})	2.5	mF
Fault resistance	1	mΩ
Dumping resistor	0.8	Ω
SMES coil (L_{SMES})	0.45	H
Supercapacitor (C_{SCES})	2.3	F
Inner current controller PI gains	1, 100	-
Outer control loops PI gains	1, 250	-

In terms of the LVFRT performances to be investigated, four different configurations are simulated, namely, CC, DR, SMES, and SCES. For the DR, an IGBT switch is used to activate the energy dissipation and limit dc-link voltage, using a PI controller with the set-point being 1.2 pu of the dc-link voltage (V_{DC}). For the SMES, the modes of operation are defined by fixed set-points, where $1.05V_{DC}$ initiates charging and $0.95V_{DC}$ initiates discharging. For the SCES, the charging and discharging functions of the SCES circuit is configured in the same manner as the SMES, with an initial charge of 30%. The reason of the higher threshold for DR is to address issues of transients to reduce the power dissipation. This is not the case for energy storage-based methods such as SMES and SCES, as the stored energy can be fed back into the system. The fault simulated is intended to demonstrate a worst-case scenario.

3.4.1 Symmetrical Fault Case

Fig. 3.6 shows the simulation results in a three-phase to ground fault at 0.3 s for a duration of 200 ms. Fig. 3.6(a-i) – Fig. 3.6(d-i) show the resultant ac voltage of 0 pu, to simulated a fault of close proximity. Fig. 3.4(a-ii) – Fig. 3.6(d-ii) show the current

waveforms during the fault, whereas Fig. 3.6(a-iii) – Fig. 3.6(d-iii) displays PCC active and reactive power. Reactive power injection post fault is visible for all fault conditions and is a result of the current limiters applied to the control system. PMSG torque and rotor speed of each case are given in Fig. 3.6(iv) and (v) respectively. For the converter system, dc-link voltage, and powers (power flowing into the dc-link, P_{in}, power delivered into the grid side converter, P_{out}, and excess power absorbed by the dc-link device, P_l) are displayed in Figs. 3.6(vi) and (vii) respectively.

Fig. 3.6(a) shows that system with CC can suppress dc-link voltage rise and current oscillation to some extent. Although the generator side converter is restricting the power flow from the turbine into the dc-link, this still results in a dc-link voltage rise to about 1.6 pu, thereby still endangering the devices. The CC technique imposes mechanical stresses on the PMSG where the torque is reduced to 0 pu, resulting in an over-speed of around 1.6 pu and effectively blocking power flow to the dc-link, see Fig. 3.6(c-iv) and (c-v). The DR performs adequately in comparison to the CC technique, with respect to containing the dc-link voltage within permissible limits, with the excessive power P_l dissipated, see Fig. 3.6(d-iv), (d-v), and (d-vii). The WECS still has a minor overshoot of active power due to the sustained 1.2 pu dc-link voltage throughout the fault, as shown in Fig. 3.6(d-iii) and (d-vi). Both SMES and SCES can absorb the power, which cannot be injected into the ac grid, with dc-link voltage tightly controlled, see Fig. 3.6(c) and (d). The level of sustained dc-link voltage throughout the fault has a direct impact on the recovery time and overshoot of power. With regulated power flow during the fault, the post-fault power recovery for SMES and SCES is improved, see Fig. 3.6(c-ii) and (d-ii), where minimal overshoot can be observed compared to other methods. The main difference between SMES and SCES techniques is the minor dc-link voltage overshoot at the early stage of the fault on the SMES, which is mainly due to the coil dynamics (high inductance causes slow current changing rate), see Fig. 3.6(c-vi). The ac current of the grid side converter is limited with DR, SMES and SCES due to the normal dc-link voltage and converter operation, see Fig. 3.6(b-iii), (c-iii), and (d-iii).

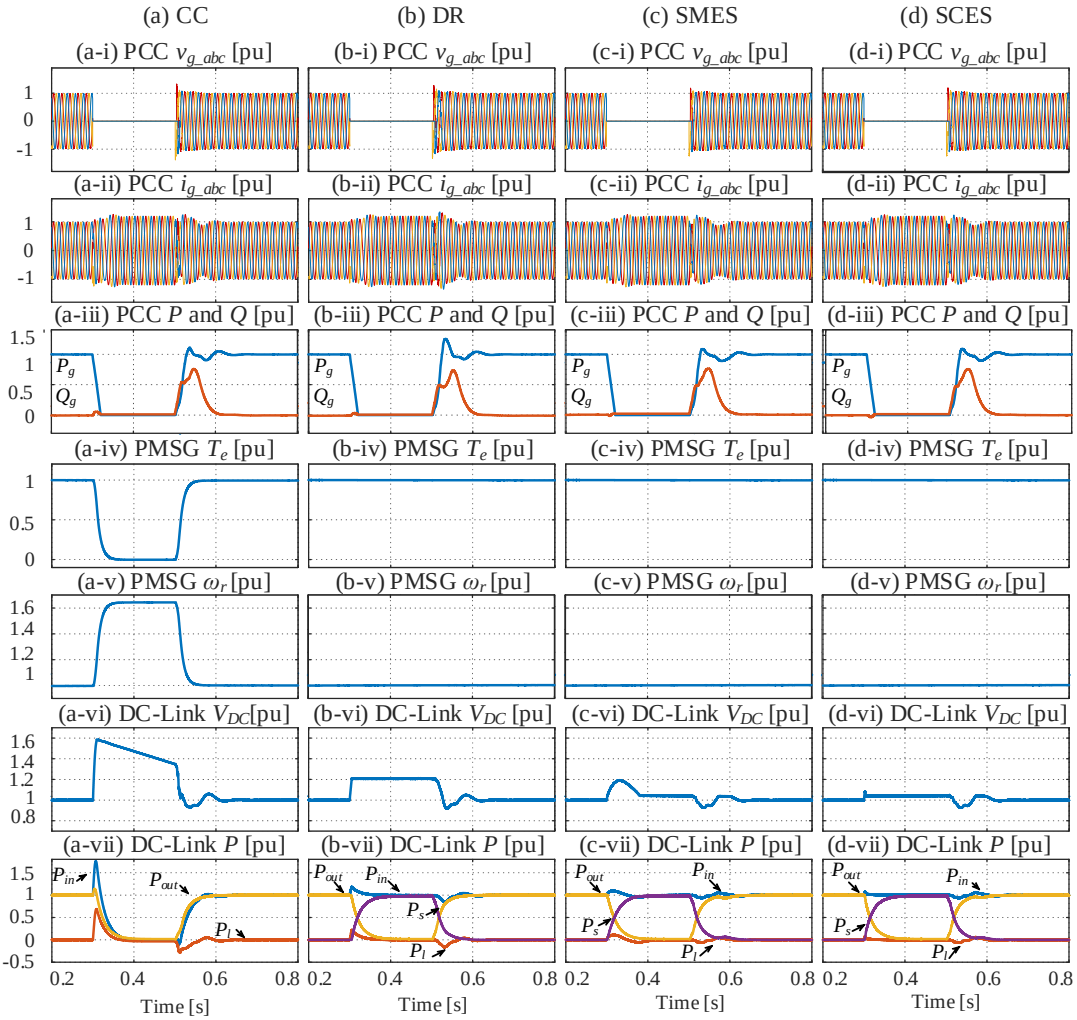

Fig. 3.6. Simulation results of three-phase to ground fault case. (a) CC. (b) DR. (c) SMES. (d) SCES.

Table 3.2 provides a numerical representation of key parameters of the WECS performance during the fault and recovery period, which forms a comparison to grid codes where applicable. The grid code selected is based on the most onerous values provided by ENTSO-E [13]. For each technique, the most onerous LVFRT of a fault that results in a 0 pu voltage fault for 200 ms has been adhered to consistently. The major difference between the techniques is the level of dc-voltage overshoot, with the highest case (CC) of 1.6 pu V_{DC} rise. This is approximately 29% higher than those of the DR and SMES cases which is approximately 42% higher than that of the SCES. On initial activation the 1.2 pu overshoot of the SMES is characterized by the large inductance resulting with the observed overshoot characteristics which can be quantified and directly compared to [27]. Thus, SCES is the most capable of maintaining the dc-link voltage within tolerable limits. The DR results in the highest

overshoot of active power to the ac network with P_g reaching 1.3 pu, being approximately 8% higher than CC and approximately 17% higher than SMES and SCES. This shows that the ESS techniques result in the lowest overshoot during recovery. Although the recovery duration of the four techniques is within the grid code stipulation of 500 ms, CC has the longest recovery of 150 ms, making it 22% slower than the ESS techniques and 40% slower than the DR technique. For verification purposes, the DR performance has been compared to [8], the SMES performance has been compared to [27], and the SCES performance has been compared to [44].

Table 3.2. Performance results of three-phase to ground fault.

Stage	Description	CC	DR	SMES	SCES	Grid Code
Fault	Min. 1ph-g grid voltage (pu)	0	0	0	0	0 - 0.15
Fault	Fault duration (ms)	200	200	200	200	140 - 200
Fault	Max. DC-link voltage (pu)	1.6	1.2	1.2	1.05	-
Recovery	PCC power overshoot (pu)	1.2	1.3	1.1	1.1	-
Recovery	PCC power recovery time (ms)	150	100	120	120	500

3.4.2 Asymmetrical Fault Case

Fig. 3.7 shows the simulation results with a single-phase to ground fault at 0.3 s for a duration of 200 ms. The presented waveforms and variables are the same as that of Fig. 3.6. For the CC, the generator converter controller restricts power flow into the dc-link during the fault until the condition where average values of P_{in} and P_{out} are matched. Due to the slow dynamics of the PMSG, an initial overshoot of P_{in} is present at the early stages of the fault, which results in an initial dc-link voltage rise of almost 1.3 pu before decaying before fault clearance, see Fig. 3.7(b-vi). In addition, there is a sustained over-speed of 1.2 pu, see Fig. 3.7(b-v), reducing the practical realisation of this technique. This value is approaching the limit of the switching device rating and prolonged faults may result in damage to devices. The DR improves the performance by keeping the dc-link voltage within the 1.2 pu set-point, see Fig. 3.7(c-vi), however, this sustained level of dc-link voltage slightly affects the recovery of the system after fault clearance, resulting in a PCC active power overshoot of almost 1.1pu and slower recovery time than the other techniques presented, see Fig. 3.7(c-iii). Performance of

the SMES and SCES, see Fig. 3.7(d) and (e) respectively, provide the most effective dc-link regulation out of the techniques presented with little distinguishable differences during such an asymmetrical fault. Also, the dc-link voltages are maintained at set-point, current regulation is correct and fast post-fault recovery is achieved.

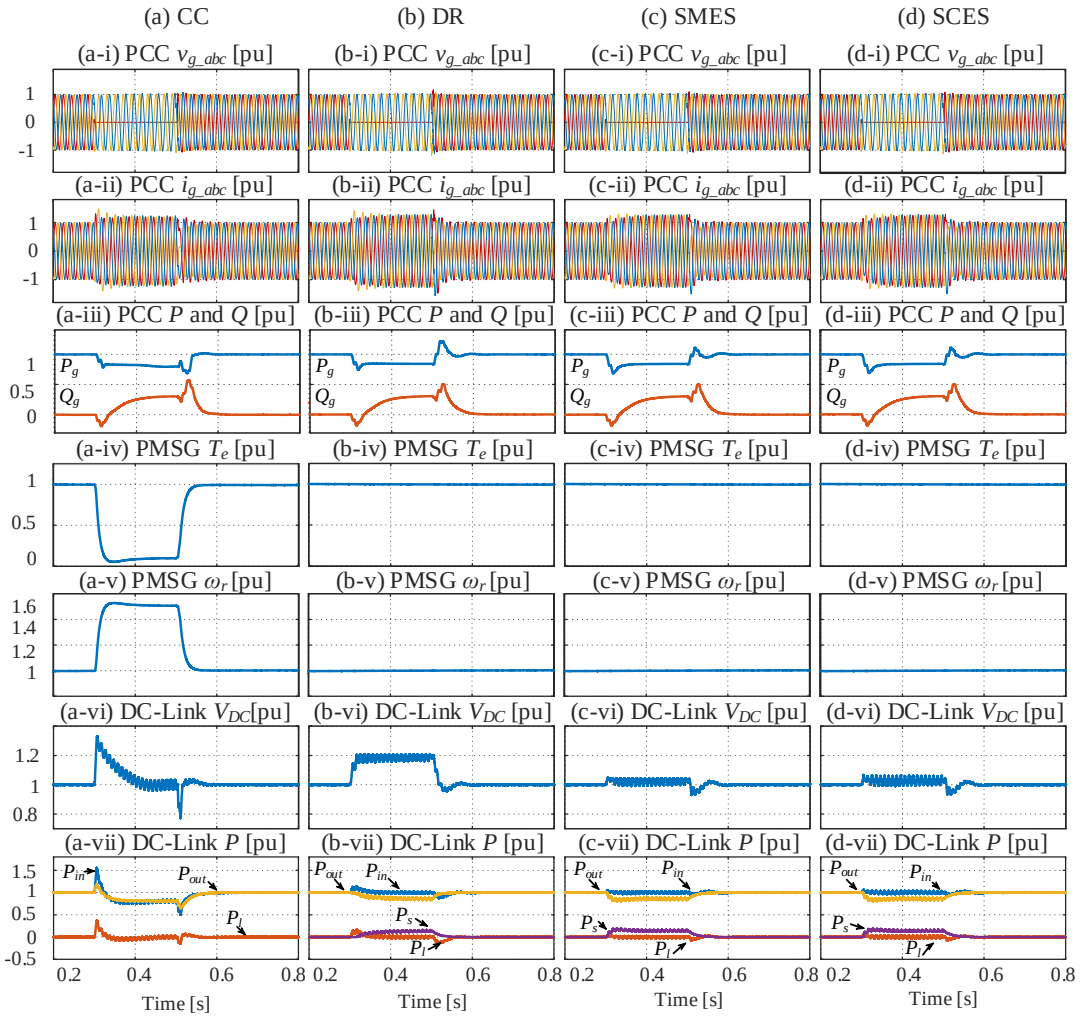

Fig. 3.7. Simulation results of single-phase to ground fault case. (a) CC. (b) DR. (c) SMES. (d) SCES.

Table 3.3 provides a numerical representation of key parameters of the WECS and converter system during the single-phase to ground fault and recovery period, which forms a comparison to grid codes where applicable. The most significant difference between the techniques is the level of dc-voltage overshoot with the highest case being CC where V_{DC} rises to 1.3 pu. This is approximately 8% higher than the DR case and approximately 17% higher than the cases with ESS techniques. Also, the DR has the highest overshoot of active power to the ac network with P_g reaching 1.2 pu,

approximately 21% higher than the ESS options and approximately 26% higher than CC (negligible overshoot during the single-phase to ground fault recovery period). All the four techniques have approximately the same recovery duration, making them indistinguishable from each other.

Table 3.3. Performance results of three-phase to ground fault.

Stage	Description	CC	DR	SMES	SCES	Grid Code
Fault	Min. 1ph-g grid voltage (pu)	0	0	0	0	0 - 0.15
Fault	Fault duration (ms)	200	200	200	200	140 - 200
Fault	Max. DC-link voltage (pu)	1.3	1.2	1.05	1.05	-
Recovery	PCC power overshoot (pu)	1	1.2	1.05	1.05	-
Recovery	PCC power recovery time (ms)	50	50	50	50	500

3.5 Practical Implementation Consideration

Practical and commercial factors are key to the decision process of implementing such engineering techniques for LVFRT. This section analyzes the practical aspects of each of the LVFRT techniques. Taking the case listed in Table 3.1 as an example, an appraisal of practical and commercial implementation regarding the investigated LVFRT solutions can be presented considering major costs, size, weight, cooling method, efficiency, etc., as given in Table 3.6, except for CC due to the minimal cost and no physical properties.

Table 3.4. Practical characteristics of the studied techniques

Considered items	DR	SMES	SCES
Volume [m^3]	0.28	12	0.3 – 0.7
Weight [kg]	80	1,100	300 – 500
Cooling method	Natural/forced convection	Cryogenic	Natural convection
Operation efficiency	N/A	80% – 99%	65% – 99%
Self-discharge percentage per day	N/A	1% – 15%	0.46% – 40%
Passive component cost [$]	40k – 90k	400k – 980k	80k – 140k
Power electronics cost [$]	1.5k	3k	3k

3.5.1 Dumping Resistor

The DR is designed based on a 2 MW dumping resistor bank such as that in [29]. Due to the heat dissipation of the resistor banks, the system requires forced convection cooling, with additional control supplies. The DR has many attractive features due to the low cost, volume, and weight. The importance of keeping cooling paths clear is stated in the manufacturer's instructions [29], showing heat management is a critical part of system. As stipulated in [29] it is imperative that the dissipated heat is managed correctly and malfunctions to the cooling system could result in failure to the DR, which in turn voids the grid code compliance of the WECS. The costs are estimated based on the suitably rated components including resistor banks [30], [31] and IGBTs [32]. Importantly, among all the techniques, it is the most technically robust and commercially mature.

3.5.2 Superconducting Magnetic Energy Storage

The information on volume, weight, and cooling method of the SMES indicate high requirements on the engineering implementation, although this technique tends to have high round-trip efficiency [21]. Due to most systems being research-based, no clear information on the commercial aspects of SMES is readily available, whereas the information in [23], [24] can be only used to ascertain a range of costs, which is high and unsuitable for wind turbine level applications. Also, this technique requires the highest number of semiconductors. Practically speaking, the SMES could be deemed unviable for wind turbine level integration due to the physical complexities involved.

3.5.3 Supercapacitor Energy Storage

The engineering consideration of the SCES system can be estimated from design, which is sized based on [33]. The cooling requirement on the SCES system can be low, while the volume and weight can result in difficult engineering constraint. The high levels of self-discharge and complexity of cell management system are also problematic. Currently, the cost of commercially available SCESs remain higher than DR [34], in addition to the dc/dc converter inductor [35]. With these factors taken into consideration, integration of SCES at wind turbine level might be practical with the cost expected to be reduced.

3.6 Analysis of Low Voltage Fault Ride Through Techniques

The key challenges during LVFRT of WECSs is to manage the active power that cannot be transferred into the faulty grid. Different techniques can be used to address that, but at the expense of imposing stresses at various points within the system. Fig.3.8 presents the performance comparison of the four studied techniques with the designated metrics.

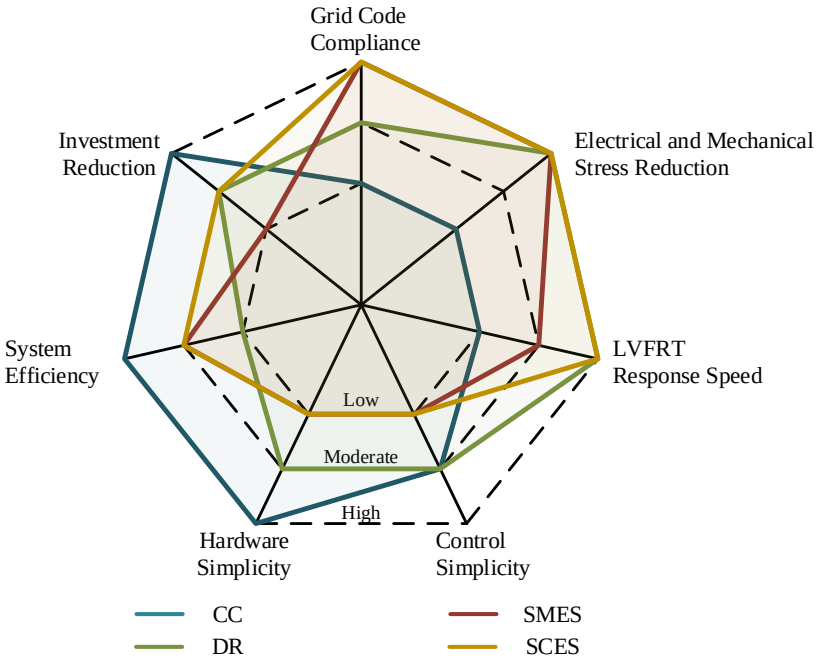

Fig. 3.8. Performance comparison of the presented techniques.

3.6.1 Grid Code Compliance

Grid codes do not provide specific values for the internal converter transient voltages and levels of fault voltages and current within the converter and state these must be based on converter capability, fault recovery limits including output power oscillations, and are permissible on recovery, providing they are adequately damped [7]. The highest level of dc-link voltage rise makes CC the least effective for grid code compliancy among the four assessed techniques, with dc-link voltage rise being approximately 29% higher than the DR and 44% higher than the ESS options: SMES and SCES. This is due to the large dc-link voltage rise during the fault. A WECS with DR can meet the grid code stipulations and the resultant power quality is superior to that of CC, however, the recovery might result in overshoot in comparison to SMES and SCES for both symmetrical and asymmetrical faults. This overshoot and prolonged period are the result of the higher permitted operating point, set to avoid spurious operation during dc-link transients that may occur in normal cases. The overshoot of active power (P_g) for the DR is 8% higher than that of CC and 17% higher than that of the ESS techniques, with SMES and the SCES presenting a superior dynamic performance compared to the CC and DR methods. However, they have a marginally slower recovery period of 120 ms seconds in comparison to the DR. All techniques adhere to the 500 ms recovery time stated by the grid codes.

3.6.2 Electrical and Mechanical Stress Reduction

The electrical stresses using CC are the highest among all techniques, due to the highest level of dc-link voltage rise. The level of voltage rise would be at such a level where the electrical components would have exceeded their rated value and in the region where failure/shutdown occurs. In addition to the electrical components on the converter, the excess rotor speed may cause overvoltage on the stator terminals, causing stresses on the stator windings. The DR, SMES and SCES mitigate electrical stresses and keep the components within their permitted values. All techniques, except for CC, inflicted minimal stresses on the PMSG, via permitting uninterrupted power flow from the generator side converter to the dc-link. The CC de-loads the PMSG, which results in a level of torque rejection proportional to the ac network voltage, thereby resulting in rotor acceleration. This rapid de-loading characteristic results in a

100% difference to the torque and 60% of the rotor speed in comparison with DR, SMES and SCES. Although electrical machines have permitted levels of over-speed depending on the rotor construction, this level of over-speed would be considered to impose high levels of mechanical stress to the WECS and may initiate a generator shutdown.

3.6.3 Low Voltage Fault Ride Through Response Speed

The CC response speed is the slowest of the techniques appraised due to the large time constants associated with the PMSG mechanical system and is difficult to improve by increasing the control loop bandwidth of the generator side control system, especially during severe faults. The DR has a fast LVFRT response as soon as it is activated the power is dissipated. To contrast this, the charging of the large SMES coils results in slow dynamics when the fault is severe. The SCES has fast LVFRT response mainly due to the low time constant of supercapacitors which results in a 1 ms settling time to set-point in comparison with the SMES which takes about 80 ms. However, it should be noted that the response speeds are highly dependent on the system sizing.

3.6.4 Control Simplicity

In general, implementing a feedback signal from the ac network voltage reference into the generator side controller torque calculation, the control for the CC, is simple. The DR also has a single PI controller with a reasonable set-point feeding a single IGBT switch. For LVFRT only and neglecting power smoothing functionality, the SMES has three operation modes, which need to be managed, as well as its energy storage (current) management. The same complexities apply to the SCES, where the system must balance the voltage across multiple cells in addition to ensuring charge and pre-charge levels are at an Acceptable level to ensure optimum LVFRT performance. This makes the control systems for SMES and SCES complex.

3.6.5 Hardware Simplicity

CC is software based so effectively has no issues regarding hardware complexity. The DR's hardware scheme is dependent on the type of resistor selected and the cooling system design, which is essential for reliability and the longevity of the system. This

is critical to the WECS. The SMES's complexities are attributed to its cryogenic cooling system, which requires specialist maintenance and highly sensitive components. The SCES is constructed of a high level of low voltage cells consisting of long series and parallel connected strings, which will all degrade at different rates depending on temperature and operating conditions.

3.6.6 System Efficiency

The system with CC can be considered the most efficient due to no additional hardware being involved. The DR by design is inefficient as all the energy captured is dissipated as heat. Theoretically, the SMES is highly efficient due to the low resistance of the superconducting material, however, self-discharging through power circuits and its own management system would affect the overall system efficiency. SMES may suffer from the power circuit internal resistance, and non-trivial levels of self-discharge.

3.6.7 Investment Reduction

The system cost with CC cannot be evaluated on the same scale as the DR, SMES and SCES due to its lack of hardware. The DR is the lowest in cost of all the schemes. Although CC mitigates hardware costs, there may be additional costs from failure or maintenance due to the higher levels of mechanical stresses to the PMSG when compared to the other techniques. The DR, which is widely used in utility scale turbines, is the lowest cost device with SMES being approximately 24 times higher at its widest price range. The SMES costs, albeit the values are academic, are very high. The SCES has a large price scale, indicating an unattractive investment being a range of 12.5% cheaper than the DR to 250% more expensive, depending on the quality and type of supercapacitor selected. However, if the lower scale cost could be practically realised in the future, the SCES would be a candidate for turbine level performance enhancement.

3.7 Assessment Findings

Table 3.5 summarizes the four LVFRT techniques with focus on the main merits and demerits of each to form a direct comparison. The coordinated control (CC) has no hardware requirements, thus is the least expensive. However, uncertainty over the effect of PMSG longevity exists as there is no empirical evidence available to quantify

the effects such stresses may have. This factor poses a risk as may lead to elevated levels of operational expenditure. The electrical stresses CC imposes, chiefly through dc-link voltage rise, could be alleviated by overrating the dc-link capacitor, however this would have physical, financial, and performance-based implications to the system. The DR is a commercially used LVFRT technique and has good performance and can meet grid code expectations. However, the main drawback to this technique is the dissipation of heat and thermal limitations (otherwise, resulting in stresses to the dc-link). In this simulation study, the set-point of 1.2 pu has been used throughout to include a safety margin as to prevent activation of the DR during wind variations which are common in steady state operation. However, in ac networks with lower SCRs, smaller disturbances cause larger voltage variation and might require higher levels of activation. Albeit increasing technology maturity, SMES has the highest cost, largest physical size, and requires specialist maintenance. SCES has the potential to replace the DR due to the presented high flexibility and controllability, however, higher weight and size are still the major challenges. Currently, with all factors taken into consideration, cost and physical limitations are dominating factors of LVFRT technique selection, whist the higher requirement on grid management may inspire the applications of energy storage-based techniques in the future.

Table 3.5. Merits and demerits of LVFRT techniques

Technique	Merits	Demerits
Coordinated control (CC)	Low cost No Hardware requirements	Electrical stresses (dc-link) Mechanical stresses (PMSG)
Dumping resistor (DR)	Low complexity Good Performance Low mechanical stress	Heat management Real power overshoots on fault recovery
Superconductive magnetic energy storage (SMES)	Good performance	Specialist maintenance requirements High cost Complex hardware requirements Physical weight and dimensions
Supercapacitor energy storage systems (SCES)	Superior performance Acceptable weight and size	High self-discharge Complex hardware requirements

3.8 Summary

In this chapter, four low voltage fault ride through (LVFRT) techniques were presented and investigated. These techniques were coordinated control (CC), dumping resistor (DR), superconductive magnetic energy storage (SMES), and supercapacitor energy storage systems (SCES). Each was presented and investigated with the aim of enhancing the performance of wind energy conversion systems (WECS), particularly during contingency periods. Even though, the CC, removes any hardware requirements it is the least effective, and not deemed suitable for LVFRT due to grid code compliance issues and the high level of dc-link voltage during faults, in turn imposing stresses to the electro-mechanical systems. The industrial standard DR was proved to be an effective method of LVFRT; however, concerns arise with the dependence on cooling and overheating due to spurious operation from poorly defined operating set-points could result in a system failure. Such a risk could be reduced by energy storage system (ESS) based methods, which have improved heat management ability and fault energy controllability. Although the simulation results show good LVFRT performance, the high levels of practical complexity and capital costs make SMES currently relatively unrealistic for integration at the wind turbine level. From a simulation perspective, the SCES can offer desirable performance and attractive benefits with flexible use of stored energy cells. Although the practical complexities are lower than SMES, SCES is still commercially immature for such turbine level applications, which is reflected in the capital costs and practical engineering challenges for integration at wind turbine level. Nevertheless, energy storage systems might be suitable for secure renewable system construction. For the remainder of this thesis the DR has been selected as the preferred method for protecting the WECS during periods of energy imbalance.

References

[1] Siegfried Heier, *Grid Integration of Wind Energy Conversion Systems*. John Wiley & Sons Ltd, 1998, ISBN 0-471-97143-X. doi: 10.1109/63.704150.

[2] M. I. Mosaad, "Model reference adaptive control of STATCOM for grid integration of wind energy systems," *IET Electr Power Appl*, vol. 12, no. 5, pp. 605–613, 2018, doi: 10.1049/iet-epa.2017.0662.

[3] S. Mishra, S. Shukla, N. Verma, and R. Ritu, "Comprehensive review on Maximum Power Point Tracking techniques: Wind Energy," *International Conference Communication, Control and Intelligent Systems, CCIS 2015*, pp. 464–469, 2016, doi: 10.1109/CCIntelS.2015.7437961.

[4] B. Wu, Y. Lang, N. Zargari, and S. Kouro, "Variable-Speed Wind Energy Systems with Synchronous Generators," *Power Conversion and Control of Wind Energy Systems*, pp. 275–316, 2011, doi: 10.1002/9781118029008.ch9.

[5] S. Li, T. A. Haskew, R. P. Swatloski, and W. Gathings, "Optimal and direct-current vector control of direct-driven PMSG wind turbines," *IEEE Trans Power Electron*, vol. 27, no. 5, pp. 2325–2337, May 2012, doi: 10.1109/TPEL.2011.2174254.

[6] A. Egea-Alvarez, S. Fekriasl, F. Hassan, and O. Gomis-Bellmunt, "Advanced vector control for voltage source converters connected to weak grids," *IEEE Transactions on Power Systems*, vol. 30, no. 6, pp. 3072–3081, Nov. 2015, doi: 10.1109/TPWRS.2014.2384596.

[7] B. Wu, Y. Lang, N. Zargari, and S. Kouro, "Power converters in wind energy conversion systems," *Power Conversion and Control of Wind Energy Systems*, pp. 87–152, 2011, doi: 10.1002/9781118029008.ch4.

[8] J. F. C. and R. F. C. Watson, R., and Watson, J.F. Conroy and R., "Low-voltage ride-through of a full converter wind turbine with permanent magnet generator," *IET Renewable Power Generation*, vol. 3, no. 1, pp. 182–189, 2007, doi: 10.1049/iet-rpg.

[9] B. Wu and M. Narimani, "High-Power Converters and AC Drives: Second Edition," *High-Power Converters and AC Drives: Second Edition*, pp. 1–451, 2016, doi: 10.1002/9781119156079.

[10] E. Hamatwi, I. E. Davidson, M. N. Gitau, and G. P. Adam, "Modeling and control of voltage source converters for grid integration of a wind turbine system," *IEEE PES PowerAfrica Conference, PowerAfrica 2016*, pp. 98–106, 2016, doi: 10.1109/PowerAfrica.2016.7556579.

[11] P. Rodríguez, J. Pou, J. Bergas, J. I. Candela, R. P. Burgos, and D. Boroyevich, "Decoupled double synchronous reference frame PLL for power converters control," *IEEE Trans Power Electron*, vol. 22, no. 3, p. 1078, 2007, doi: 10.1109/TPEL.2007.894351.

[12] National Grid Electricity System Operator Limited, "The Grid code | National Grid," no. 5, pp. 1–998, 2019.

[13] European Network of Transmission System Operators for Electricity (ENTSO-E), "Requirements for grid connection applicable to all generators," *ENTSOE Standards*, no. October, p. 86, 2013.

[14] IEEE Standard Association, *IEEE Std. 1547-2018. Standard for Interconnection and Interoperability of Distributed Energy Resources with Associated Electric Power Systems Interfaces*. 2018. doi: 10.1109/IEEESTD.2018.8332112.

[15] D. B. W. Abeywardana, B. Hredzak, V. G. Agelidis, and G. D. Demetriades, "Supercapacitor sizing method for energy-controlled filter-based hybrid energy storage systems," *IEEE Trans Power Electron*, vol. 32, no. 2, pp. 1626–1637, 2017, doi: 10.1109/TPEL.2016.2552198.

[16] C. Wu, S. Gao, Y. Liu, H. Han, and S. Jiang, "Wind power smoothing with energy storage system: A stochastic model predictive control approach," *IEEE Access*, vol. 9, pp. 37534–37541, 2021, doi: 10.1109/ACCESS.2021.3063740.

[17] C. Abbey and G. Joos, "Supercapacitor energy storage for wind energy applications," *IEEE Trans Ind Appl*, vol. 43, no. 3, pp. 769–776, 2007, doi: 10.1109/TIA.2007.895768.

[18] R. Basak, G. Bhuvaneswari, and R. R. Pillai, "Low-Voltage Ride-Through of a Synchronous Generator-Based Variable Speed Grid-Interfaced Wind Energy Conversion System," in *IEEE Transactions on Industry Applications*, Institute of Electrical and Electronics Engineers Inc., Jan. 2020, pp. 752–762. doi: 10.1109/TIA.2019.2946125.

[19] G. P. Adam, K. H. Ahmed, S. J. Finney, and B. W. Williams, "AC fault ride-through capability of a VSC-HVDC transmission systems," *2010 IEEE Energy Conversion Congress and Exposition, ECCE 2010 - Proceedings*, pp. 3739–3745, 2010, doi: 10.1109/ECCE.2010.5617786.

[20] H. S. Salama and I. Vokony, “Voltage and Frequency Control of Balanced / Unbalanced Distribution System Using the SMES System in the Presence of Wind Energy,” pp. 205–224, 2021.
[21] S. Sabihuddin, A. E. Kiprakis, and M. Mueller, “A numerical and graphical review of energy storage technologies,” *Energies (Basel)*, vol. 8, no. 1, pp. 172–216, 2015, doi: 10.3390/en8010172.
[22] C. Huang, X. Y. Xiao, Z. Zheng, and Y. Wang, “Cooperative Control of SFCL and SMES for Protecting PMSG-Based WTGs under Grid Faults,” *IEEE Transactions on Applied Superconductivity*, vol. 29, no. 2, Mar. 2019, doi: 10.1109/TASC.2019.2891908.
[23] C. K. Das, O. Bass, G. Kothapalli, T. S. Mahmoud, and D. Habibi, “Overview of energy storage systems in distribution networks: Placement, sizing, operation, and power quality,” *Renewable and Sustainable Energy Reviews*, vol. 91, no. November 2016, pp. 1205–1230, 2018, doi: 10.1016/j.rser.2018.03.068.
[24] H. A. Behabtu *et al.*, “A review of energy storage technologies’ application potentials in renewable energy sources grid integration,” *Sustainability (Switzerland)*, vol. 12, no. 24, pp. 1–20, 2020, doi: 10.3390/su122410511.
[25] S. Wang, A. M. Massoud, and B. W. Williams, “A t-type modular multilevel converter,” *IEEE J Emerg Sel Top Power Electron*, vol. 9, no. 1, pp. 843–857, 2021, doi: 10.1109/JESTPE.2019.2953007.
[26] O. P. Mahela, N. Gupta, M. Khosravy, and N. Patel, “Comprehensive overview of low voltage ride through methods of grid integrated wind generator,” *IEEE Access*, vol. 7, pp. 99299–99326, 2019, doi: 10.1109/ACCESS.2019.2930413.
[27] Q. Xie, Z. Zheng, C. Huang, and T. Dai, “Coordinated Fault Ride Through Method for PMSG-Based Wind Turbine Using SFCL and Modified Control Strategy,” *IEEE Transactions on Applied Superconductivity*, vol. 31, no. 8, pp. 1–5, Aug. 2021, doi: 10.1109/tasc.2021.3103730.
[28] E. Sathya and P. Maruthupandi, “Enhancement of Low Voltage Ride Through Capability for PMSG Based Wind Energy Conversion System with Super Capacitor,” *Proceedings of the 4th International Conference on Electrical Energy Systems, ICEES 2018*, pp. 57–60, 2018, doi: 10.1109/ICEES.2018.8443259.
[29] S. P. E. E. & Components, “Braking Chopper CHT,” 2021.
[30] Newark, “WDBR5-150RKT Through Hole Thick Film Resistor.” https://www.newark.com/tt-electronics-welwyn/wdbr5-150rkt/through-hole-thick-film-resistor/dp/71P4644?ost=wdbr5-150rkt (accessed Jul. 13, 2021).
[31] Digi-key, “TE Connectivity Passive Product TE2500B100RJ.” https://www.digikey.co.uk/product-detail/en/te-connectivity-passive-product/TE2500B100RJ/A121354-ND/2367863 (accessed Jul. 29, 2021).
[32] Newark, “FZ1600R17HP4B2BOSA2 IGBT MODULE, 1.7KV, 1.6KA, 10.5KW.” https://www.newark.com/infineon/fz1600r17hp4b2bosa2/igbt-module-1-7kv-1-6ka-10-5kw/dp/38AJ3608?ost=fz1600r17hp4_b2&autoc=fz1600r17hp4b2 (accessed Jul. 12, 2021).
[33] M. Technologies, “2.7v 100f ultracapacitor cell,” pp. 6–7.
[34] Newark, “XLM-62R1137A-R Supercapacitor, Module, 130 F, 62.1 V, Threaded Stud, XLM Series, +20%, -0%.” https://www.newark.com/eaton-bussmann/xlm-62r1137a-r/supercapacitor-130f-62-1v/dp/84AC4632?st=super+capacitors (accessed Jul. 13, 2021).
[35] B. S. Transformer, “Chassis Mount CH / CL Series Single, Filter Chokes Windings, Dual,” pp. 0–3, 2021.

Chapter 4

A Fault Resilient Series-Connected Offshore Wind Farm

The series-connected offshore wind farm (SC-OWF) is a promising offshore wind generation solution to mitigate the need of centralized offshore high-voltage/power converter stations. Predominantly, other researchers have focused on the steady-state operation and control of SC-OWFs, without considering the system-level characteristics and ability to ride-through dc side and ac network faults. This chapter proposes an enhanced system for SC-OWF applications with fault-resilient capability, where comprehensive circuit configuration and protection strategies are articulated to minimize the negative effects caused by various types of dc and ac faults. For the offshore system architecture, a grouping scheme is adopted where a disconnector and diode-based substation is proposed to realize prompt fault bypass/isolation and protection functions in the event of offshore collector faults. Additionally, an onshore fault-tolerant modular multilevel converter (MMC) with modified dc-system-oriented control is employed to enable smooth and secure operation under steady-state and fault conditions. The proposed SC-OWF system is quantitatively substantiated by time-domain simulations where four ac/dc fault cases are considered, and the results consolidate the feasibility of the proposed configuration and control, indicating fault resilience of the SC-OWF system. Additionally, size, weight and cost estimations of the proposed offshore substation is presented and compared to a conventional MMC offshore station, to further highlight the merits of the presented solution.

4.1 Series-Connected Offshore Wind Farm Architecture and control

The proposed SC-OWF system architecture is presented in Fig. 4.1. The offshore SC-OWF units are configured into N groups whereas each group consists of U individual units. A total of $N \times U$ WECSs are therefore connected through HVDC cables to an onshore converter station (for example, the hybrid MMC as illustrated) that transfer power into the ac grid. The offshore wind farm configuration can improve system fault resiliency, whilst the onshore station ensures well-regulated operation in both normal

and fault cases. Each of the following subsections details the major elements of the proposed system in terms of configuration and control.

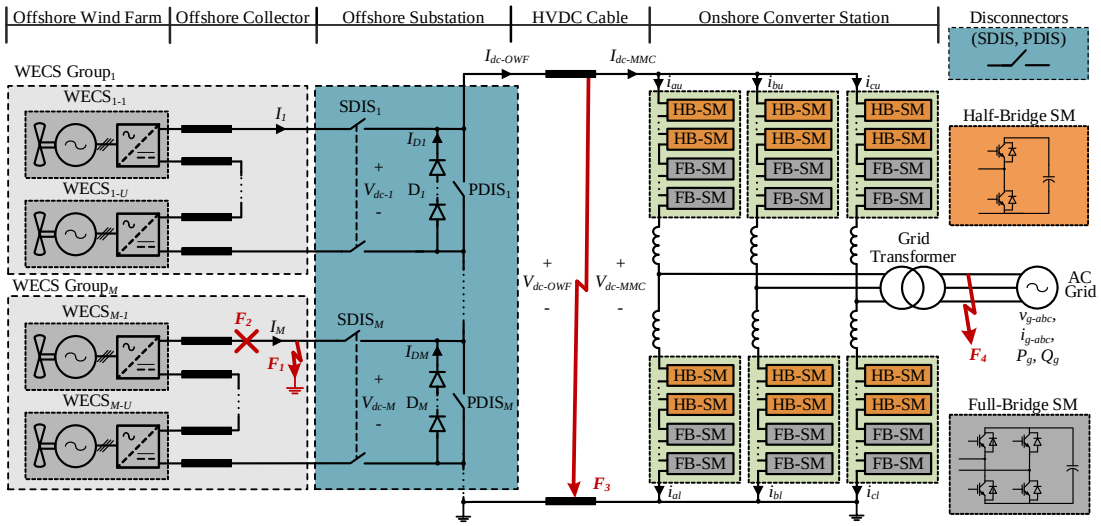

Fig. 4.1. Architecture of the proposed SC-OWF system.

4.1.1 Wind Energy Conversion System

In general, the applicable WECS configurations and topologies vary, whereas the conversion stages and technologies aligning with those in [1] are adopted herein, as presented in Fig. 4.2. Dimensions of permanent magnet synchronous generators (PMSGs) can vary with the overall SC-OWF setup, where both low and medium voltage variants are applicable [2]–[5]. The PMSG side ac/dc conversion stage employs IGBT switches, thereby being advantageous in terms of controllability and ripple propagation [6]. The active energy dissipation device, assumed to be a DR, is employed within dc bus protection stage, as per [7]. The galvanic isolation of the WECS is of significant importance and can be achieved by an air core MFT with the aim of reducing mass and losses while operating at medium frequencies [5]. The high transformation ratio of the proposed dc/dc conversion stage has been proposed in [8] and will be applied herein. Fig. 4.2 presents the dc/dc converter as an aggregated system for simplicity, where a practical system may form a modular topology presented in [4] and articulated by one or more IGBT active bridges driving one or more MFTs with a rectification stage. Compared with controlled output rectifier stages in [3], [9], [10], the diode rectification stage proposed features relatively low capital costs and operational losses, and simple converter design, which is especially beneficial for such applications requiring galvanic isolation and high-voltage ratings.

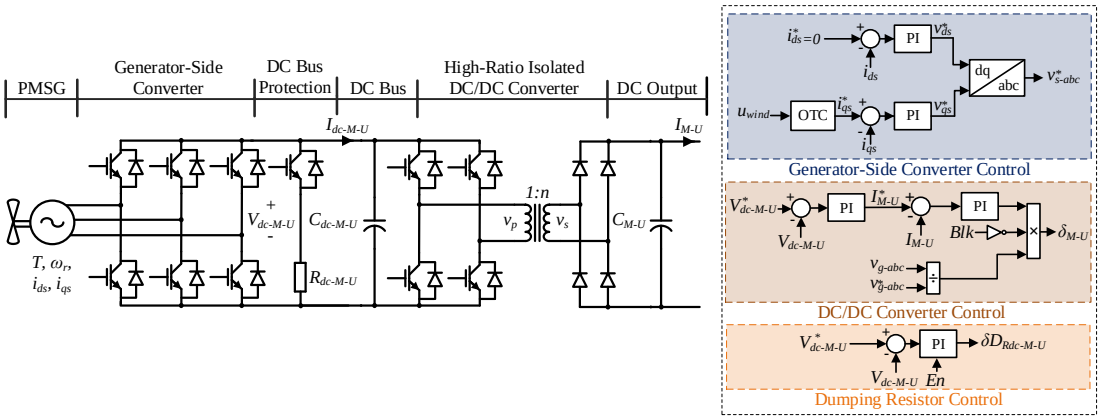

Fig. 4.2. Schematic diagram and control structure of WECS.

Considering a generic WECS (like the U^{th} of the M^{th} group), the generator-side control ensures wind power injection into the dc bus based on wind speed based on the control system described in Chapter 3.1.

The dual-loop dc/dc converter control regulates the dc-bus voltage ($V_{dc\text{-}M\text{-}U}$), therefore the WECS output dc voltage $V_{M\text{-}U}$ varies depending on the available wind power, affecting the total offshore string output voltage (assuming a controlled and constant dc-link current) [4]. The control structure akin to [1], inner-loop output controller is expressed by (4.1) with the PI controller represented by $K_{pi\_\delta}(s)$, the duty cycle by $\delta_{M\text{-}U}$ and output current by $I_{M\text{-}U.}$ The outer-loop controller regulates the dc-link voltage ($V_{dc\text{-}M\text{-}U}$) and expressed by (4.2), with the PI controller represented by $K_{pi\_i}(s)$.

$$\delta^*_{M-U} = K_{pi\_\delta}(s)(I^*_{M-U} - I_{M-U}) \tag{4.1}$$

$$I^*_{M-U} = K_{pi\_I}(s)(V^*_{dc-M-U} - V_{dc-M-U}) \tag{4.2}$$

Importantly, inter-WECS voltage balancing is not challenging in such a system with single string offshore WECSs, controlled dc-link current and the maximum WECS output voltage would be the rated [11]. A blocking signal *Blk* (equal to 1 in steady state) will be used in fault cases, *Blk* = 0 is applied to block power transfer with the diode rectification bridge entering in a freewheeling state. During contingency periods, the DR devices will maintain dc bus voltage ($V_{dc\text{-}M\text{-}U}$) within limits, thereby mitigating PMSG electromechanical stresses. The control structure of the DR is shown in Fig. 4.2, where the PI controller ($K_{pi\_dr}(s)$) is enabled during contingency periods via the *En* port. Furthermore, the control setpoint is configured to be marginally higher than the dc-bus rated voltage so that during contingencies the additional energy can be

consumed without interfering with steady-state operation. The control structure is represented by (4.3).

$$\delta D^{*}_{Rdc-M-U} = K_{pi\_dr}(s)(V^{*}_{dc-M-U} - V_{dc-M-U}) \tag{4.3}$$

To allow for prompt de-loading (balancing) during the onshore ac grid faults, a coordination mechanism via high-speed communications is included between the offshore WECS and the onshore integrated grid, as shown in Fig. 4.2. In steady-state operation, the grid voltage is at approximately nominal value ($V_{g\text{-}abc}$ = 1 pu); therefore, there is no reliance on the communication mechanism during normal operation. When a grid fault occurs, the dc/dc converter duty cycle ($\delta D_{M\text{-}U}$) can be altered based on the onshore grid voltage ($V_{g\text{-}abc}$), which allows reduction of the WECS's generation contribution to the HVDC-link, thereby effectively maintaining system power balance. In extreme cases, (e.g., simultaneous communication failure and onshore grid fault), the WECS DR and MMC local protection (as per [12]) can still ensure the system are maintained within tolerable limits. Such manipulation of WECS energy contribution can be used for more advanced system management such as frequency containment reserve depending on system operators.

4.1.2 Wind Energy Conversion System Grouping Configuration and Offshore Substation

In the proposed system, each of the WECS groups is interfaced into the HVDC system (e.g., group *M*) via a two-pole series disconnector ($SDIS_M$), a parallel disconnector ($PDIS_M$) and diode unit(s) (D_M), as shown in Fig. 4.1 (relevant auxiliary protective components such as surge arresters are omitted for simplicity). Conventional SC-OWFs have no external current path apart from the series-connected wind turbines, where a single wind farm fault will be cascading system wide and affects overall power export. Also, to isolate the fault, the entire system must be isolated. In contrast, the proposed WECS grouping arrangement employs a separate offshore substation to provide external current paths (in parallel with the wind turbines). The additional offshore substation introduces greater flexibility and enables circuit manipulation during SC-OWF faults. The selection of numbers of groups and WECSs within the group involves many factors such as device manufacturing capacity, cable failure probability, design complexity, cost, engineering factors, etc. In terms of functionality,

the SDIS is used to isolate the WECS group, where the PDIS ensures bypass of the group for long-term periods (e.g., fault isolation or normal maintenance). The substation can be a common bus array with reasonable isolation and insulation margins, thereby minimizing susceptibility of internal faults. The grouping method allows the diode strings and PDISs to be rated to the group nominal voltage; whereas the voltage ratings of the SDISs can vary depending on the group position within the string (lower the position, lower the rating), leading to a positive effect on the choice of component ratings and space requirements practically [28]. This design eliminates the requirement for complex and costly dc circuit breakers (DCCB), with detailed operation during offshore system faults given in section 4.2.

4.1.3 Onshore Converter Station

The onshore converter station can be implemented by MMCs with the dc fault ride-through (zero dc-side voltage operation) capability [13], such as topologies equipped with sufficient full-bridge submodules (FB-SMs) as shown in Fig. 4.1 [14], [15].

The MMC control system is critical to maintain system security within tolerable limits during steady-state operation and faults, whereas the proposed MMC control is shown in Fig. 4.3. In this research, the grid-connected control system is designed and operated based on grid-following strategy through the implementation of a phase locked loop (PLL) generating a grid angle reference (θ_g) [16], and applied and tuned as per methods described in Chapter 3.2. Given that the onshore MMC station is a voltage source converter type, it can be anticipated that potential grid-forming control schemes are also applicable. The MMC ac side *d-q* current control references are regulated by average capacitor voltage controller and grid voltage (or reactive power) controller respectively, analogous to [17] and outer loop controllers can be expressed by (4.4) and (4.5) for the *dq*-axis current references respectively. The converter average capacitor voltage ($V_{c\text{-}ave}$) controller is represented by $K_{pi\_Vc}(s)$ and ac grid voltage (V_g) controller by $K_{pi\_Vg}(s)$.

$$i_d^* = K_{pi\_vc}(s)(V_{c-ave}^* - V_{c-ave}) \tag{4.4}$$

$$i_q^* = K_{pi\_Vg}(s)(V_{g-abc}^* - V_{g-abc}) \tag{4.5}$$

The dc-link current control is achieved by regulating MMC common mode current

($I_{cm\text{-}MMC}$); the reference can be optimized for low power operation in low wind or contingent cases, which allows the dc-link voltage regulation down to zero [11]. To maintain the balance of capacitor voltages within the MMC, correction signals for inter-phase and inter-arm capacitor balancing are implemented and controlled using PI controllers as detailed and tuned as per [18]. Outputs of dc current, inter-phase voltage and inter-arm voltage controllers are fed into the proportional-integral-resonant (PIR) controller [18]. The PIR controller implemented (K_{pir_ci}) can be expressed by (4.6) with K_{r_ci} and ω_{ci} representing the resonant gain and angular velocity with the frequency tuned to 2 times the nominal system frequency ($2\omega_n$) [19]. The tuning method adopted were based on [19].

$$K_{pir\_ci}(s) = K_{p\_ci} + \frac{2K_{r\_ci}\omega_{ci}s}{s^2 + 2\omega_{ci}s + \omega_n^2} \tag{4.6}$$

Importantly, to effectively maintain onshore and offshore power balance in both steady-state and abnormal cases, a dc offset modifier (DOM) is adopted, shown in Fig. 4.3. The MMC dc-terminal voltage can be promptly adjusted with the offshore dc voltage ($V_{dc\text{-}OWF}$) through high-speed communications (a minor delay in ms level is tolerated for both sides). Unlike other proposals utilising current control methods [4], [20], the DOM inherently responds to wind variations, adjusting the MMC port voltage, while maintaining rated dc-link current without energy curtailment. Importantly, the DOM can also Accept a local dc-terminal voltage measurement ($V_{dc\text{-}MMC}$), acting as suitable system redundancy for the scheme in the event of potential communication failures. Therefore, a universal linear control scheme can be realised in normal and fault scenarios without switching between different control modes.

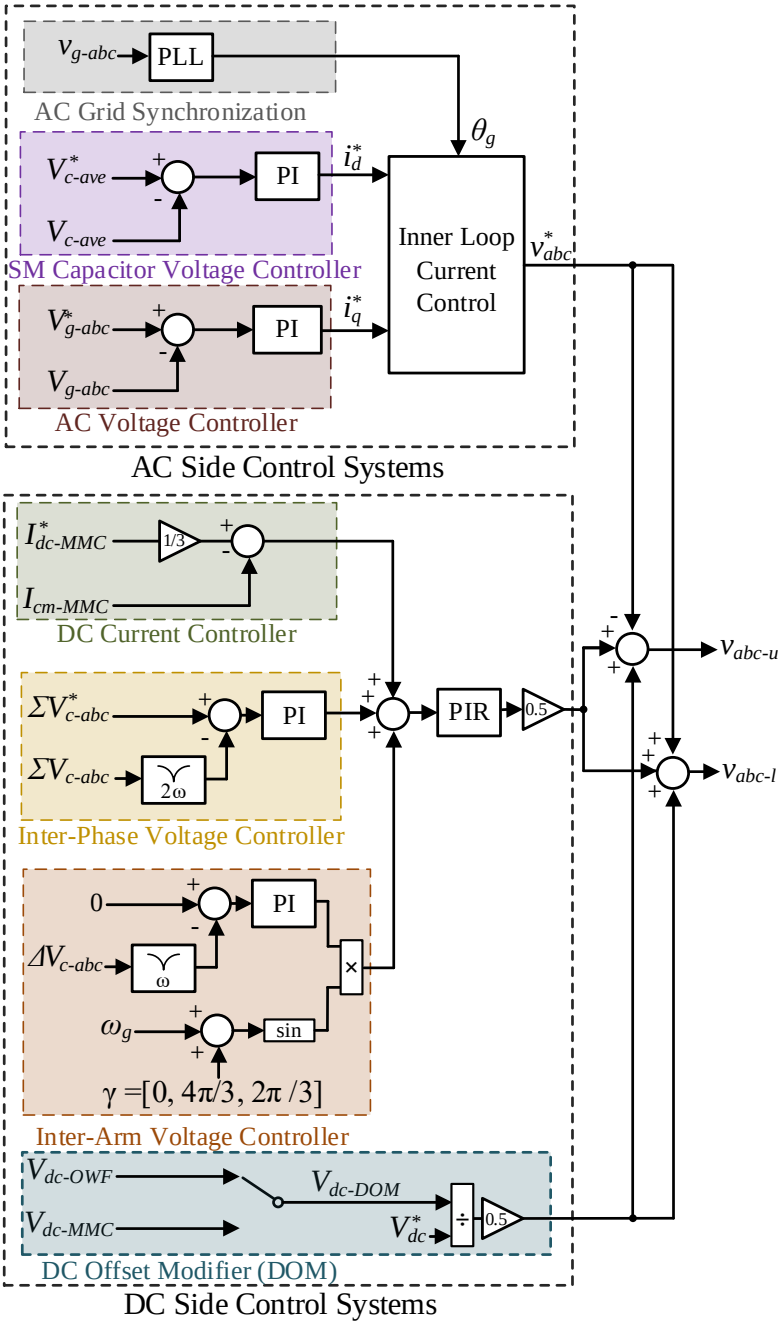

Fig. 4.3. Control structure of the onshore MMC station.

4.2 Series Connected Offshore Wind Farm Fault-Ride Through Strategy

System fault management and power transfer reliability are critical of the SC-OWF systems. This section articulates operational behaviour and fault ride-through strategies of the proposed SC-OWF system considering four fault types, which are highlighted in Fig. 4.1, as follows:

- *F_1: Offshore Collector Cable Short Circuit Fault*
- *F_2: Offshore Collector Cable Open Circuit Fault*
- *F_3: HVDC Cable Short Circuit Fault*
- *F_4: AC Grid Fault*

The studied faults comprehensively represent typical cases that occur within the SC-OWF system, with common causes attributed to insulation degradation (short circuit), external aggressors (open and short circuit) and mechanical fatigue at termination points (open circuit) [21]. The system is represented by average voltage source blocks for the simplicity.

4.2.1 System Coordination and Dependencies

Fig.4.4 represents a high-level block diagram of the system showing the interdependencies and measurements required for the coordinated control system and used as part of the Fault-ride through strategy.

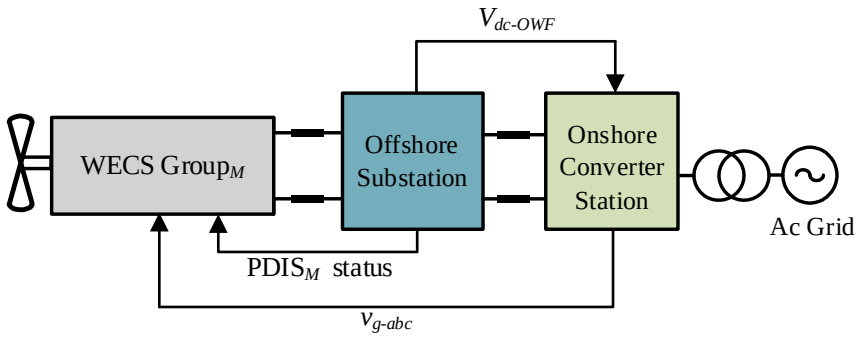

Fig. 4.4. Block diagram of SC-OWF showing interdependencies and coordination.

To precisely and promptly de-load the individual WECS contained within generic Group *M*, on the occurrence of an ac network fault, resulting in a voltage depression, a grid voltage ($v_{g\text{-}abc}$) reference signal is required. The signal issued via

communications link from the onshore converter station, is distributed to each of the WECS for precise de-loading corresponding to the grid voltage.

A reference dc voltage ($V_{dc\text{-}OWF}$) signal between the offshore substation and onshore converter station provides. This allows the prompt adjustment of the onshore converter stations dc port voltage ensure balancing of the system. In the event of a communications link failure a local voltage reference can be utilised.

A PDIS and SDIS status signal is issued between the relevant group to provide open / closed status of the disconnector switches and the signal distributed to each of the WECS connected within the group to minimise the occurrence of the WECS feeding into an open / short circuit. In the event of a communications failure the local WECS protection system will activate and prevent system failure.

4.2.2 Offshore Collector Cable Short Circuit Fault

Conventionally, SC-OWFs are inherently susceptible to offshore side faults with cascading effects. A cable to ground short circuit fault at the offshore collector affects the power transfer of all WECSs units connected within the string, potentially leading to a system shutdown and lasting for prolonged durations. Such revenue losses can be significantly minimised by employing the proposed system with WECS units, grouping philosophy and offshore substation.

Assuming the F_1 fault occurs at the first WECS unit of the group *M*, Fig. 4.5 shows an equivalent representation of an SC-OWF section configured into groups *M* and *N*, each containing *U* WECSs. In steady-state operation, as shown in Fig. 4.5(a), the section output voltage is determined by the voltage sum of groups *M* and *N* ($V_M + V_N$) and string current $I_{dc\text{-}OWF}$ is regulated by onshore MMC. Fig. 4.5(b) depicts the section behaviour when a grounding fault (with impedance of Z_{f1}) occurs to the upper side collector of group *M*, this cascades to both groups through the fault conduction path to earth. After the fault occurs, both WECS groups can effectively stop power contribution with their output voltage regulated to zero (the blocking signal $Blk = 1$ is issued, with surplus power from the generators consumed by WECS local DRs). With groups *M* and *N* ceasing their power contribution, fault currents decay within the duration which is mainly dependent on the total damping resistance in the fault loop. Furthermore, the dc current is transferred from the WECS units to the diode units D_M

and D_N situated at the offshore substation, as per the circuit shown in Fig. 4.5(c). Simultaneously, power balancing between the onshore and offshore sides is maintained mainly by the DOM mechanism of the onshore MMC, where MMC dc-terminal voltage $V_{dc\text{-}MMC}$ and ac power P_g are reduced based on the available SC-OWF group capacity.

With the current flow through $SDIS_M$ reduced to an acceptable level, $SDIS_M$ can be opened to eliminate residual current and achieve fault isolation; meanwhile, SC-OWF current flows through D_M. Blocking signals of group *N* WECSs can be cleared (*Blk* = 0), allowing output voltage restoration and power transfer recovery. In addition, $PDIS_M$ can be closed to achieve long-term isolation of the fault from the system. Fig. 4.5(d) shows the SC-OWF section with group *M* isolated, and the system retains operation with group *N*. Additionally, the onshore MMC dc voltage should be decreased correspondingly to allow reduced power transfer, whilst dc-link current can be maintained. This configuration eliminates the requirement for DCCBs and allows WECS units connected below group *M* in the string to retain long-term operation, thereby greatly improving system resiliency. The generation degradation level mainly related to grouping configuration/numbers.

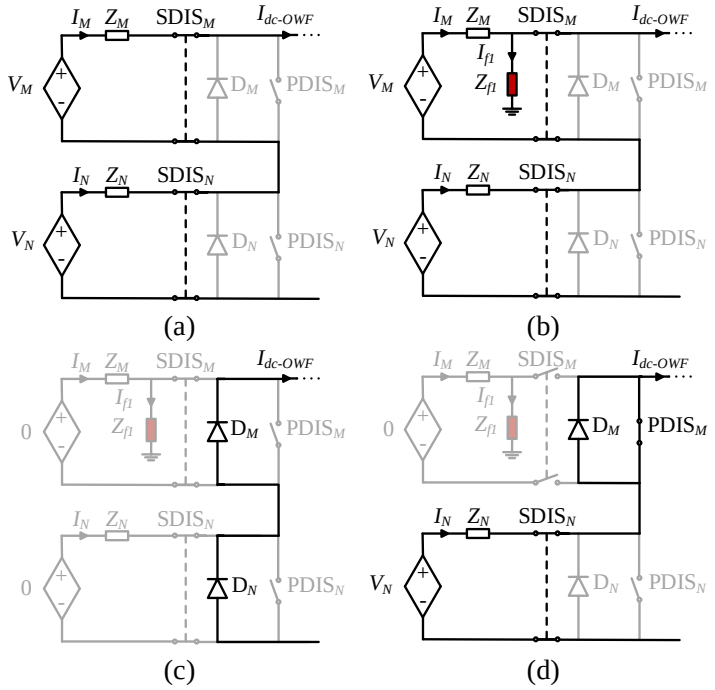

Fig. 4.5. Equivalent circuits of SC-OWF section in F_1 fault case. (a) Steady-State operation. (b) Fault occurrence at group *M*. (c) Fault condition with ceased power transfer of groups *M* and *N*. (d) Bypass and isolation of the faulty group *M* (separate).

4.2.3 Collector Cable Open Circuit Fault

Open circuit faults result in a full power transmission loss, potentially for prolonged durations, which poses a serious reliability concern for conventional SC-OWFs. By applying the proposed offshore substation equipped with diode-based bypassing capability, offshore collector open circuit faults can be promptly managed, allowing power production to continue.

Fig. 4.6(a) shows the steady-state configuration of the SC-OWF represented by two groups *M* and *N*. At the occurrence of the fault, WECSs contained in group *M* will cease power transfer and extra energy will be consumed by its DR. Simultaneously, D_M becomes forward-biased and conducts dc-link current. As the transmitted power is reduced, the onshore MMC, via DOM, can be manipulated to reduce $V_{dc\text{-}MMC}$ in an effective manner, with dc-link current control maintained at the operational setpoint.

As no current presents in group *M*, $SDIS_M$ can be opened to isolate the fault from the network; $PDIS_M$ can be closed to ensure a safe bypass path and gain lower losses. Fig. 4.6(b) shows the network condition where the normal dc-link current can flow through D_M (predominantly $PDIS_M$, if closed) allowing the smooth operation of group *N*. By implementing the offshore substation configuration with the coordinated control, system resiliency is enhanced against the collector open circuit faults.

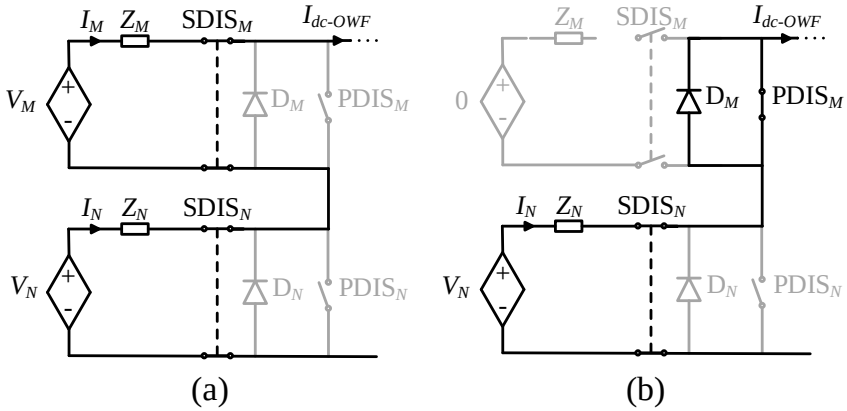

Fig. 4.6. Equivalent circuit of SC-OWF section in F_2 fault case. (a) Steady-State operation (b) Bypass and isolation of the faulty group *M*.

4.2.4 HVDC Cable Short Circuit Fault

The SC-OWF system is required to safely ride-through HVDC cable faults, which pose high risk to device safety and power transmission similar to other HVDC systems. As shown in Fig. 4.1, at the occurrence of a dc-link fault, the system is split into two major circuitry loops (by the short circuit point). The WECSs are blocked (Blk = 1) to cease power transfer (with surplus power generation dissipated by DRs). Current within the offshore loop will begin to decay at a rate corresponding to the total loop damping resistance. Meanwhile, onshore the MMC fault blocking capability is activated, to effectively reduce MMC dc terminal voltage, maintain sub module (SM) capacitor voltage, and regulate $I_{dc\text{-}MMC}$ to zero (export power Pg is stopped). In addition, the MMC can still deliver reactive power, if required, operating in static compensation mode.

4.2.5 AC Grid Fault

Generally, grid code regulations specify the fault severity and duration to which wind farm systems are expected to remain connected to the ac network to ensure system security and stability. The key challenge of the SC-OWF is to address power transfer coordination between onshore and offshore units herein as the ac power transfer is limited/eliminated.

By employing an ac voltage signal to the offshore WECSs, overall system power management is achieved in a coordinated manner, even extending to ac grid disturbances. After a short communication period in ms, the WECSs output is reduced proportionally with the grid voltage magnitude, with surplus WECS energy consumed by DRs. The MMC dc-terminal voltage is adjusted in a dynamic way through DOM mechanism, inherently responding to the offshore voltage reduction, with the dc-link current maintained.

4.3 Case Study Based Verification

This section details study cases and results based on MATLAB/Simulink simulation of the proposed SC-OWF system, as illustrated in Fig. 4.7. In addition, a comparison of estimated volume, mass and cost between an offshore HVDC-MMC station and the proposed offshore substation is presented.

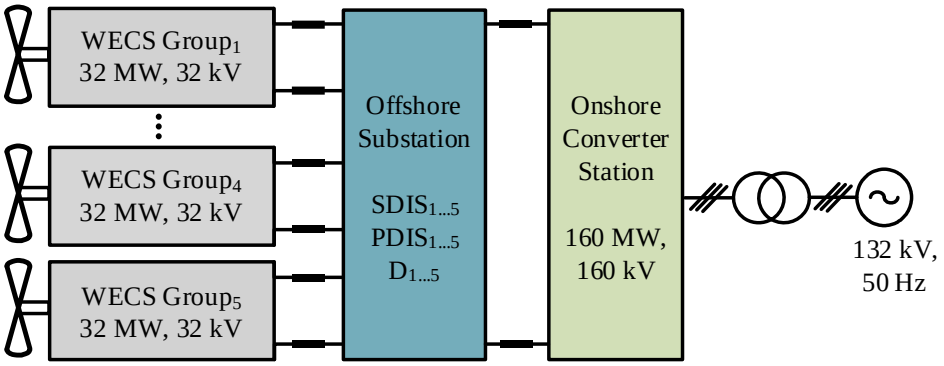

Fig. 4.7. Schematic diagram of simulated SC-OWF system.

Table 4.1 lists key system parameters utilised for system modelling, where the system architecture and control are configured as presented in section 4.1. In this case study, low-voltage (0.69 kV) PMSGs are adopted, which align with commercial products [32] – [34]. The wind turbine properties are assumed to be extrapolated from [35]. The cable distance between two adjacent wind turbines within one group is assumed to be 7D, while detailed sub-siting/sub-string arrangements are not considered herein [36]. Also, a multi-section π-model is used to represent dc cables in the simulation, which aligns with [19], [37]. The four types of faults (detailed in Section 3.2) are applied with 1 ms fault detection duration and communication delay between onshore and offshore sides is applied for all cases. All studied faults are assumed to be temporary from 0.3 s to 0.5 s to include system recovery performance. The onshore station operates with 1 pu active power injection at unity power factor. PI gains have been applied though parameter estimation and iterative trialling of parameters.

Table 4.1. System parameters for SC-OWF case studies.

Items		Values
Offshore WECSs	Wind turbine rotor diameter (D)	167 m
	Rated power per WECS unit	8 MW
	PMSG rated (rms) voltage	0.69 kV
	WECS dc bus rated voltage	1.2 kV
	WECS dc bus capacitance	110 mF
	WECS IGBT switching frequency	1 kHz
	WECS dc output rated voltage	8 kV
	WECS dc output capacitance	2.5 mF
	SC-OWF WECS group No. (N)	5
	WECS units No. per group (U)	4
	Total WECS No. ($N \times U$)	20
Offshore Substation	Total No. diodes (D2601NH90T)	40
	Total No. of SDISs	10
	Total No. of PDISs	5
Offshore Collectors & Cables	Distance between two near WECSs	1.2 km
	Total cables No. per group	5
	Total cable length per group	6 km
	HVDC cable length	40 km
	Cable resistance	35 mΩ/km
	Cable inductance	1 mH/km
	Cable capacitance	0.172 μF/km
Onshore Converter Station	Rated power capacity	160 MVA
	Rated dc voltage	160 kV
	Total MMC SM No. per arm	80
	MMC HB-SM No. per arm	40
	MMC FB-SM No. per arm	40
	MMC SM capacitance	8 mF
	MMC SM rated voltage	2 kV
	MMC arm inductance	28.6 mH
AC Grid	Interfacing transformer ratio	1:1.47
	Interfacing transformer leakage	0.2 pu
	Frequency	50 Hz
	Rated (rms) voltage	132

4.3.1 Collector Cable Short Circuit Fault Case

A short circuit fault (F_1) is applied at the uppermost collector cable of group 4 with groups 1 to 3 above and group 5 below in the string (both of which are normal/healthy). Simulation results of this case are presented in Fig. 4.7, with the 1 Ω impedance fault applied between 0.3 s and cleared at 0.5 s.

With the occurrence of F_1, the SC-OWF cascading nature leads to initial voltage collapses of groups 4 and 5 (V_4 and V_5), with groups 1 to 3 voltages ($V_{1\text{-}3}$) remaining at the pre-fault output (32 kV per group), as shown in Fig. 4.8(a), where the overvoltage surges can be absorbed by protective devices practically. Simultaneously, the output current of group 4 (I_4), and currents of WECS group 5 and its substation diode unit (I_5 and I_{D5}) rise in different dynamics due to the fault current flow and different cable impedances, as shown in Fig. 4.8(c) to approximately 6 kA, this value will dictate the design rating of the output diodes of the dc-dc converter and may require multiple units. Shortly after detecting the fault, WECSs of groups 4 and 5 are blocked (with Blk = 1 triggered) and group output currents begin to decrease due to the stray resistive impedance within the fault loop (Stage I). Substation diode units D_4 and D_5 begin to conduct the current at about 0.34 s, as shown in Fig. 4.8(c) and (d), indicating that there is an increasing amount of current to be carried by groups 4 and 5 bypass diode units within the offshore substation (Stage II). Therefore, as groups 1 to 3 remain connected (as main offshore power contributors), offshore overall output voltage $V_{dc\text{-}OWF}$ reduces to 96 kV and dc-terminal voltage of the onshore MMC $V_{dc\text{-}MMC}$ is promptly reduced, through the proposed DOM mechanism, as shown in Fig. 4.7(b). Also, the dc-link current $I_{dc\text{-}MMC}$ is maintained by the MMC control system during the fault, see Fig. 4.8(e). The active power injected into the grid P_g is reduced correspondingly to be 96 MW, as shown in Fig. 4.8(f) and (g). Throughout the fault duration, the MMC SM capacitor voltages and arm currents are regulated within acceptable limits, as shown in Fig. 4.8(h) and (i) respectively.

The proposed system can retain the normal/healthy group 5 back into the generation mode with a successful current commutation. At approximately 0.44 s (Stage III), D_4 and D_5 are carrying sufficient dc current share, allowing group 4 series-connected disconnector ($SDIS_4$) to be safely opened, thereby isolating the faulty section (group 4). WECSs of group 5 can resume power transfer into the HVDC system by re-

establishing its output voltage ($Blk = 0$). The development of V_5 includes an acceptable stabilizing period due to control system, which allows the increase of $V_{dc\text{-}MMC}$ and thus P_g (to be about 128 MW), with I_{D5} current nullified. This action maximises wind power generation of available/normal WECSs in long term operation.

If F_4 is cleared (at 0.5 s), $SDIS_4$ can be closed and WECSs of group 4 can restore back to the generation mode ($Blk = 0$), facilitating a smooth power recovery to the pre-fault value at about 0.6 s (Stage IV).

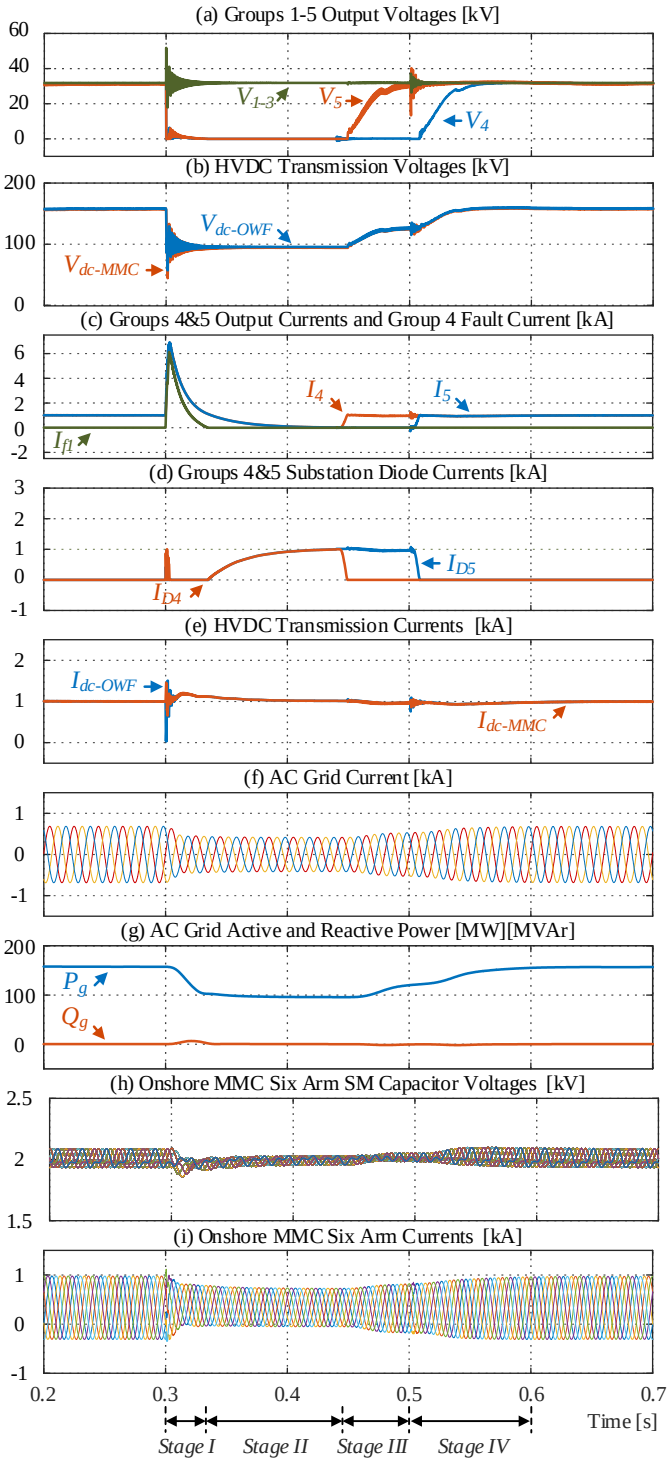

Stage I: Fault occurs and Groups 4&5 power transfer ceased
Stage II: Bypass path established through D_4 and D_5
Stage III: Fault isolated, Group 5 power transfer resumes
Stage IV: Fault cleared and Group 4 power transfer resumes

Fig. 4.8. Simulation results of collector cable short circuit fault (F_1) case.

4.3.2 Collector Cable Open Circuit Fault Case

Fig. 4.8 shows system performance with a collector cable open circuit fault (F_2) located at the uppermost cable of group 4.

At 0.3 s, group 4 power contribution to the HVDC system is stopped, resulting in the elimination of output voltage (V_4) and current (I_4), as shown in Fig. 4.9(a) and (c). During the fault, the offshore substation diode D_4 becomes forward-biased to promptly establish a conduction path for the offshore dc current ($I_{dc\text{-}OWF}$), and group 4 energy production is consumed locally by WECS DRs, as shown in Fig. 4.9(c) and (d). Simultaneously, the healthy group voltages $V_{1\text{-}3}$ and V_5 remain at the pre-fault values, subsequent to a short oscillation/surge period, caused by circuit interruption (which can be suppressed by protective devices), as shown in Fig. 4.9(b). Offshore dc-link voltage is reduced (to be 128 kV), where onshore MMC reacts quickly via the DOM mechanism, with dc-link current regulated, as shown in Fig. 4.9(b) and (d). The MMC avoids power elimination risks, with regulated ac current and reduced active power of about 128 MW, see Fig. 4.9(e) and (f). Throughout the fault, the MMC SM capacitor voltages and arm currents are maintained within acceptable operational limits, see Fig. 4.9(g) and (h).

After the fault clearance at 0.5 s, group 4 power production can be restored, allowing smooth system recovery back to nominal power transfer at 0.55 s. For a permanent fault, group 4 series, and parallel disconnectors ($SDIS_4$ and $PDIS_4$ respectively) can be opened and closed, respectively.

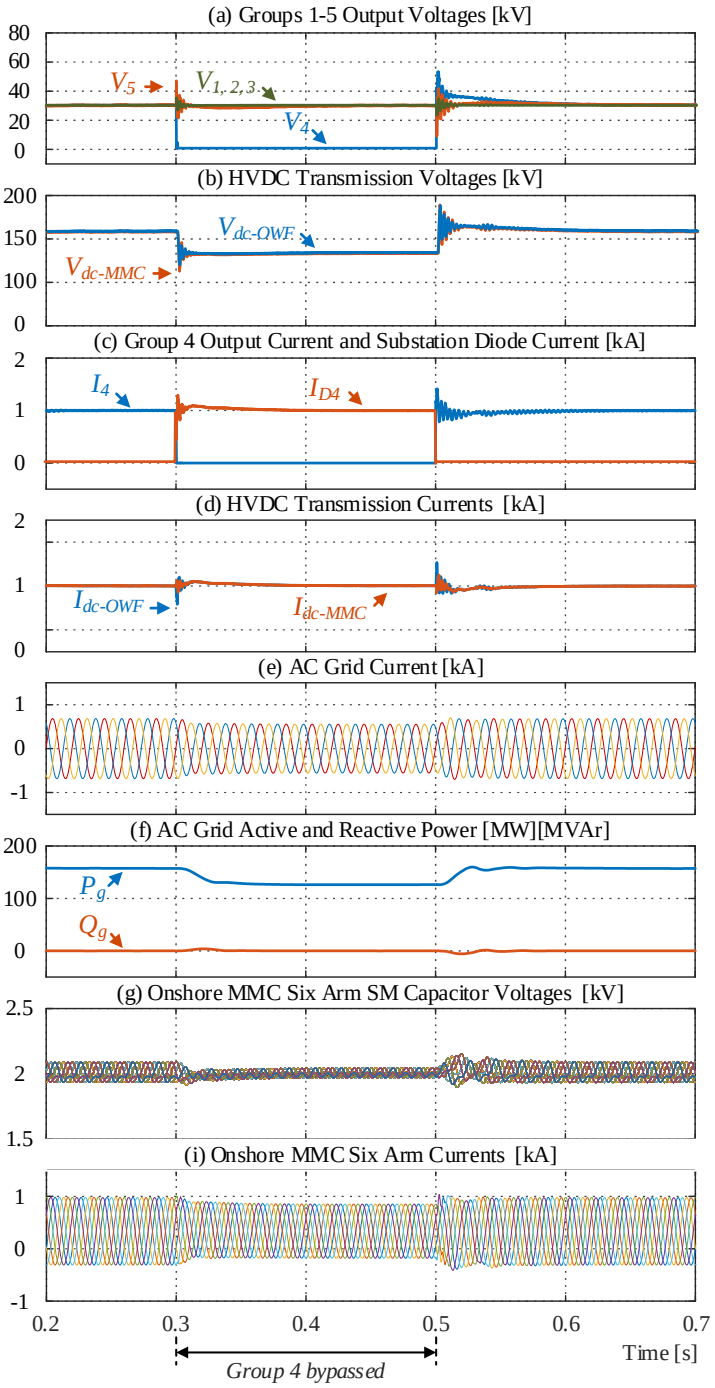

Fig. 4.9. Simulation results of collector cable open circuit fault (F_2).

4.3.3 HVDC Cable Short Circuit Fault Case

Fig. 4.10 shows system performance during an HVDC cable short circuit fault (F_3), which is assumed to be located at 20 km from the onshore substation with 1 Ω impedance.

At 0.3 s, the total offshore voltage $V_{dc\text{-}OWF}$ reduces sharply with $V_{dc\text{-}MMC}$ aligning promptly due to the DOM mechanism, shown in Fig. 4.10(a). The offshore current $I_{dc\text{-}OWF}$ rises to a peak value of approximately 4.2 kA (shortly, tolerated by diodes), and begins to decrease at a rate determined by the damping resistance of the cable impedance after blocking the WECSs (*Blk* = 1, and excess energy is dissipated by WECS DRs), as shown in Fig. 4.10(b). The MMC reference current $I^*_{dc\text{-}MMC}$ is set to 0 shortly and therefore holds $I_{dc\text{-}MMC}$ (offshore fault loop) to 0 A. The onshore ac grid currents and MMC arm currents become zero in this case, as shown in Fig. 4.10(d) and (g), and the active power transfer ceases, see Fig. 4.10(e). A minor discharge of SM capacitor voltages occurs to be about 1.9 kV, but is stopped quickly, as shown in Fig. 4.10(f), indicating the brief period of the detection delay and fault blocking.

At 0.5 s, the fault is cleared and the WECS blocking signal (*Blk* = 0) can be removed. Group terminal voltages can be established to allow recovery of $V_{dc\text{-}OWF}$ and $V_{dc\text{-}MMC}$, which also enables smooth MMC active power injection recovery.

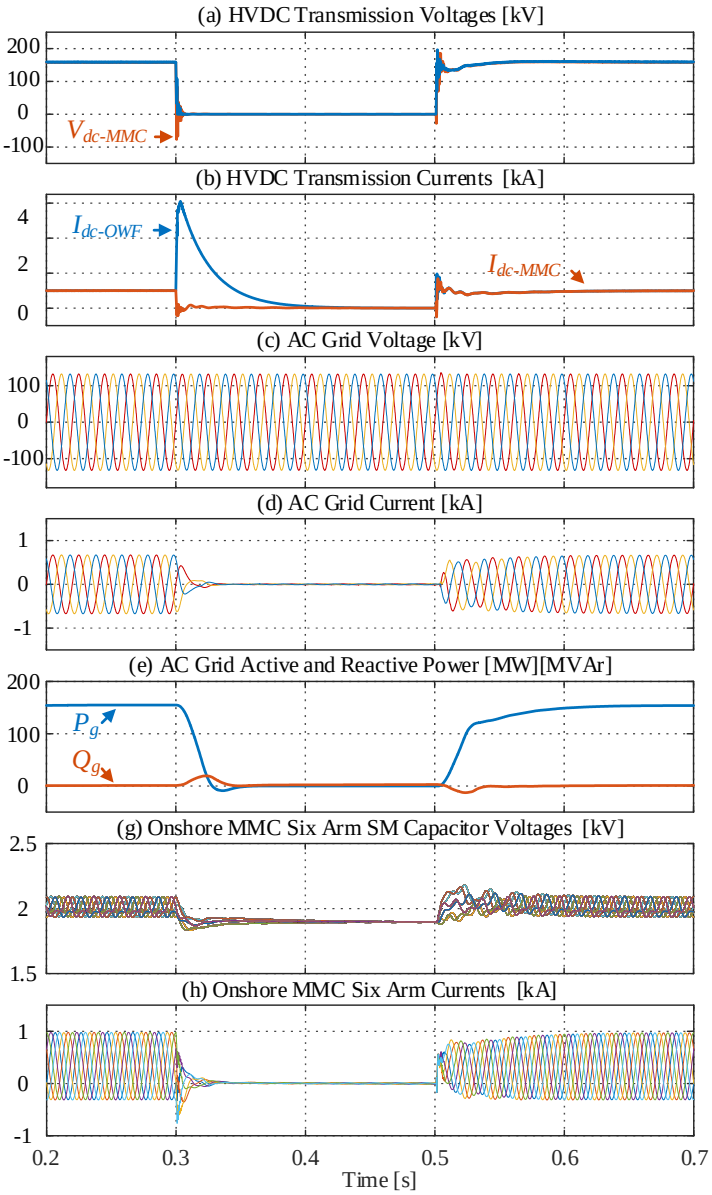

Fig. 4.10. Simulation results of HVDC cable short circuit fault (F_3) case.

4.3.4 AC Grid Fault Case

Simulation results in Fig. 4.11 show system behaviour in an asymmetrical (single-phase to ground) ac grid fault (F_4) case, where one phase voltage is collapsed as shown in Fig. 4.11(c).

At the occurrence of the fault, offshore WECS units respond proportionally to the V_g, effectively de-loading with $V_{dc\text{-}OWF}$ becoming about 106 kV, as shown in Fig. 4.11(a), where the undeliverable WECSs power is consumed by local DRs. Through the DOM mechanism, $I_{dc\text{-}OWF}$ and $I_{dc\text{-}MMC}$ are maintained at 1 kA with minor oscillation, as shown in Fig. 4.11(b). During the fault, ac grid current i_{abc} is controlled at 1.2 pu, as shown in Fig. 4.10(d). The power injection from the MMC into the grid is about 106 MW, where the MMC also injects about 56 MVAr reactive power to regulate the grid voltage depression, see Fig. 4.11(e). MMC SM capacitor voltages range between 1.8 kV to 2.2 kV shortly after a control stabilization period, whereas the arm currents remain controlled and within the limits, as shown in Fig. 4.11(f) and (g).

After the grid fault is cleared, grid voltage is re-established, allowing the onshore MMC to inject the rated power, therefore the offshore SC-OWF retain power recovery with $V_{dc\text{-}OWF}$ and $V_{dc\text{-}MMC}$ (via DOM) restored.

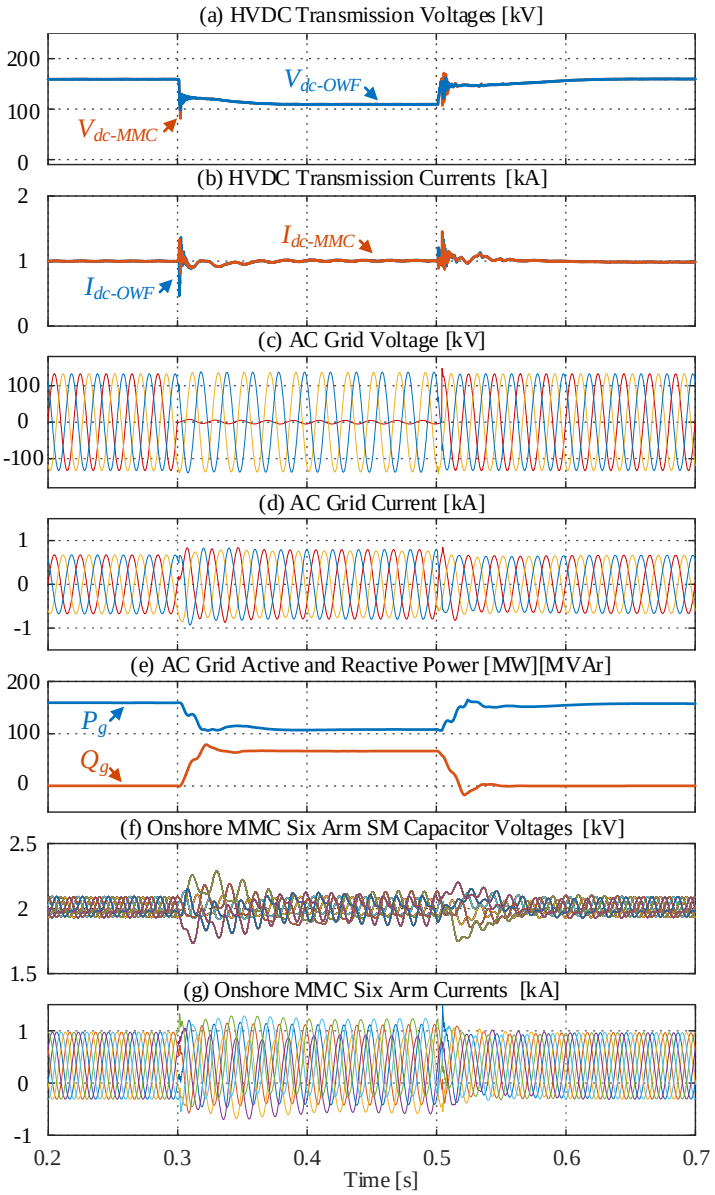

Fig. 4.11. Simulation results of asymetrical ac grid fault (F_4) case.

4.3.5 Offshore Substation Volume, Weight, and Cost Analysis

This subsection presents estimated volume, weight, and cost in order to give a comparison between the proposed substation and an offshore HVDC-MMC station.

The estimation of the proposed substation can be achieved by considering diodes and disconnectors, with reasonable margins included. For the selected diode unit (D2601NH90T), volume, mass and cost are estimated to be 0.05 m^3/pcs, 5 kg/pcs and 3k $/pcs respectively, considering auxiliary circuits, heat sinks, and additional units required to withstand fault current etc. Therefore, for the 160 MW system of the

studied case, the size, weight, and cost of 40 diode units within the proposed substation are 2 m^3, 200 kg and \$120k respectively. For the sake of generality and simplicity, it is assumed that disconnectors are the same for different groups, with the dimension and weight being 6 m^3 and 500 kg respectively [22], where margins are included for spacing between units [23]. Also, the mechanical switch cost can be estimated at 570º\$/MW [24]. Thus, 15 disconnectors of the proposed substation require approximately 90 m^3, 7500 kg and \$274k respectively.

For an MMC-HVDC offshore substation, per MW parameters can be used due to the existence of commercially available projects, namely, volume of 54ºm^3/MW, mass (electrical equipment) of 1,875 kg/MW and cost of 115k \$/MW approximately [24]–[27].

Comparatively, Table 4.2 shows the estimated values of an assumed offshore HVDC-MMC station and the proposed offshore substation (same power ratings are assumed as the studied case in the main manuscript). The physical parameters and cost of the proposed offshore substation is significantly lower, where the volume, weight, and cost count for approximately 1.1%, 2.6%, and 2.1% of an offshore HVDC-MMC station, showing a very competitive solution for offshore wind integration.

Table 4.2. Volume, Mass, and Cost Comparison.

Items	HVDC-MMC Station	Proposed Substation
Power [MW]	160	160
Volume [m^3]	8640	92
Weight [tonne]	300	7.7
Cost [\$]	18400k	394k

4.4 Summary

This chapter proposed a series-connected offshore wind farm (SC-OWF) system with novel architecture and control, which prioritise, thus enhance, resiliency against typical faults of high severity. The proposed offshore substation arrangement and manipulation strategies allow the series-connected wind energy converter systems (WECSs) to be electrically grouped, achieving effective fault isolation/bypassing, and reducing the risks of permanent generation loss. Also, offshore network complexity and costs are low, through the collective implementation of the WECSs with diode rectifier output stage and the offshore substation utilising diodes and disconnectors.

The onshore subsystem employs a dc-fault-tolerant modular multilevel converter (MMC) with constant dc current control and a dc offset modifier (DOM) mechanism, which can maximise power generation during normal operation and ensure transmission system safety during dc/ac faults. System behaviour in four typical dc/ac fault cases were presented, indicating the operational effectiveness. The proposed system can eliminate the requirement of massive offshore converter stations with significantly reduced cost, which was confirmed by a comparative estimation between an offshore MMC station and the proposed system. The proposed SC-OWF system would be applicable for future offshore wind generation applications. However, the power export capability of the windfarm may be limited due to limitations on component and cable ratings.

References

[1] H. Zhang, F. Gruson, D. M. F. Rodriguez, and C. Saudemont, "Overvoltage limitation method of an offshore wind farm with DC series-parallel collection grid," *IEEE Trans Sustain Energy*, vol. 10, no. 1, pp. 204–213, Jan. 2019, doi: 10.1109/TSTE.2018.2829929.

[2] F. Rong, G. Wu, X. Li, S. Huang, and B. Zhou, "All-DC offshore wind farm with series-connected wind turbines to overcome unequal wind speeds," *IEEE Trans Power Electron*, vol. 34, no. 2, pp. 1370–1381, Feb. 2019, doi: 10.1109/TPEL.2018.2834965.

[3] M. Guan, "A series-connected offshore wind farm based on modular dual-active-bridge (DAB) isolated DC–DC converter," *IEEE Transactions on Energy Conversion*, vol. 34, no. 3, pp. 1422–1431, May 2019, doi: 10.1109/tec.2019.2918200.

[4] Q. Wei, B. Wu, D. Xu, and N. R. Zargari, "A medium-frequency transformer-based wind energy conversion system used for current-source converter-based offshore wind farm," *IEEE Trans Power Electron*, vol. 32, no. 1, pp. 248–259, Jan. 2017, doi: 10.1109/TPEL.2016.2524635.

[5] A. O. Almeida, I. F. Lopes, P. M. Almeida, M. A. Tomim, J. A. Passos Filho, and P. G. Barbosa, "Series-DC connection of offshore wind generating units: Modeling, control and galvanic isolation.," *Electric Power Systems Research*, vol. 195, Jun. 2021, doi: 10.1016/j.epsr.2021.107149.

[6] Y. Xia, K. H. Ahmed, and B. W. Williams, "A pwm current source-based DC transmission system for multiple wind turbine interfacing," *IEEE J Emerg Sel Top Power Electron*, vol. 2, no. 4, pp. 784–796, 2014.

[7] J. Tait, S. Wang, K. Ahmed, and G. P. Adam, "Comparative assessment of four low voltage fault ride through techniques (lvfrt) for wind energy conversion systems (wecss)," *Alexandria Engineering Journal*, vol. 61, no. 12, pp. 10463–10476, Dec. 2022, doi: 10.1016/j.aej.2022.04.003.

[8] H. Liu, M. S. A. Dahidah, J. Yu, R. T. Naayagi, and M. Armstrong, "Design and control of unidirectional DC-DC modular multilevel converter for offshore DC collection point: Theoretical analysis and experimental validation," *IEEE Trans Power Electron*, vol. 34, no. 6, pp. 5191–5208, Jun. 2019, doi: 10.1109/TPEL.2018.2866787.

[9] H. J. Bahirat and B. A. Mork, "Operation of DC series-parallel connected offshore wind farm," *IEEE Trans Sustain Energy*, vol. 10, no. 2, pp. 596–603, Apr. 2019, doi: 10.1109/TSTE.2018.2839712.

[10] G. Guo, K. Zha, J. Zhang, Z. Wang, F. Zhang, and J. Cao, "Grounding fault in series-connection-based offshore wind farms: Fault clearance," *IEEE Trans Power Electron*, vol. 35, no. 9, pp. 9357–9367, Sep. 2020, doi: 10.1109/TPEL.2020.2971640.

[11] A. O. Almeida, M. A. Tomim, P. M. Almeida, and P. G. Barbosa, "A control strategy for an offshore wind farm with the generating units connected in series with a VSC-HVDC

transmission link," *Electric Power Systems Research*, vol. 180, Mar. 2020, doi: 10.1016/j.epsr.2019.106121.

[12] General Electric Company, "Hvdc valves power electronics for hvdc schemes," 2019. Accessed: Sep. 20, 2022. [Online]. Available: https://resources.gegridsolutions.com/hvdc/hvdc-valves-brochure

[13] E. Shahriari, F. Gruson, P. Vermeersch, P. Delarue, F. Colas, and X. Guillaud, "A novel dc fault ride through control methodology for hybrid modular multilevel converters in hvdc systems," *IEEE Transactions on Power Delivery*, vol. 35, no. 6, pp. 2831–2840, Dec. 2020, doi: 10.1109/TPWRD.2020.2998535.

[14] G. Guo *et al.*, "Series-connected-based offshore wind farms with full-bridge modular multilevel converter as grid- and generator-side converters," *IEEE Transactions on Industrial Electronics*, vol. 67, no. 4, pp. 2798–2809, Apr. 2020, doi: 10.1109/TIE.2019.2912777.

[15] M. Pape and M. Kazerani, "A generic power converter sizing framework for series-connected dc offshore wind farms," *IEEE Trans Power Electron*, vol. 37, no. 2, pp. 2307–2320, Feb. 2022, doi: 10.1109/TPEL.2021.3106578.

[16] A. Egea-Alvarez, S. Fekriasl, F. Hassan, and O. Gomis-Bellmunt, "Advanced vector control for voltage source converters connected to weak grids," *IEEE Transactions on Power Systems*, vol. 30, no. 6, pp. 3072–3081, Nov. 2015, doi: 10.1109/TPWRS.2014.2384596.

[17] W. Yang, Q. Song, and W. Liu, "Decoupled control of modular multilevel converter based on intermediate controllable voltages," *IEEE Transactions on Industrial Electronics*, vol. 63, no. 8, pp. 4695–4706, Aug. 2016, doi: 10.1109/TIE.2016.2549001.

[18] S. Wang, G. P. Adam, A. M. Massoud, D. Holliday, and B. W. Williams, "Analysis and assessment of modular multilevel converter internal control schemes," *IEEE J Emerg Sel Top Power Electron*, vol. 8, no. 1, pp. 697–719, Mar. 2020, doi: 10.1109/JESTPE.2019.2899794.

[19] H. Wu, X. Wang, and L. H. Kocewiak, "Impedance-based stability analysis of voltage-controlled MMCs feeding linear AC systems," *IEEE J Emerg Sel Top Power Electron*, vol. 8, no. 4, pp. 4060–4074, Dec. 2020, doi: 10.1109/JESTPE.2019.2911654.

[20] G. Guo *et al.*, "HB and FB MMC based onshore converter in series-connected offshore wind farm," *IEEE Trans Power Electron*, vol. 35, no. 3, pp. 2646–2658, Mar. 2020, doi: 10.1109/TPEL.2019.2929689.

[21] W. Wang, X. Yan, S. Li, L. Zhang, J. Ouyang, and X. Ni, "Failure of submarine cables used in high-voltage power transmission: Characteristics, mechanisms, key issues and prospects," *IET Generation, Transmission and Distribution*, vol. 15, no. 9. John Wiley and Sons Inc, pp. 1387–1402, May 01, 2021. doi: 10.1049/gtd2.12117.

[22] Cleaveland / Price Inc., "Aluminum center break switch bulletin db-126b18," 2022. Accessed: Sep. 20, 2022. [Online]. Available: https://www.cleavelandprice.com/wp-content/uploads/2018/10/No-crop-lines-CP_CBA-VBrochure_3.16.18_FA_LOW-RES.pdf

[23] Siemens Energy, "Cpv2/cpv2s circuit switchers and 3ap live-tank breakers." Accessed: Sep. 20, 2022. [Online]. Available: https://assets.siemens-energy.com/siemens/assets/api/uuid:3e08d087-f191-413f-a047-896455a1df37/brochure-cpv2-cpv2s-circuit-switchers-3ap-lt-breakers-us.pdf

[24] Matthias Heidemann, Gregor Nikolic, Armin Schnettler, Ala Qawasmi, Nils Soltau, and Rik W. De Donker, "Circuit-breakers for medium-voltage dc grids," *IEEE PES Transmission & Distribution Conference and Exposition*, 2016.

[25] X. Xiang *et al.*, "Comparison of cost-effective distances for lfac with hvac and hvdc in their connections for offshore and remote onshore wind energy," *CSEE Journal of Power and Energy Systems*, vol. 7, no. 5, pp. 954–975, Sep. 2021, doi: 10.17775/CSEEJPES.2020.07000.

[26] S. Hardy, K. Van Brusselen, S. Hendrix, and D. Van Hertem, "Techno-economic analysis of HVAC, HVDC and OFAC offshore wind power connections.," *2019 IEEE Milan PowerTech*, 2019.

[27] P. Lundberg, "HVDC light: Power from shore," 2016. Accessed: Sep. 20, 2022. [Online]. Available: https://new.abb.com/docs/librariesprovider46/pw2016/seminars/r607-en-abb_hvdc_light_power_from_shore.pdf?sfvrsn=2

[28] P. Bresesti, W. L. Kling, R. L. Hendriks, and R. Vailati, "Hvdc connection of offshore wind farms to the transmission system," *IEEE Transactions on Energy Conversion*, vol. 22, no. 1, pp. 37–43, Mar. 2007, doi: 10.1109/TEC.2006.889624.

Chapter 5

A DC-Based Offshore Wind Farm Featuring Reduced Mass Requirements

---

This chapter proposes a modular-series-parallel topology, facilitating advantageous elements from other researchers previously published schemes, and presenting comprehensive circuit configuration and protection strategies with the aim of minimizing the detrimental effects caused by dc cable faults to ensure system security in a cost-effective manner. The system architecture employs a grouping scheme, where each group consist of a string of series connected wind energy converter systems (WECS) interfaced to uni-directional high gain dc/dc converter with parallel connection at the high voltage dc (HVDC) transmission point. The modular uni-directional high gain dc-dc converter is achieved through use of single active bridge modular multilevel converter (MMC) comprising of half bridge submodules (HB-SM) at medium voltage dc (MVDC) level with diode rectification at HVDC level. The system configuration allows the containment off collector faults within each of the groups allowing secure system operation via control and balancing systems, with power quality achieved through an adaptive phase-shift control function on the dc output of the offshore converter station. The proposed system is quantitatively substantiated by time-domain simulations, where three dc fault cases are considered. In addition, a weight/size assessment is conducted to demonstrate the benefits of the presented system in comparison to conventional HVDC systems with ac collectors.

5.1 Proposed DC-based Offshore Wind Farm Configuration

The proposed system configuration is shown in Fig. 5.1. At the offshore side, there are *M* wind energy conversion system groups (WGs) parallel-connected to HVDC) link, and each WG consists of *N* WECSs series-connected via cables forming a MVDC link, and an offshore dc-dc converter. An onshore MMC (such as the HB-MMC) station is used to integrate the HVDC link into the grid.

In general, the multiple WGs arrangement for the OWF facilitates flexible configuration and expandable structure. Although, different WGs use the common

HVDC link, the operation can be decoupled given the constant dc-link voltage. Also, with such a multi-terminal dc (MTDC) system, WGs can be located far away from each other, which is particularly advantageous for OWF applications.

The subsequent subsections detail the key elements of the proposed OWF architecture including configuration, hardware components, and control.

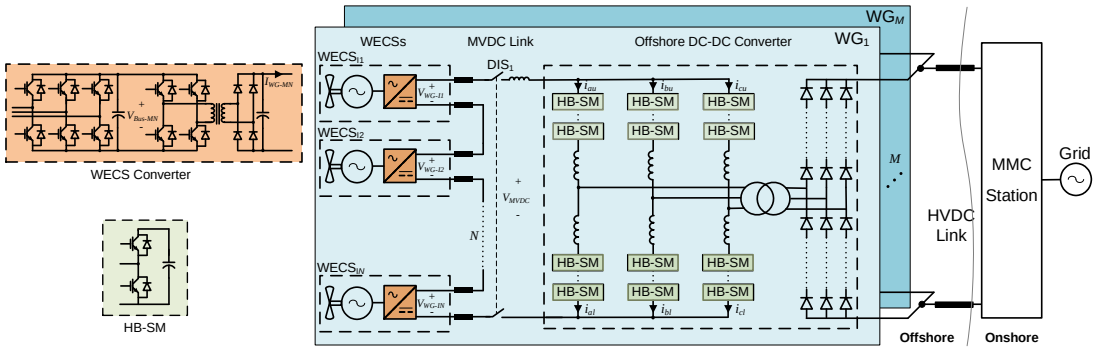

Fig. 5.1. System architecture of proposed OWF.

5.1.1 Wind Energy Conversion System

The stator terminal voltages and dimensioning of the wind turbine vary with both low and medium voltage variants (as in [1]– [4]), whilst it is obvious that the voltage level can increase with higher power rating requirements.

Various power converter topologies are applicable as the WECS converter, which is used to interface the wind turbine and the medium voltage (MV) side. Sufficient voltage gain of the dc-dc conversion stage has been proposed in [5] and described in Chapter 4.1.1. Currently, a two-level IGBT-based converter is usually used as the generator-side converter. The output rectification stage employs a single active bridge type converter, with a MF transformer to provide isolation, and a diode bridge as the output stage to interface the MV side. This design aligns with that articulated in [6], where sufficient isolation (for the dc bias at MV voltage levels) can be achieved by an air-core MF transformer, reducing weight and losses in comparison to iron-core counterparts [2].

5.1.2 Medium Voltage DC-Link

As shown in Fig.5.1, the dc collection system of the proposed OWF is rated at MV level, which is opposed to mainstream SC-OWF schemes rated at HV level. Both systems construct the dc system by series connection of WECSs, however, the WECS

offset voltage stresses of the proposed system are significantly reduced due to the MVDC (typically less than 66 kV).

For isolation and protection, the MVDC link within each WG is equipped with disconnectors (DISs) to provide proper isolation during contingency (e.g., faults) or maintenance period. Also, a dc reactor is connected to suppress current surges during short-circuit faults at the MVDC link or WECS strings, whilst the inductance depends on overcurrent tolerances, detection periods, etc.

5.1.3 Offshore DC-DC Converter

The offshore dc-dc converter is employed to boost the MVDC to HVDC with essential fault isolation. The dc-dc converter mainly consists of a dc-ac conversion stage, a medium frequency transformer (MFT), and a diode rectification stage. The intermediate ac system within the dc-dc converter is operated at medium frequency (MF) ranges (hundreds Hz), which is especially advantageous in terms of both converter ratings and transformer weight/size.

The dc-ac conversion is achieved by a three-phase HB-MMC. Such an HB-MMC operating at the MV level is the only MMC within the overall OWF, which reduces engineering and isolation/insulation difficulties compared to the conventional MMC-HVDC systems operating at hundreds kV levels. Besides, with the MF ac operation, the required stored energy and circuit filter ratings can be reduced for a pre-determined power rating, which leads to smaller submodule (SM) capacitors and arm inductors. The isolation transformer operates at MF ranges, which would lead to reduced overall physical dimensions and weight in comparison to the 50/60 Hz equivalents [7].

The output stage of the dc-dc converter is achieved through three-phase diode rectifier, which allows unidirectional power flows. The high-robustness and low-cost characteristics make the diodes advantageous in this application, especially considering the salient capability and simplicity to isolate WGs from the HVDC link in cases of WG fault. Thus, an MTDC-based architecture is realised through the parallel connection of WGs.

5.2 System Control and Contingency Management

This section details the control system design and system arrangement against two typical contingency cases, namely, short circuit fault on the WG collector cable (F_1) and short circuit fault on HVDC transmission cable (F_2).

5.2.1 Control System

For the proposed OWF, multiple WGs are connected and controlled with their respective power flows injected into the HVDC link. The HVDC link voltage is maintained by the onshore converter station, where an HB-MMC could be used, for HVDC integration and grid support functions [8].

As shown in Fig. 5.2, the generator-side converter controller within the WECS generates ac output references with conventional methods, where the *d*-axis current (i_{dg}) is controlled zero and the *q*-axis current (i_{qg}) loop is for optimum torque control (OTC) function, as detailed in [9] and control system described in Chapter 4.1.1. By controlling the *q*-axis current (the added reference signal from the WECS power control), power flow from the wind turbine can be regulated to maintain the balance of WECS output voltages ($V_{WG\text{-}MN}$) in short terms, while wind turbine level control over the pitch angle could ensure long-term balance (essentially, power balance in long terms). The curtailment controller provides a reduction signal to the summation point of the q-axis current refence and is represented by a PI controller ($K_{pi\_vc}(s)$) expressed in (5.1).

$$i^*_{q\_mod} = K_{pi\_vc}(s)(V^*_{WG-MN} - V_{WG-MN}) \tag{5.1}$$

Simply, the practices of voltage balancing for SC-OWF schemes could be adopted for the series-connected WECSs of the proposed OWF, which, in the proposed OWF, is operating at MV levels [10]– [13].

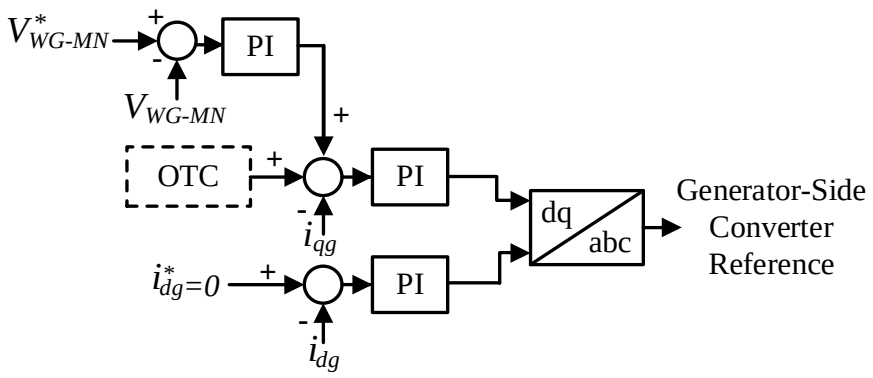

Fig. 5.2. Generator-Side converter control system.

As shown in Fig. 5.3, the WECS dc output converter (dc-dc converter) control adopts a dual-loop architecture as detailed in Chapter 4.1.1, with the inner loop controlling WECS dc output current ($I_{WG\text{-}MN}$) and the outer loop regulates the WECS dc output voltage, thus varying the output voltage ($V_{Bus\text{-}MN}$) via the dc-dc converter modulation index. Also, the dc-dc converter can be blocked with the enabling signal $En_1 = 0$, to cease the WECS power injection into the MVDC link.

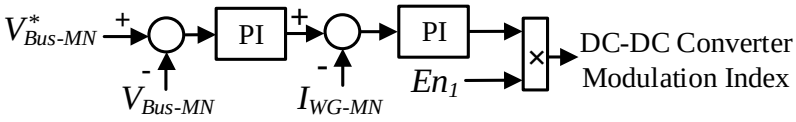

Fig. 5.3. WECS dc-dc converter control system.

The control structure of the offshore dc-dc converter within a generic WG is presented in Fig. 5.4. An enabling signal ($En_2 = 1$) is included to indicate normal operation, which will be useful to block the HB-MMC ac-side output during HVDC link fault. The MVDC voltage controller (detailed in Chapter 3.2.2) regulates the MVDC side voltage (V_{MVDC}) via the magnitude variation of the HB-MMC ac-side output (with the predetermined frequency at MF ranges).

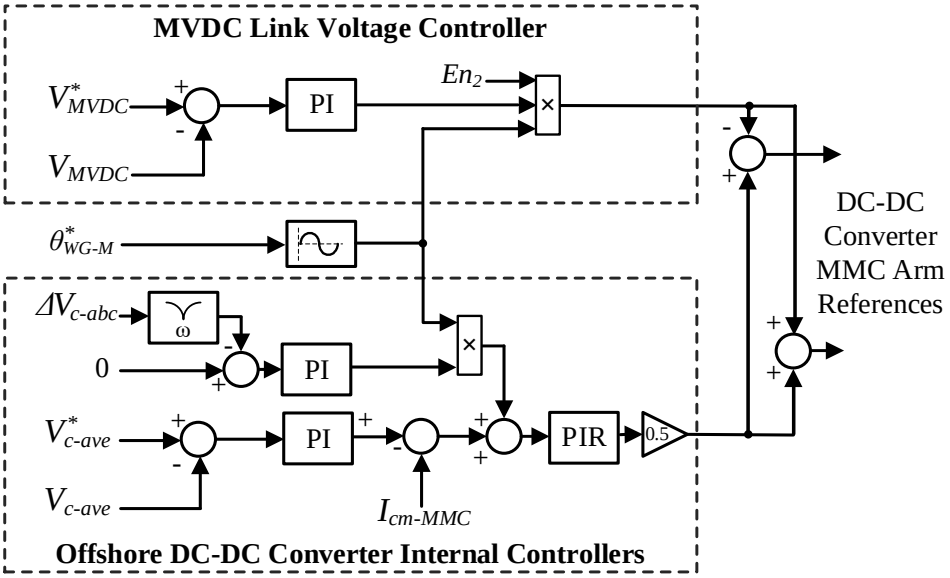

Fig. 5.4. Control system of offshore dc-dc converter.

Also, a phase angle is assigned and used to generate a base sinusoidal signal for the ac output. With multiple WGs connected at the HVDC link, phase-shifted diode rectifier outputs can be implemented to minimise the ripple of overall HVDC link. Considering flexible connection/disconnection of the multiple WGs (such as in WG fault cases), an adaptive phase-shift assignment algorithm is designed herein, where the dc-dc converter internal ac voltage (and thereby diode rectifier output voltage) phase shift, namely θ^*_{WG-M} in Fig. 5.4, is dynamically calculated and assigned. For the generic M^{th} WG, the HB-MMC ac-side output voltage phase angle can be expressed by (5.2)

$$\theta^*_{WG-M} = (M-1)\frac{N_C}{2\pi} \tag{5.2}$$

where, N_C is the total number of the instantaneously connected WGs. Generally, a design with more parallel-connected WGs will lead to lower HVDC link harmonics.

As shown in Fig. 5.4, the dc-dc converter HB-MMC internal control is similar to that of a conventional HB-MMC, as described in Chapter 4.1.3 and tuning described as per [14]. The assigned base sinusoidal signal is used as the fundamental frequency ac reference fed into the proportional-integral-resonant (PIR) controller for MMC inter-arm balance. Capacitor voltage controller, inter-leg balancing controller, and circulating current suppression controller are also included to synthesise the HB-MMC arm references, as in [14].

5.2.2 Wind Turbine DC collector short Circuit Fault

This subsection presents the fault-tolerant capability against the wind turbine dc collector short circuit fault, which is illustrated as F_1 at WG_1 in Fig. 5.5. One of the advantageous features of the proposed OWF system is that the wind turbine side faults can be simply isolated and contained within one WG. This is mainly due to the parallel connection and decoupled operation of different WGs.

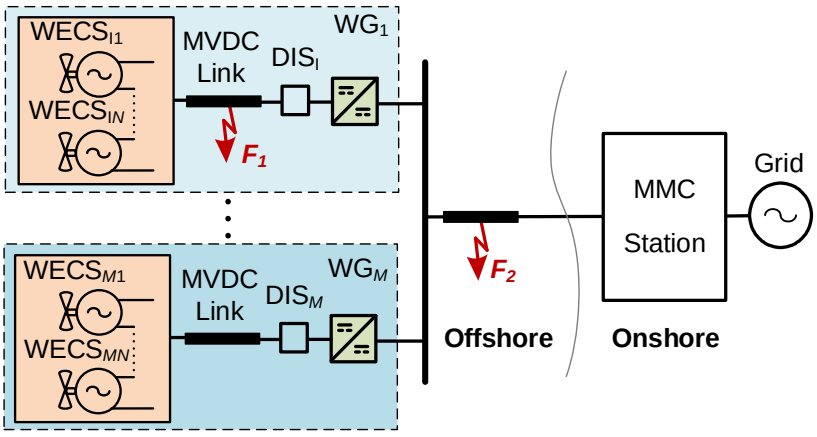

Fig. 5.5. Single line diagram of OWF.

In terms of the faulty WG_1, when F_1 occurs and has been detected, all WECS controllers within the faulty WG_1 are disabled (by setting $En_1 = 0$ in Fig. 5.3) with additional energy being dissipated by the local protection to ensure the system operates within its correct operating boundaries. Simultaneously and in a coordinated manner, the HB-MMC with the WG_1 offshore dc-dc converter is blocked, to prevent the SMs from discharging during such an MVDC link fault, and to cease the contribution to the dc collector fault point.

From the perspective of the HVDC link, the faulty WG_1 stops injecting power during the F_1 fault, leading to a power reduction of total transmission. Besides, the remaining connected WGs will adapt the respective dc-dc converter ac reference phase angle ($\theta^*_{WG\text{-}M}$), in order to minimise the HVDC link ripple with the shifted phases.

If a temporary fault is cleared, the MVDC link voltage can be rebuilt, and the dc-dc converter operation can be retained to allow the restoration of power transfer from MVDC to HVDC link. For a long-term fault, once the MVDC link fault current decays to zero (mainly depending on the collector system impedance characteristics), the DIS_I with the WG_1 can be operated to safely isolate WECS string (WECSs and collectors) from the dc-dc converter to wait for operator intervention.

5.2.3 HVDC Cable Short Circuit Fault

Besides inevitable power export interruption, the HVDC link fault (marked as F_2 in Fig. 5.5) would potentially pose high risks to both offshore and onshore equipment. Therefore, it is imperative that all subsystems are secured throughout.

For the proposed OWF, all WGs should cease the power injection into the HVDC link with the offshore dc-dc converter modulation index references set to zero ($En_2 = 0$ in Fig. 5.4). With the zero ac-side voltage, all diode rectifiers interfacing the HVDC link would not transfer power from ac (essentially, the WG MVDC links) to dc (HVDC link) side, with only forward biasing to allow the fault current flow and decay. Fortunately, diodes are very robust and tolerant to fault current surges. Simultaneously, the power contribution from WECSs should be interrupted (by setting $En_1 = 0$ in Fig. 5.3) with the extra energy dissipated within each WECS. For the onshore converter station, the HB-MMC should be blocked once the HVDC link fault is detected, with ac-side circuit breakers tripped to stop the current flowing from ac grid to the faulty dc link.

Thus, although the fault current is extinguished in a passive way, no component of the proposed system is endangered by high/transient voltages and/or currents, whilst the power generation would be able to restore once the fault is cleared.

5.3 Case Studies of Proposed Offshore Wind Farm

To verify the operational feasibility and fault ride-through performance, a case study is established and simulated based on MATLAB/Simulink software, considering the two fault cases (F_1 and F_2 as shown in Fig. 5.5). Also, comparison of the estimated weight and volume between the conventional MMC-HVDC and the proposed OWF systems is presented to highlight the feature of reduced weight and size requirements. Table 5.1 gives the key parameters utilised for the case study. For the wind turbine level, the low-voltage PMSG is assumed herein, which aligns with commercial offerings available in [15] – [17]; nevertheless, the trends towards higher voltage levels exist. With the adopted wind turbine system [18], the distance between two adjacent turbines is assumed to be seven times the turbine rotor diameter [19], while detailed wind turbine sub-siting arrangement is neglected herein for a generic study. The offshore collector cable parameters are chosen aligning with [20], with multi-section

π-model used for the simulation [21]. A 1 ms delay is assumed to represent the fault processing/detection actions in fault scenarios. In steady-state (pre-fault) operation, all elements such as WECSs, offshore and onshore converter stations are operated at 1 pu with power transferred into the onshore grid.

Table 5.1. Case study simulation parameters

Items		Values
Overall System	HVDC link voltage rating	200 kV
	HVDC power rating	200 MW
	HVDC link length	40 km
	WG number (M)	5
	WECS number per WG (N)	5
	Total WECS number ($M \times N$)	25
WECS	Wind turbine rotor diameter (D)	167 m
	WECS rated power	8 MW
	WECS rated output voltage ($V_{WG\text{-}MN}$)	8 kV
MVDC Link	Distance between two near turbines	1.2 km
	Collector cable number per WG	6
	Collector cable resistance	17.8 mΩ/km
	Collector cable inductance	0.158 mH/km
	Collector cable capacitance	0.275 μF/km
Offshore DC-DC Converter	Rated active power	40 MW
	Rated input dc voltage	40 kV
	Rated output dc voltage	200 kV
	HB-MMC SM number per arm	20
	HB-MMC SM capacitance	1.5 mF
	HB-MMC SM rated voltage	2 kV
	HB-MMC arm inductance	1 mH
	MF transformer ratio	1:8
	MF transformer leakage	0.2 pu
	Internal ac frequency (MF)	400 Hz
Onshore MMC Station & Grid	Power rating	200 MVA
	HB-MMC SM number per arm	100
	HB-MMC SM capacitance	8 mF
	HB-MMC SM rated voltage	2 kV
	HB-MMC arm inductance	19.3 mH
	Grid frequency	50 Hz
	Grid voltage	132 kV

5.3.1 WECS Group Offshore Collector Cable Short Circuit Fault Case

In this subsection, system performance, with a rail-to-rail short circuit fault (F_1) to the WG_1 dc collector from 0.3 s to 0.5 s, is presented in Fig. 5.6.

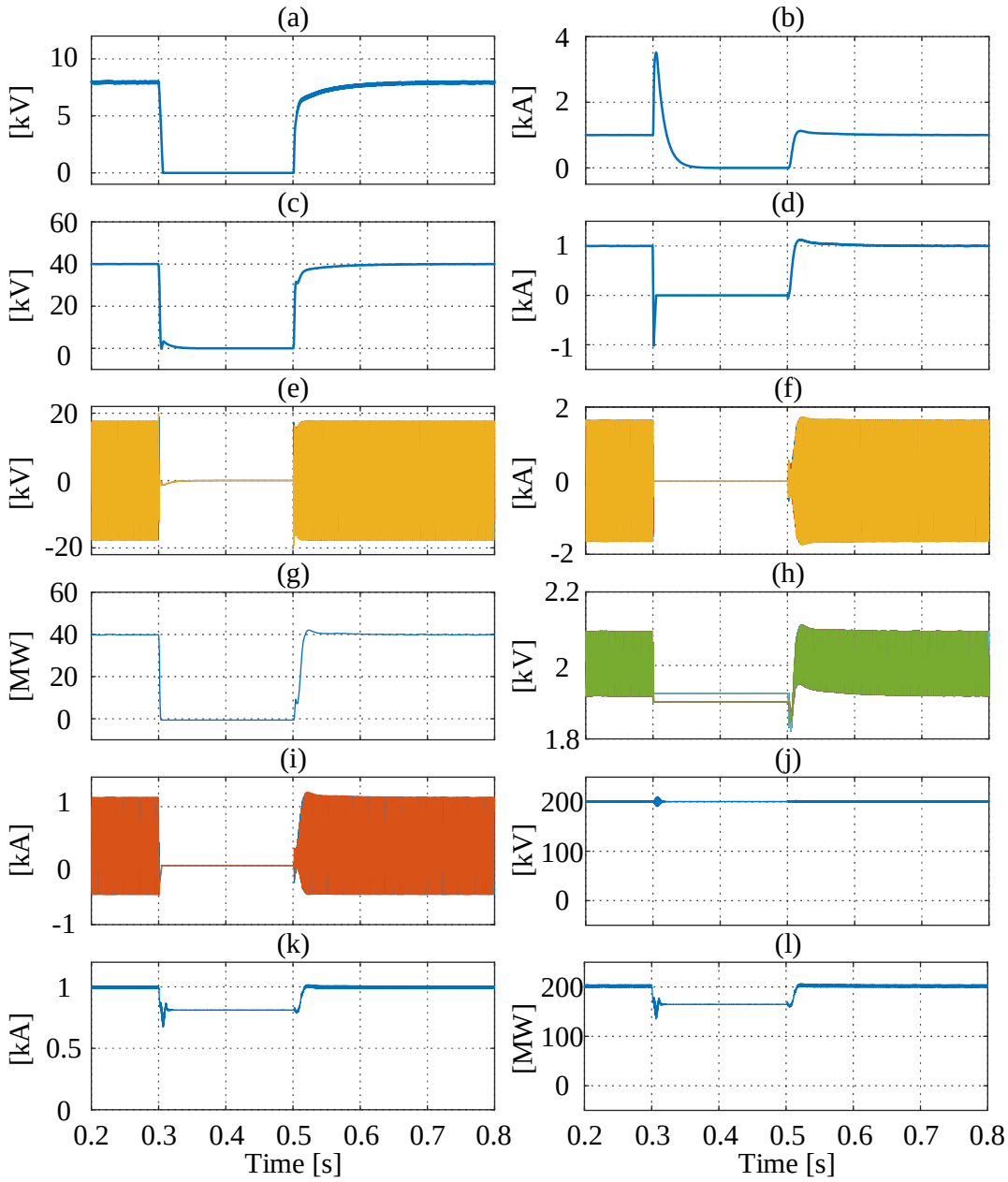

Fig. 5.6. Simulation results of dc collector cable short circuit fault (F_1). (a) WG_1 $WECS_{11}$ output voltage. (b) WG_1 $WECS_{11}$ output current. (c) WG_1 MVDC link voltage. (d) WG_1 MVDC link current. (e) WG_1 dc-dc converter ac bus voltage. (f) WG_1 dc-dc converter ac bus current. (g) WG_1 dc-dc converter power. (h) WG_1 dc-dc converter MMC capacitor voltage. (i) WG_1 dc-dc converter MMC arm current. (j) HVDC link voltage. (k) HVDC link OWF-side current. (l) HVDC link power.

With the F_1 fault, WG_1 WECS output voltage (thereby MVDC link voltage) collapses, as shown in Fig. 5.6(a) and (c), while the output current of WECSs endures a high current surge (at approximately 3.5 pu, which is acceptable for the output stage diode rectifier, if sized correctly) at the occurrence of F_1 and decays in about 50 ms, see Fig.5.6(b). Such a quick decay is due to the deactivation of WECSs ($En_1 = 0$) at 0.301 s, thereby the power contribution to the fault can be stopped. For the offshore dc-dc

converter within the WG_1, a simultaneous blocking action of the MV-level HB-MMC prevents its SM capacitors from discharging (with a short discharge/reverse current period of 1 ms, until the offshore dc-dc converter is disabled by setting $En_2 = 0$), as shown in Fig. 5.6(d). During the fault, with the WG_1 dc-dc converter HB-MMC blocked, the converter ac-side voltage, current and power are nullified, see Fig. 5.6(e)-(g). Also, the HB-MMC operation is stopped as shown in Fig. 5.6(h) and (i).

In terms of the HVDC link, the voltage is negligibly affected due the effective isolation of WG_1 diode rectification stage, as shown in Fig. 5.6(j). Also, with the phase-shift reconfiguration of the remaining WGs, HVDC link power quality is maintained high. With the ceased power transfer of WG_1 (rated at 40 MW), overall power is reduced from 200 MW to 160 MW throughout the fault duration. Once the fault has been cleared, the WECSs and dc-dc converter can be enabled (with $En_1 = 1$ and $En_2 = 1$), allowing the smooth power transfer restoration of WG_1, therefore overall, 200 MW power transmission retains, see Fig. 5.6(k) and (l).

5.3.2 HVDC Cable Short Circuit Fault Case

The severity of HVDC cable faults is extremely high as the full power transfer is eliminated. One of the key operating objectives throughout is to secure components against harmful transient high voltages and/or currents. An HVDC cable fault (marked as F_2 in Fig. 55) is applied from 0.3 s to 0.5 s, and the time-domain simulation results are shown in Fig. 5.7.

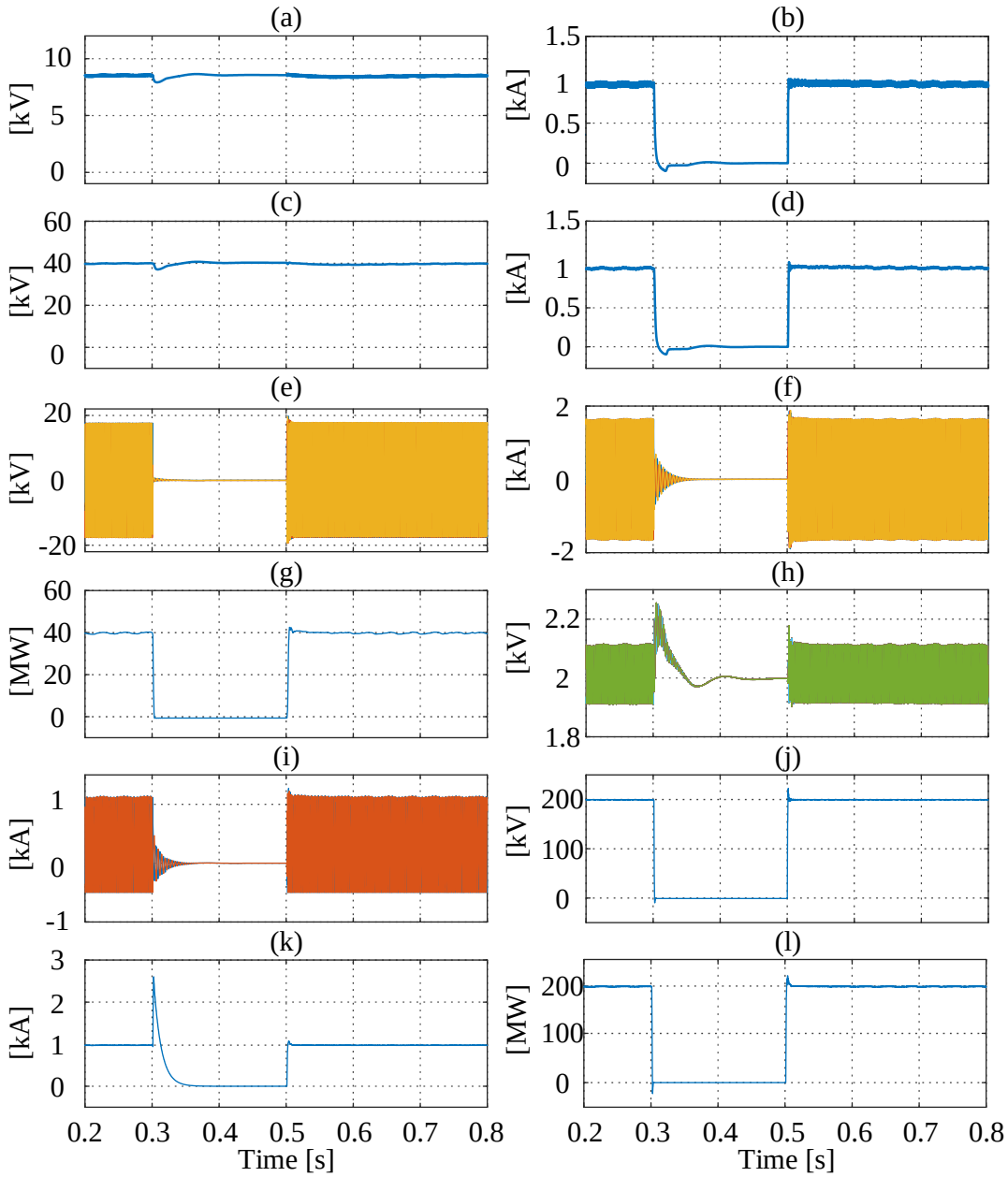

Fig. 5.7. Simulation results of HVDC cable short circuit fault (F_2). (a) WG_1 $WECS_{11}$ output voltage. (b) WG_1 $WECS_{11}$ output current. (c) WG_1 MVDC link voltage. (d) WG_1 MVDC link current. (e) WG_1 dc-dc converter ac bus voltage. (f) WG_1 dc-dc converter ac bus current. (g) WG_1 dc-dc converter power. (h) WG_1 dc-dc converter MMC capacitor voltage. (i) WG_1 dc-dc converter MMC arm current. (j) HVDC link voltage. (k) HVDC link OWF-side current. (l) HVDC link power.

With the fault occurrence, the HVDC voltage is depressed to 0 as shown in Fig. 5.7(j), and the OWF-side HVDC link current encounters a sharp discharge current at about 2.5 pu (which can be tolerated by the rectification stage diodes) as shown in Fig. 5.7(k). Also, the HVDC link current decays with zero power transferrable, see Fig. 5.7(k) and (l). In terms of the WGs, as all WGs are operated to follow the same operation after the fault is detected at approximately 0.301 s, only WG_1 waveforms are given herein.

The WG_1 dc-dc converter can stop its ac bus voltage synthesis, with its current decays to zero shortly, as shown in Fig. 5.7(e) and (f); therefore, the HB-MMC operation and the WG (and dc-dc converter) power transfer are stopped as well, see Fig 5.7(g)-(i). The minor overvoltage at the HB-MMC SM capacitor is due to the collective effects of WECS operation and the stray parameters of the dc collectors. The WECSs are blocked, effectively ceasing all power contribution to the HVDC system, and consequently ceasing power transfer through the MVDC links, which reduces the MVDC current to zero without breaching current limits, as in Fig. 5.7(b) and (d). The HB-MMC can still operate, although without power transfer, to maintain the MVDC link voltage, as shown in Fig. 5.7(a) and (c). When the fault is cleared at 0.5 s, all WGs can retain normal operation, and the system recovery can be promptly initiated.

5.3.3 Weight and Volume Comparison Case Study

This subsection presents weight and volume comparison between the offshore platforms of the conventional MMC-HVDC based OWF and the proposed OWF. The conventional MMC-HVDC system illustrated as per Fig. 5.1(a) is detailed in [22], where ac-based wind turbines are connected to a centralised offshore HB-MMC station via step-up transformers. As specific information regarding weight and volume of specific converter and magnetic components are proprietary, weight and volume of three-phase step-up transformers can be estimated to be 620 kg/MW and 2 m^3/MW respectively [23]. The weight and volume of the offshore HB-MMC (excluding power transformer) can be estimated to be 1250 kg/MW and 50 m^3/MW respectively [24]. These data can be used to qualify minimum weight and size requirements of the conventional MMC-HVDC station on its platform. Due to the importance in such a centralised system, the converter transformer is typically deployed with redundancy, which will significantly increase weight and size requirements on the offshore platform. However, for simplicity, design for redundancy and protection is not considered throughout this assessment. Thus, the offshore converter station mainly consists of a fully sized HB-MMC and a fully sized transformer. The offshore platforms for the proposed OWF are mainly for the WG dc-dc converters, each of which mainly consists of an HB-MMC, a three-phase ac transformer, and a three-phase diode rectifier. One of the main differences herein is that the dc-dc converter internal

ac bus is operating at MF ranges (hundreds Hz), which would lead to reduced weight/volume of passive components [25]. For the HB-MMC, higher frequency would lead to lower submodule (SM) capacitance and arm inductance [26]. The sizing/selection of SM capacitors and arm inductors for practical applications are dependent on various considerations such as operation points, frequency selection, tolerated ripples, manufacturing limitations, etc.; therefore, the estimation can be performed based on the effects of increased frequency, with reasonable margins included [27], [28]. Given that the SM capacitor account for around 80% weight and 50% size, it can be estimated that the weight and volume of the HB-MMC reduce to 0.4 and 0.6 times the conventional HB-MMC, respectively [29], [30], whereas the reduction of arm inductors is ignored due to the strict isolation and insulation requirements within the equipment. With the MF ac bus, transformer weight and volume are estimated to be 0.6 and 0.7 times the conventional 50 Hz ac transformer respectively, according to [31] and including margins for isolation and insulation. For the diode rectifier, the weight and volume can be estimated to be 40 kg/MW and 0.3 m^3/MW [32]. For the studied case, the diode rectifier for the proposed system has the weight of about 8 tonnes and a volume of about 60 m^3, which are negligible considering the overall values.

Fig. 5.8(a) shows the comparison of transformer, converter and overall system weights for the case-studied 200 MW system, whilst Fig. 5.8(b) shows the volume comparison. In general, the offshore station of the proposed OWF system is estimated to be approximately 49% and 61% of the weight and volume of a conventional MMC-HVDC system respectively. It is noted that the estimated weight and volume reduction of the proposed system is based on high-level study considering conservative design margins. The actual weight and volume values are highly related to the offshore dc-dc converter parameter selection and engineering optimisation. Philosophically, the proposed dc-based OWF architecture successfully overcomes the weight/volume reduction limitation of conventional 50/60 Hz MMC-HVDC systems. Instead, in the proposed OWF system, the internal ac system within dc-dc converters enables much higher design/optimisation flexibility and thereby can operate at a significantly higher frequency (at MF ranges). Thus, the proposed OWF system could achieve a significant

reduction in terms of weight and size requirements on offshore platforms, which is one of the most attractive features of the proposed system.

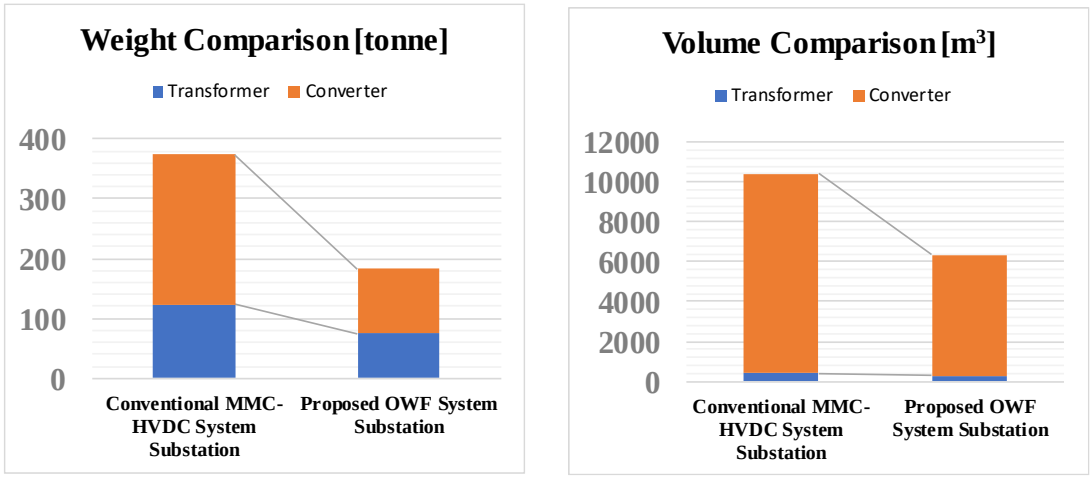

(a) (b)

Fig. 5.8. Weight and Volume comparison. (a) Estimated weight comparison. (b) Estimated volume comparison.

5.4 Summary

This chapter proposed a novel dc-based offshore wind farm (OWF) architecture, incorporating multiple medium-voltage dc (MVDC) collector systems and a high-voltage dc (HVDC) transmission system with reduced power conversion stages in comparison to published research. The MVDC-level system is achieved through series connected wind turbine units incorporating dc-dc converters as presented in chapter 4. The HVDC link is achieved through the proposed lightweight unidirectional dc-dc converter, which employs a medium-frequency (MF) internal ac bus between a modular multilevel converter (MMC) and a diode rectifier. A grouping philosophy has been presented in this paper to facilitate the parallel connection of the dc-dc converters, enabling flexible and robust multi-terminal dc (MTDC) configuration. Critical control systems have been developed to ensure reliable operation and secure fault ride-through. System performance was substantiated by time-domain simulation, verifying system resiliency in both MVDC collector and HVDC cable fault cases. Also, the presented assessment demonstrated that the proposed architecture leads to significant reduction in terms of the overall offshore weight and volume requirements, compared to a centralised MMC-based OWF system. The proposed dc based OWF concept,

which features high resiliency against faults and reduced offshore weight/size requirement, would be competitive in future OWF applications.

References

[1] F. Rong, G. Wu, X. Li, S. Huang, and B. Zhou, "All-DC offshore wind farm with series-connected wind turbines to overcome unequal wind speeds," *IEEE Trans Power Electron*, vol. 34, no. 2, pp. 1370–1381, Feb. 2019, doi: 10.1109/TPEL.2018.2834965.

[2] A. O. Almeida, I. F. Lopes, P. M. Almeida, M. A. Tomim, J. A. Passos Filho, and P. G. Barbosa, "Series-DC connection of offshore wind generating units: Modeling, control and galvanic isolation.," *Electric Power Systems Research*, vol. 195, Jun. 2021, doi: 10.1016/j.epsr.2021.107149.

[3] M. Guan, "A series-connected offshore wind farm based on modular dual-active-bridge (DAB) isolated DC–DC converter," *IEEE Transactions on Energy Conversion*, vol. 34, no. 3, pp. 1422–1431, May 2019, doi: 10.1109/tec.2019.2918200.

[4] Q. Wei, B. Wu, D. Xu, and N. R. Zargari, "Further study on a PWM current-source-converter-based wind energy conversion system considering the DC-link voltage," *IEEE Trans Power Electron*, vol. 34, no. 6, pp. 5378–5387, Jun. 2019, doi: 10.1109/TPEL.2018.2866045.

[5] H. Liu, M. S. A. Dahidah, J. Yu, R. T. Naayagi, and M. Armstrong, "Design and control of unidirectional DC-DC modular multilevel converter for offshore DC collection point: Theoretical analysis and experimental validation," *IEEE Trans Power Electron*, vol. 34, no. 6, pp. 5191–5208, Jun. 2019, doi: 10.1109/TPEL.2018.2866787.

[6] H. Zhang, F. Gruson, D. M. F. Rodriguez, and C. Saudemont, "Overvoltage limitation method of an offshore wind farm with DC series-parallel collection grid," *IEEE Trans Sustain Energy*, vol. 10, no. 1, pp. 204–213, Jan. 2019, doi: 10.1109/TSTE.2018.2829929.

[7] H. Liu, M. Dahidah, R. T. Naayagi, M. Armstrong, and J. Yu, "A novel modular multilevel step-up DC/DC converter for offshore systems," in *IEEE International Symposium on Industrial Electronics*, Institute of Electrical and Electronics Engineers Inc., Aug. 2017, pp. 576–581. doi: 10.1109/ISIE.2017.8001310.

[8] S. Wang, K. H. Ahmed, G. P. Adam, A. M. Massoud, and B. W. Williams, "A novel converter station structure for improving multiterminal HVDC system resiliency against AC and DC faults," *IEEE Transactions on Industrial Electronics*, vol. 67, no. 6, pp. 4270–4280, Jun. 2020, doi: 10.1109/TIE.2019.2926036.

[9] B. Wu, Y. Lang, N. Zargari, and S. Kouro, "Power converters in wind energy conversion systems," *Power Conversion and Control of Wind Energy Systems*, pp. 87–152, 2011, doi: 10.1002/9781118029008.ch4.

[10] A. O. Almeida, M. A. Tomim, P. M. Almeida, and P. G. Barbosa, "A control strategy for an offshore wind farm with the generating units connected in series with a VSC-HVDC transmission link," *Electric Power Systems Research*, vol. 180, Mar. 2020, doi: 10.1016/j.epsr.2019.106121.

[11] H. J. Bahirat and B. A. Mork, "Operation of DC series-parallel connected offshore wind farm," *IEEE Trans Sustain Energy*, vol. 10, no. 2, pp. 596–603, Apr. 2019, doi: 10.1109/TSTE.2018.2839712.

[12] G. Guo, K. Zha, J. Zhang, Z. Wang, F. Zhang, and J. Cao, "Grounding fault in series-connection-based offshore wind farms: Fault clearance," *IEEE Trans Power Electron*, vol. 35, no. 9, pp. 9357–9367, Sep. 2020, doi: 10.1109/TPEL.2020.2971640.

[13] J. Tait, S. Wang, and K. H. Ahmed, "An Enhanced Series-Connected Offshore Wind Farm (SC-OWF) System Considering Fault Resiliency," *IEEE Transactions on Power Delivery*, pp. 1–11, 2022, doi: 10.1109/TPWRD.2022.3219373.

[14] S. Wang, G. P. Adam, A. M. Massoud, D. Holliday, and B. W. Williams, "Analysis and assessment of modular multilevel converter internal control schemes," *IEEE J Emerg Sel Top Power Electron*, vol. 8, no. 1, pp. 697–719, Mar. 2020, doi: 10.1109/JESTPE.2019.2899794.

[15] ABB, "ABB wind turbine converters : ACS880, 800 kW to 8 MW," 2018. Accessed: Sep. 20, 2022. [Online]. Available: https://search.abb.com/library/Download.aspx?DocumentID=3AUA0000231755&LanguageCode=en&DocumentPartId=&Action=Launch

[16] Siemens, “The new benchmark for highest availability and maximum energy yield: Sinamics W180,” 2022. https://new.siemens.com/us/en/markets/wind/equipment/energy-generation/wind-converters.html (accessed Sep. 20, 2022).
[17] A. Bensalah, G. Barakat, and Y. Amara, “Electrical generators for large wind turbine: trends and challenges,” *Energies (Basel)*, vol. 15, no. 18, p. 6700, Sep. 2022, doi: 10.3390/en15186700.
[18] Siemens Gamesa Renewable Technology, “SG 8.0-167 DD offshore wind turbine,” 2022. https://www.siemensgamesa.com/products-and-services/offshore/wind-turbine-sg-8-0-167-dd (accessed Sep. 20, 2022).
[19] P. Hou, W. Hu, M. Soltani, and Z. Chen, “Optimized placement of wind turbines in large-scale offshore wind farm using particle swarm optimization algorithm,” *IEEE Trans Sustain Energy*, vol. 6, no. 4, pp. 1272–1282, Oct. 2015, doi: 10.1109/TSTE.2015.2429912.
[20] S. Cui, N. Soltau, and R. W. de Doncker, “A high step-up ratio soft-switching DC-DC converter for interconnection of MVDC and HVDC grids,” in *IEEE Transactions on Power Electronics*, Institute of Electrical and Electronics Engineers Inc., Apr. 2018, pp. 2986–3001. doi: 10.1109/TPEL.2017.2702207.
[21] D. van Hertem, O. Gomis-Bellmunt, and J. Liang, *HVDC grids: For offshore and supergrid of the future*. IEE, 2016.
[22] U. Karaagac, J. Mahseredjian, L. Cai, and H. Saad, “Offshore wind farm modeling accuracy and efficiency in MMC-based multiterminal HVDC connection,” *IEEE Transactions on Power Delivery*, vol. 32, no. 2, pp. 617–627, Apr. 2017, doi: 10.1109/TPWRD.2016.2522562.
[23] U.S Department of Energy, “Large power transformers and the U.S. electric grid.” Accessed: Nov. 19, 2022. [Online]. Available: https://www.energy.gov/sites/prod/files/Large%20Power%20Transformer%20Study%20-%20June%202012_0.pdf
[24] P. Lundberg, “HVDC light: Power from shore,” 2016. Accessed: Sep. 20, 2022. [Online]. Available: https://new.abb.com/docs/librariesprovider46/pw2016/seminars/r607-en-abb_hvdc_light_power_from_shore.pdf?sfvrsn=2
[25] M. Zygmanowski, B. Grzesik, and R. Nalepa, “Capacitance and inductance selection of the modular multilevel converter,” in *2013 15th European Conference on Power Electronics and Applications (EPE)*, IEEE, Sep. 2013, pp. 1–10. doi: 10.1109/EPE.2013.6634446.
[26] G. P. Adam, I. A. Gowaid, S. J. Finney, D. Holliday, and B. W. Williams, “Review of dc–dc converters for multi-terminal HVDC transmission networks,” *IET Power Electronics*, vol. 9, no. 2, pp. 281–296, Feb. 2016, doi: 10.1049/iet-pel.2015.0530.
[27] Y. Tang, L. Ran, O. Alatise, and P. Mawby, “Capacitor selection for modular multilevel converter,” *IEEE Trans Ind Appl*, vol. 52, no. 4, pp. 3279–3293, Jul. 2016, doi: 10.1109/TIA.2016.2533620.
[28] J. E. Huber and J. W. Kolar, “Volume/weight/cost comparison of a 1MVA 10 kV/400 V solid-state against a conventional low-frequency distribution transformer,” in *2014 IEEE Energy Conversion Congress and Exposition (ECCE)*, IEEE, Sep. 2014, pp. 4545–4552. doi: 10.1109/ECCE.2014.6954023.
[29] Y. Tang, M. Chen, and L. Ran, “A compact MMC submodule structure with reduced capacitor size using the stacked switched capacitor architecture,” *IEEE Trans Power Electron*, pp. 1–1, 2015, doi: 10.1109/TPEL.2015.2511189.
[30] D. Han, J. Noppakunkajorn, and B. Sarlioglu, “Comprehensive efficiency, weight, and volume comparison of SiC- and Si-based bidirectional DC–DC converters for hybrid electric vehicles,” *IEEE Trans Veh Technol*, vol. 63, no. 7, pp. 3001–3010, Sep. 2014, doi: 10.1109/TVT.2014.2323193.
[31] U. Drofenik, “A 150 kW medium frequency transformer optimized for maximum power density,” in *2012 7th International Conference on Integrated Power Electronics Systems (CIPS)*, Nuremberg, Germany: IEEE, Mar. 2012.
[32] Mouser Electronics, “Infineon technologies D2601NH90T,” 2022. https://www.mouser.co.uk/ProductDetail/Infineon-Technologies/D2601NH90T?qs=667VNtDUsoOVEkZ6DWM0uw%3D%3D (accessed Sep. 20, 2022).

Chapter 6

Conclusions

6.1 General conclusions

This research focussed on securing offshore wind farms, with a particular focus on dc collector offshore networks with series connected wind turbines. Various topologies, network structures and control methods have been introduced and verified through means of time-domain simulations and qualitative substantiation.

Chapter 2 reviewed proposed research regarding aspects of reliability, resilience, and secure system operation during ac grid and dc collector faults. The review investigated this at both wind turbine and wind farm level. At wind turbine level the review suggests that current techniques regarding wind turbine level security can be achieved using energy storage systems. However, each technology presents their own practical, financial, and technical challenges for wind turbine level integration. The use of coordinated control systems in addressing energy imbalance may inflict stresses to the mechanical and electrical components of the wind turbine if not coordinated with other methods. Offshore wind farms utilising series connected wind turbines as a means of directly establishing transmission voltage without offshore infrastructure have been investigated. The outcomes of the review suggested that the literature is only focused on steady state operation of such systems and no deep investigation has been carried out for major risks to resiliency in the event of a dc network fault, which demonstrates cascading phenomena. The use of dc link voltage control in series connected systems requires the use of curtailment and or energy storage to ensure balancing during inter-string wind speed variability. If balancing is not addressed promptly system overvoltage's can occur, which may pose risks to system reliability. The use of dc link current control can off benefits to the system balancing if applied correctly, however can incur additional system losses at low power export levels. Systems configured in a series parallel configuration are subject to the same security risks as series connected systems, particularly regarding interesting and intergroup balancing. Due to the parallel connection of multiple series strings voltage control is often proposed, as current control is technically difficult to apply to such a structure sue the inter group

voltage fluctuations. Series parallel systems often rely on dc circuit breakers to provide prompt isolation of a faulted section of network. Although effective, implementation incurs cost, weight, and volume penalties to the offshore substations.

In Chapter 3, four low voltage fault ride through (LVFRT) techniques, namely, coordinated control (CC), dumping resistor (DR), superconductive magnetic energy storage (SMES), and supercapacitor energy storage systems (SCES), were presented, and investigated to enhance the performance of wind energy conversion systems (WECS) to ensure reliability of the system during ac network faults. General design has been introduced, and the performance and features have been comprehensively assessed by time-based simulations and critical performance metrics. Although mitigating hardware requirements, the CC is the least effective, and not suitable for LVFRT due to grid code compliance issues and the high level of dc-link voltage during faults. Although CC has advantages when used in coordination with additional techniques, allowing reduced size and cost of additional components. The DR, which has been widely used in industry, was proved to be an effective method of LVFRT; however, concerns arise with the dependence on cooling and overheating due to spurious operation from poorly defined operating set-points could result in a system failure. Such a risk could be reduced by energy storage system (ESS) based methods, which have improved heat management ability and fault energy controllability. Although the simulation results show good LVFRT performance, the high levels of practical complexity and capital costs make SMES currently relatively unrealistic for integration at the wind turbine level. From a simulation perspective, the SCES can offer desirable performance and attractive benefits with flexible use of stored energy cells. Although the practical complexities are lower than SMES, SCES is still commercially immature for such turbine level applications, which is reflected in the capital costs and practical engineering challenges for integration at wind turbine level. Nevertheless, energy storage systems might be suitable for secure renewable system construction.

Chapter 4 proposed a series-connected offshore wind farm (SC-OWF) system with novel architecture and control, which prioritise, thus enhance, resiliency against typical faults of high severity. The proposed offshore substation arrangement and manipulation strategies allow the series-connected wind energy converter systems

(WECSs) to be electrically grouped, achieving effective fault isolation/bypassing and reducing the risks of permanent generation loss. Also, offshore network complexity and costs are low, through the collective implementation of the WECSs with diode rectifier output stage and the offshore substation utilising diodes and disconnectors. The onshore subsystem employs a dc-fault-tolerant modular multilevel converter (MMC) with constant dc current control and a dc offset modifier (DOM) mechanism, which can maximise power generation during normal operation and ensure transmission system safety during dc/ac faults. System behaviour in four typical dc/ac fault cases were presented, indicating the operational effectiveness. The proposed system can eliminate the requirement of massive offshore converter stations with significantly reduced cost, which was confirmed by a comparative estimation between an offshore MMC station and the proposed system. The proposed SC-OWF system would be applicable for future offshore wind generation applications, however limitations exist regarding component rating and future expansion of the SC-OWF limiting the overall power export capability of the wind farm. In addition, the scheme presented is reliant on an onshore converter station which utilises full-bridge sub modules (FB-SM), although the architecture proposes a hybrid system aiming to reduce the number of FB-SM required, there is a cost and weight penalty involved.

Chapter 5 proposed a novel dc-based offshore wind farm (OWF) architecture, incorporating multiple medium-voltage dc (MVDC) collector systems and a high-voltage dc (HVDC) transmission system. The MVDC-level system is realised by the series connection of wind turbine units, and the HVDC link is achieved through lightweight dc-dc converters, where a medium-frequency (MF) internal ac bus is used between a modular multilevel converter (MMC) and a diode rectifier. A grouping concept has been proposed in this thesis to allow parallel connection of the dc-dc converters, enabling flexible and robust multi-terminal dc (MTDC) configuration. Essential control systems were designed to ensure reliable operation and secure fault ride-through. System performance was substantiated by time-domain simulation, verifying system resiliency in both MVDC collector and HVDC cable fault cases. Also, the presented assessment demonstrated that the proposed architecture leads to significant reduction in terms of the overall offshore weight and volume requirements, compared to a centralised MMC-based OWF system. The proposed dc based OWF

concept, which features high resiliency against faults and reduced offshore weight/size requirement, would be competitive in future OWF applications. The system eliminates the requirements for dc circuit breakers and provides a lightweight alternative reducing infrastructure costs. However, the system proposed is reliant on curtailment of energy during contingency periods and steady wind variation. The dc-dc converter employed for the scheme was selected for its robust nature to faults however poses limitations through the application of a single active bridge topology.

6.2 Author's Contributions

The following highlights what is deemed to be the significant contributions of this thesis:

- A comprehensive assessment of the evaluated techniques as the potentially feasible LVFRT techniques.
- A control structure facilitating current control mode was proposed, which provides instantaneous balancing between offshore wind turbines and onshore conversion system, which is suitable for both ac and dc network faults.
- A new control structure for series connected wind turbines connected in a series connected wind farm was proposed, which automatically de-loads during an ac grid fault.
- A fault ride through methodology was proposed for series connected offshore wind farms.
- A lightweight, low complexity bypass station was proposed for series connected offshore wind farms, which provides an external bypass function, greatly increasing the security and reducing risk of total power loss during open and short circuit faults on the dc network.
- A reduced converter stage multi-terminal dc applicable offshore wind farm was proposed implementing a unidirectional lightweight converter station.
- An adaptive phase shift control algorithm was implemented to the lightweight converter station to overcome power quality issues associated with diode bridges.

- A control algorithm was established based on voltage control mode for series connected wind farm groups allowing lower cost half-bridge modules for the unidirectional offshore converter station.

6.3 Future Research

- Improved control structure to remove communications from instantaneous balancing off proposed series connected offshore wind farm.
- Cost reduction analysis and investigation into loss reduction algorithm for modular-multilevel converters operating in current control mode.
- Real time digital simulation (RTDS), implementing hardware, where practical, for the proposed series connected wind farm to further verify its performance and feasibility.
- Investigation into wind turbine level dc-dc converters for offshore wind farms facilitating dc collectors. Although a single active bridge has been proposed in this thesis, additional benefits may be achieved through the adoption of higher performance converters.
- Further investigation into control structure, for series connected wind turbines connected in voltage control mode. Currently there is a reliance on curtailment and energy storage options could be a viable option to prevent this.
- More detailed fault analysis on both series and lightweight series parallel topologies, which includes additional fault scenarios including internal converter faults.

Appendix A. *Low Voltage Fault Ride Though Simulink Model Sample*

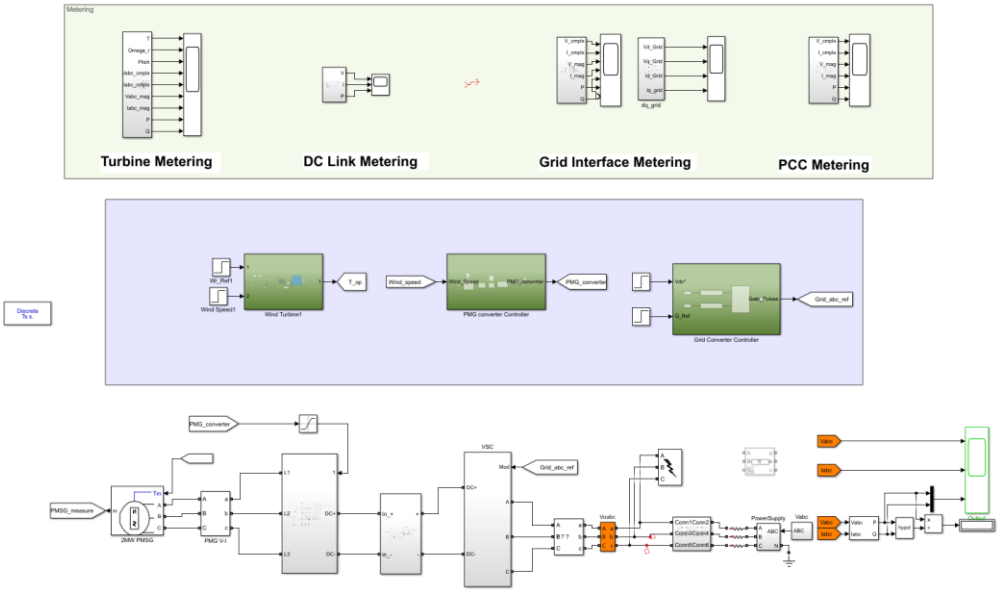

Fig. A1.1 Network overview of grid connected low voltage fault ride through model.

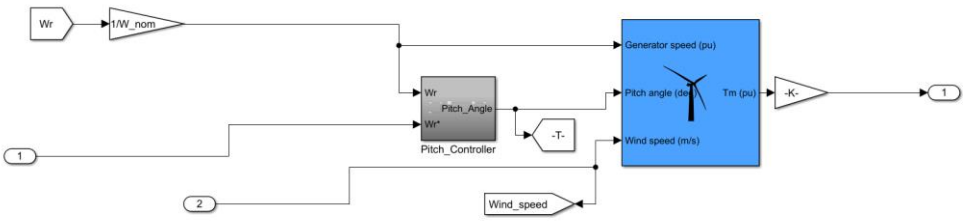

Fig. A1.2 Overview of wind turbine model of grid connected low voltage fault ride through model.

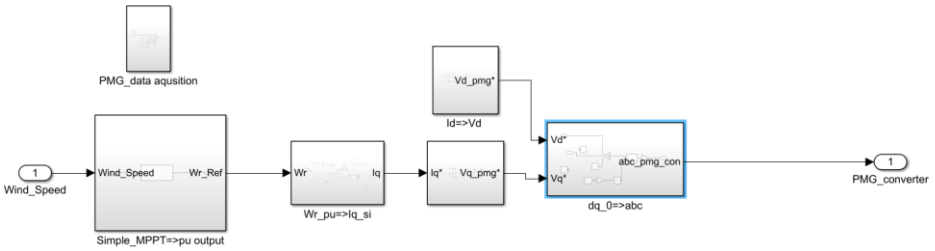

Fig. A1.3 Overview of generator side control structure of grid connected low voltage fault ride through model.

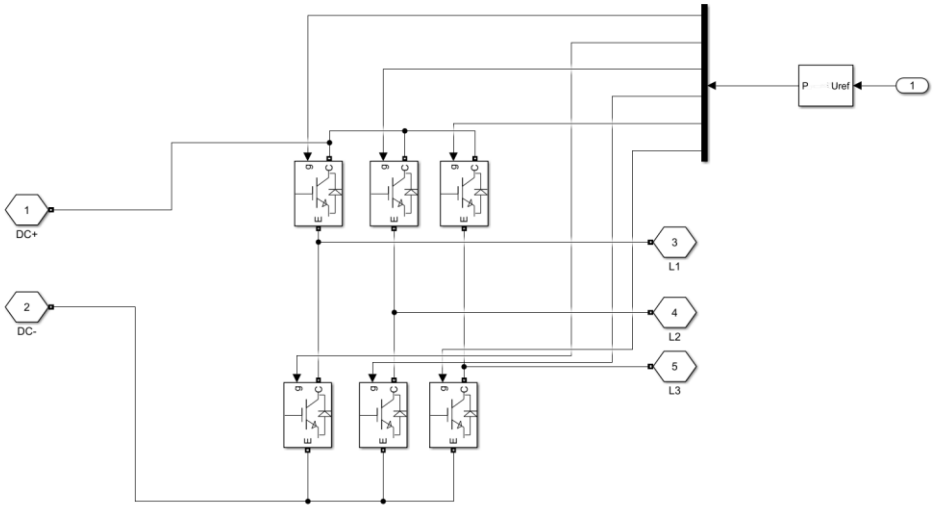

Fig.A1.4 Overview of generator-side and grid side converter of grid connected low voltage fault ride through model.

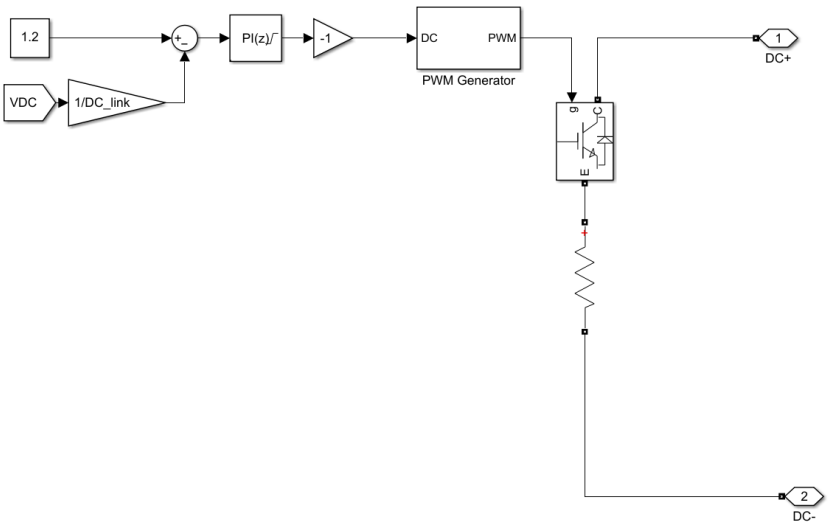

Fig.A1.5 Overview of dumping resistor and control of grid connected low voltage fault ride through model.

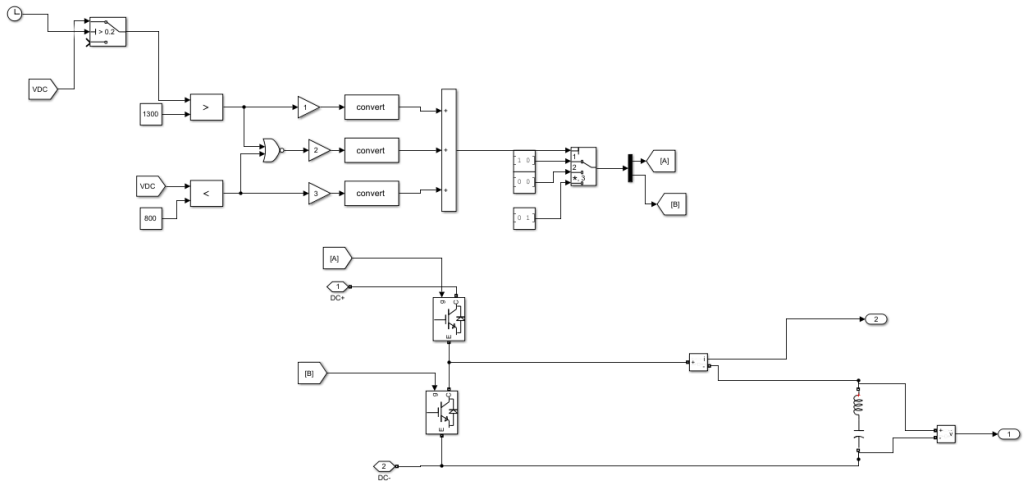

Fig.A1.6 Overview of supercapacitor energy storage and control of grid connected low voltage fault ride through model.

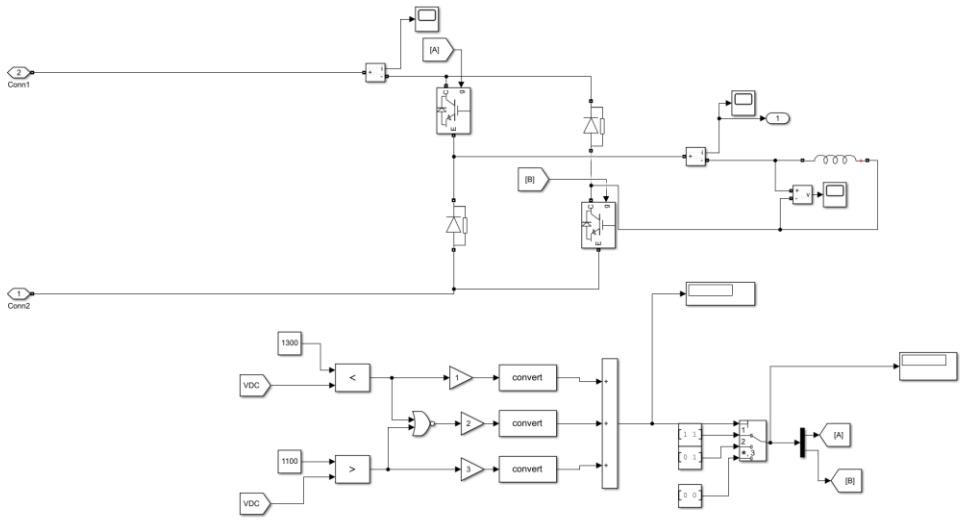

Fig.A1.7 Overview of superconductive magnetic energy storage and control of grid connected low voltage fault ride through model.

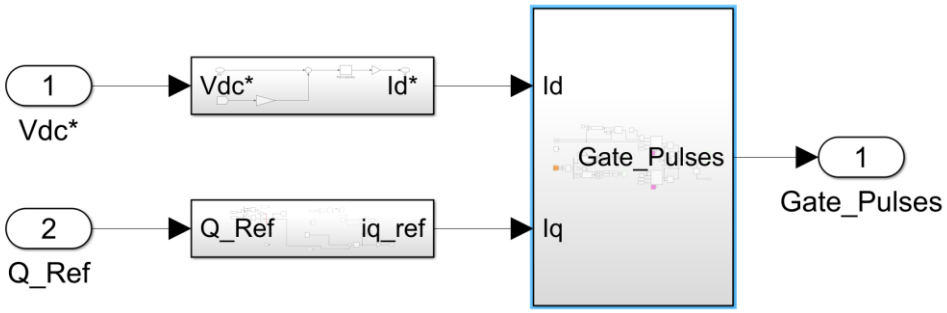

Fig.A1.8 Overview of grid-side control of grid connected low voltage fault ride through model.

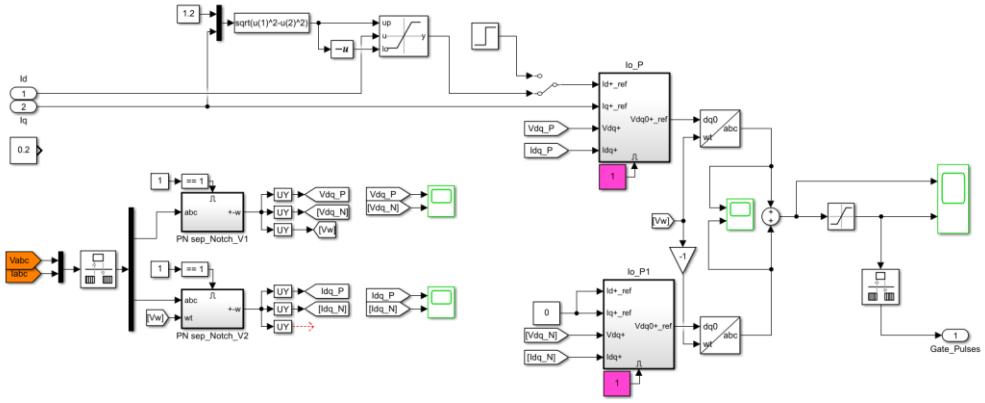

Fig.A1.9 Overview of inner-loop current control and PLL of grid connected low voltage faut ride through model.

Appendix B. *Series-Connected Wind Farm Simulink Model Sample*

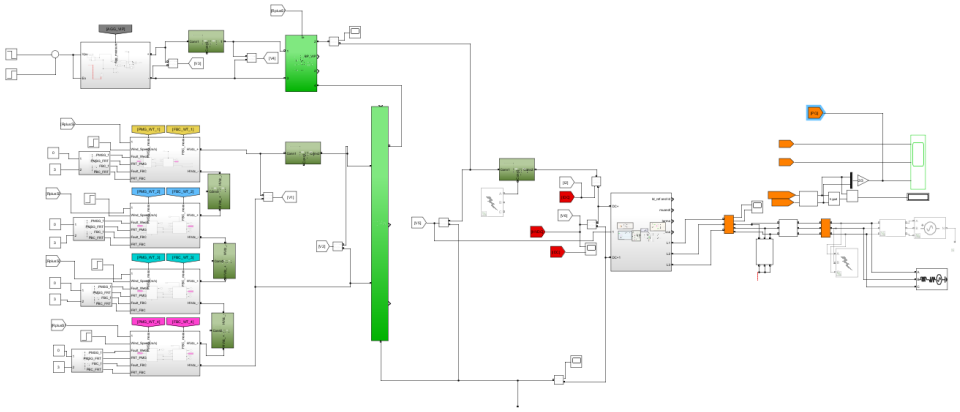

Fig.A2.1 Overview of network for series-connected wind farm model.

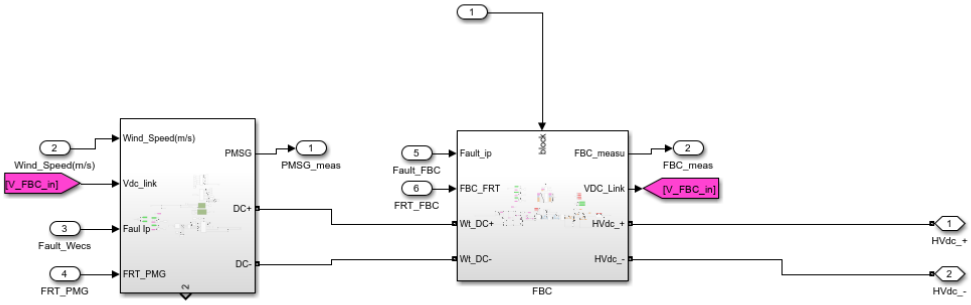

Fig.A2.2 Overview of wind energy conversion system for series-connected wind farm model.

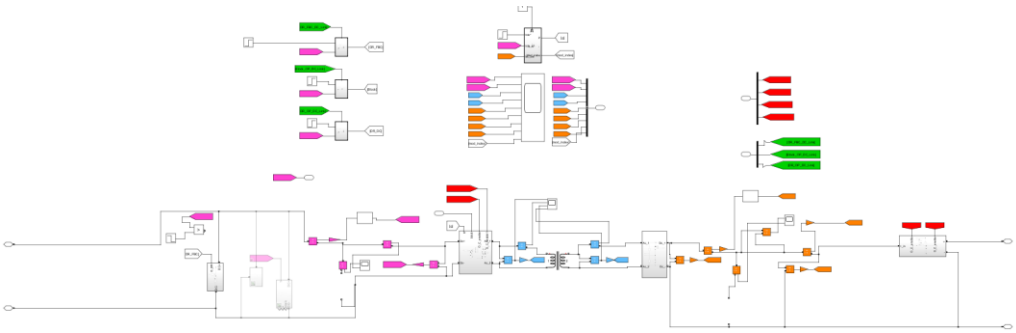

Fig.A2.3 Overview of dc-dc converter for series-connected wind farm model.

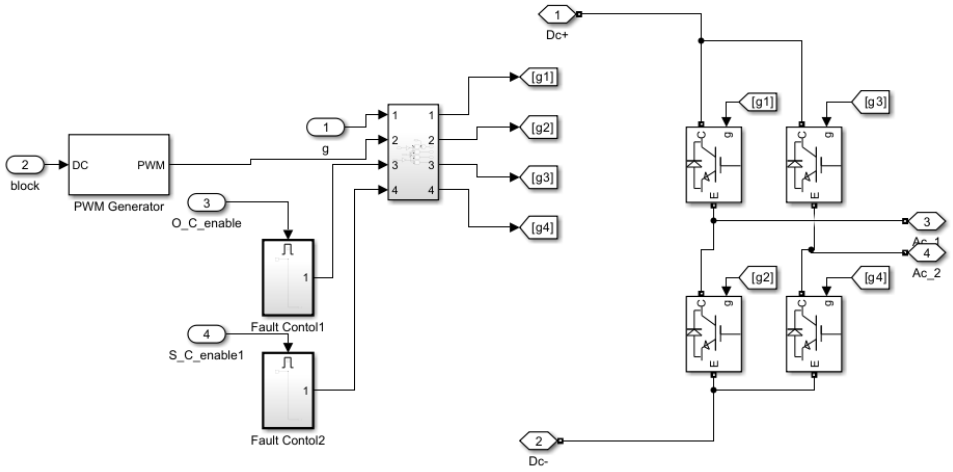

Fig.A2.4 Overview of single active bridge for dc-dc converter for series-connected wind farm model.

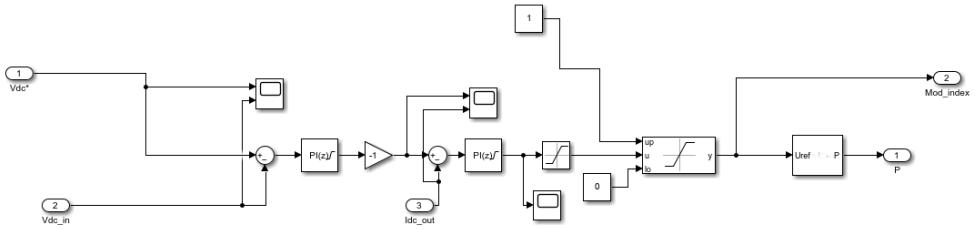

Fig.A2.5 Overview of single active bridge control structure for dc-dc converter for series-connected wind farm model.

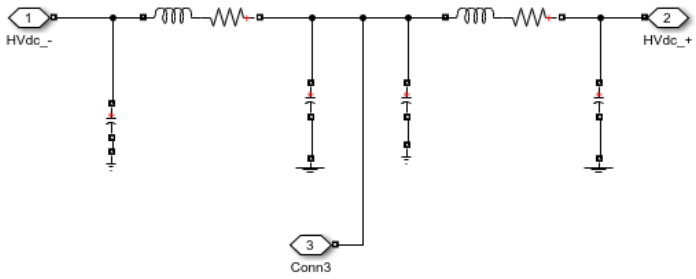

Fig.A2.6 Overview of dc cable for series-connected wind farm model.

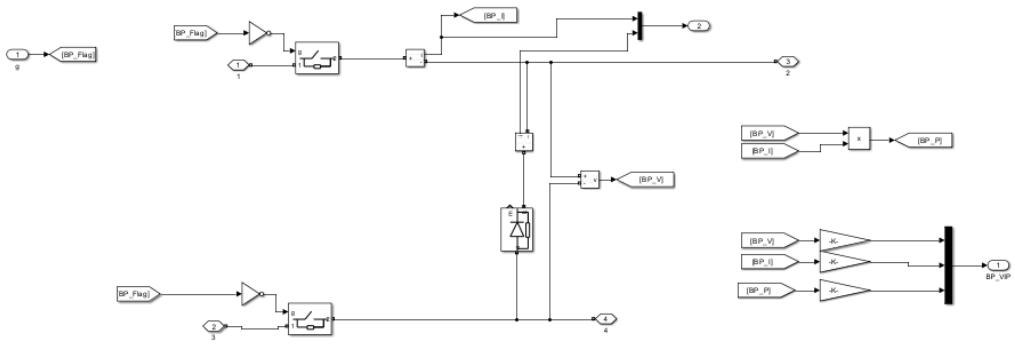

Fig.A2.7 Overview of offshore substation for series-connected wind farm model.

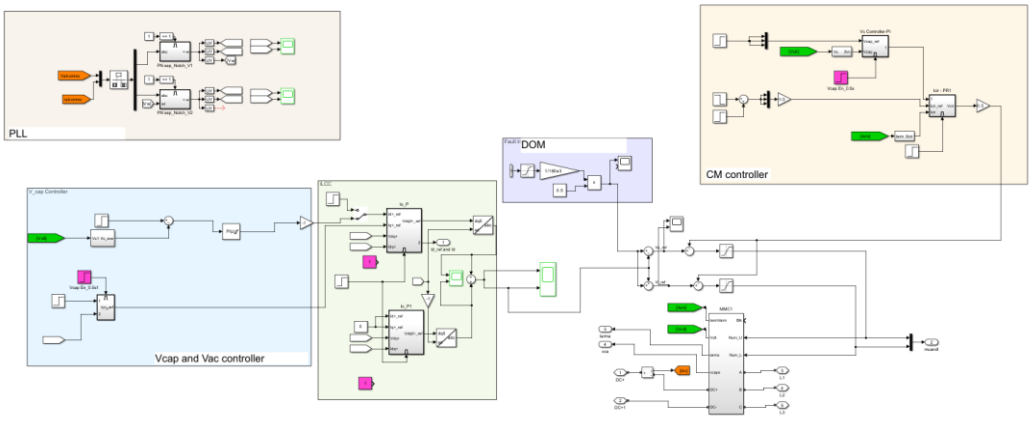

Fig.A2.8 Overview of MMC control structure for series-connected wind farm model.

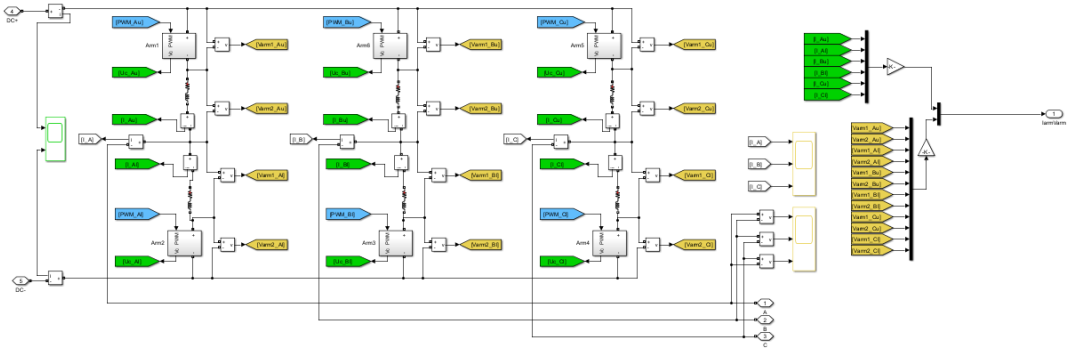

Fig.A2.9 Overview of FB-MMC for series-connected wind farm model.

Appendix C. *Series-Parallel-Connected Wind Farm Simulink Model Sample*

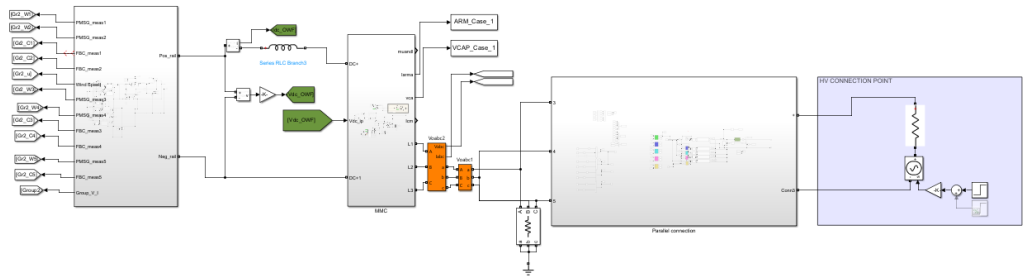

Fig.A3.1 Overview of network for series-parallel-connected wind farm model.

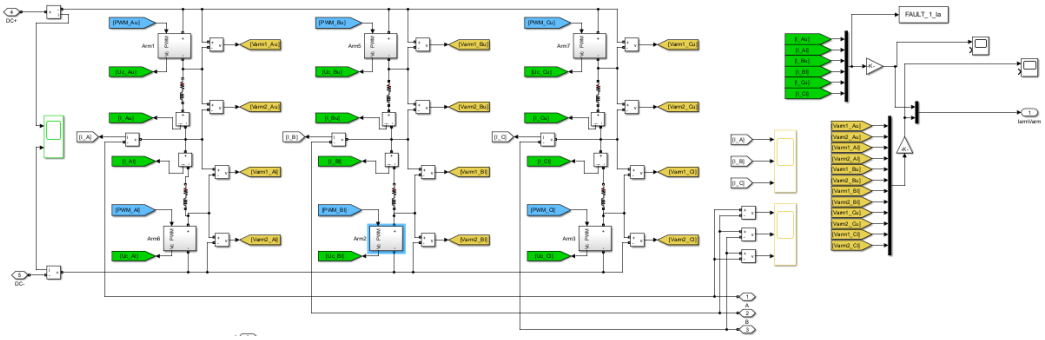

Fig.A3.1 Overview of HB-MMC for series-parallel-connected wind farm model.

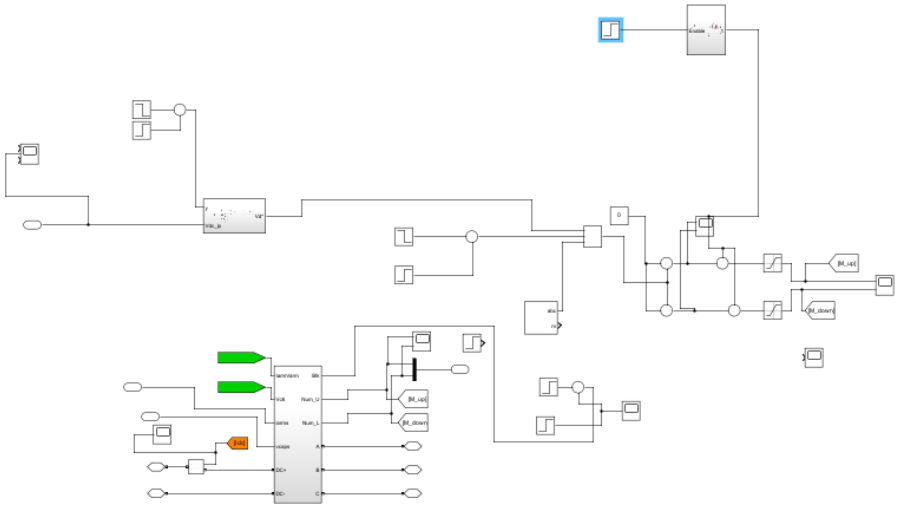

Fig.A3.1 Overview of HB-MMC control structure for series-parallel-connected wind farm model.

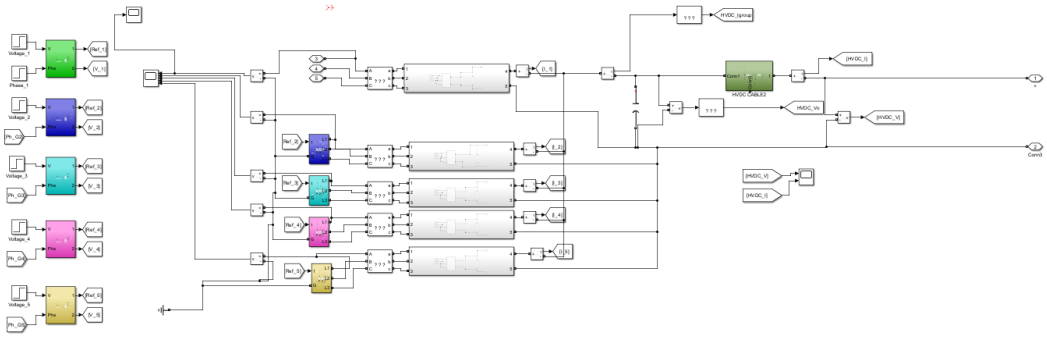

Fig.A3.1 Overview of adaptive phase shift control and HVDC connection point for series-parallel-connected wind farm model.

Appendix D. *Sample Generator and Converter Parameters*

```
%%%%%%%%%%%%%%%%%%%%%%%%%%%%%%%%%%%%%%%%%%%%%%%%%%%%
%%  8 MW PMSG Settings
%%%%%%%%%%%%%%%%%%%%%%%%%%%%%%%%%%%%%%%%%%%%%%%%%%%%
P_nom_wt=8e6;       %Wind Turbine nominal Power
V_nom_wt=0.69e3;    %Wind Turbine nominal Voltage
T_nom_wt=3.4e6;     %Wind Turbine nominal Torque
F_nom_wt=9.75;      %Nominal Frequency
Omega_nom_wt=2.356;  %Wind Turbine nominal rotor speed
Pole_paris_wt=26;    %PMSG Pole Pairs
Flux_link_wt=5.8624; %PMSG Flux linkage
R_s_wt=0.205e-3;     %PMSG Stator resistance
Ld_wt=0.3931e-3;     %PMSG d-axis inductance
Lq_wt=0.393e-3;     %PMSG q-axis inductance

%%%%%%%%%%%%%%%%%%%%%%%%%%%%%%%%%%%%%%%%%%%%%%%%%%%%
%% 8MW Full Bridge converter Ratings
%%%%%%%%%%%%%%%%%%%%%%%%%%%%%%%%%%%%%%%%%%%%%%%%%%%%
Fs_FBC=1e3;         %Switching Frequency
F_tx_FBC=1e3;       %Transformer Frequency
P_nom_Tx_FBC= 8e6;  %Transformer Rated Power
V_tx_FBC_p=1.2e3;   %Transfomer Primary Voltage
V_tx_FBC_s=10e3;    %Transformer Secondary Voltage
I_tx_FBC_p=P_nom_Tx_FBC/V_tx_FBC_p;     %Primary FLC
I_tx_FBC_s=P_nom_Tx_FBC/V_tx_FBC_s;     %Secondary FLC
Tx_FBC_Ltpu=0.2;    %Transformer Leakage reactance
Tx_FBC_Rtpu=0.01;   %Transformer Leakage resistance
DC_V_Nom=8e3;       %Nominal DC link Voltage
DC_I_Nom=P_nom_Tx_FBC/DC_V_Nom; %Nominal DC link Current

%%%%%%%%%%%%%%%%%%%%%%%%%%%%%%%%%%%%%%%%%%%%%%%%%%%%
% 8MW Passives Calculation
%%%%%%%%%%%%%%%%%%%%%%%%%%%%%%%%%%%%%%%%%%%%%%%%%%%%
Tau_C_in=10e-3;     %Capacitor Time Constant
Tau_C_out=10e-3;    %Capacitor Time Constant
Tau_L_out=1e-3;     %Capacitor Time Constant
C_tx_FB_p= (Tau_C_in*P_nom_Tx_FBC)/0.5/(V_tx_FBC_p^2);  %Input Capacitor
C_tx_FB_s= (Tau_C_out*P_nom_Tx_FBC)/0.5/(DC_V_Nom^2);   %Output Capacitor
L_tx_FB_s= (Tau_L_out*P_nom_Tx_FBC)/0.5/(DC_I_Nom^2);   %Output Inductor
```

Appendix E. *List of Figures*

Appendix F. *List of Tables*

Appendix G. *Author's Publications*

- **James Tait,** Khaled Ahmed**,** Grain Adam, "Comparative Analysis of Three Low Voltage Fault Ride Through Techniques for Wind Energy Conversion Systems", *2020 9th International Conference on Renewable Energy Research and Application (ICRERA)*, September 2020.

  Abstract - This paper compares the performances of three different Low Voltage Fault Ride- Through (LVFRT) techniques for Wind Energy Conversion Systems (WECS). The comparison aims to identify the most effective technique for alleviation of adverse impacts of ac faults on WECS electrical and mechanical parts, which include dc voltage rise and generator over-speed. The comparison is based on a critical qualitative review of existing literature on the selected LVFRT techniques, which are further supported by quantitative substantiation using simulations. The major findings of this comparative study are highlighted, with emphasis on metrics, which account for practical implementation, hardware, cost, and complexity issues. They are important to assess the overall effectiveness of the techniques evaluated. Although practical and commercial limitations exist, the initial findings suggest that an energy storage solution would be suitable for the enhancement of LVFRT for WECS in future power networks, and if the stored energy is utilised correctly, offer further attractive benefits.

- **James Tait**, Shuren Wang, Khaled Ahmed, Grain Philip Adam, "Comparative assessment of four low voltage fault ride through techniques (LVFRT) for wind energy conversion systems (WECSs)", *Alexandria Engineering Journal*, Volume 61, Issue 12, December 2022.

  Abstract - This paper presents a comparative assessment of four low voltage fault ride through (LVFRT) techniques that alleviate the effects of power imbalance during ac network faults for voltage source converter (VSC)-based wind energy conversion systems (WECSs). The techniques appraised include a software-based coordinated control (CC) technique, commercially available dumping resistor (DR) technique, and two energy storage techniques,

namely, superconductive magnetic energy storage (SMES) and supercapacitor energy storage (SCES). The techniques presented are technically viable solutions for alleviating impacts of ac network faults on the WECS. The techniques have previously been assessed by performance-based metrics, whereas this paper aims to form a more comprehensive assessment by expanding the scope from the performance-based comparison to include economic considerations and practical limitations. Based on qualitative review of technically viable designs, this study presents quantitative substantiation with time-domain simulations of symmetrical and asymmetrical ac network faults. The comparative assessment is formulated based on assessing key performance metrics including grid code compliance, electrical and mechanical stress reduction, LVFRT response speed, hardware implementation, system efficiency and investment reduction. The assessment findings suggest that a performance-based study fails to highlight the potential financial and practical barriers that may exist regarding the implementation of the LVFRT solutions especially with energy storage-based techniques. However, the flexibility, benefits and increasing feasibility regarding energy storage systems may make them a preferred option for LVFRT of critical WECSs.

- **James Tait**, Shuren Wang, Khaled H. Ahmed, "An Enhanced Series-Connected Offshore Wind Farm (SC-OWF) System Considering Fault Resiliency", *IEEE Transactions on Power Delivery (Early Access).*

  Abstract - The series-connected offshore wind farm (SC-OWF) is a promising offshore wind generation solution to mitigate the need of centralised offshore high-voltage/power converter stations. Predominantly, researchers have focused on the steady-state operation and control of SC-OWFs, without considering the system-level characteristics and ability to ride-through dc side and ac network faults. This paper proposes an enhanced system for SC-OWF applications with fault-resilient capability, where comprehensive circuit configuration and protection strategies are articulated to minimise, the negative effects caused by various types of dc and ac faults. For the offshore wind farm

architecture, a grouping scheme is adopted where a substation based on disconnectors and diodes is proposed to realise prompt fault bypass/isolation and protection functions in the event of offshore system faults. Additionally, an onshore fault-tolerant modular multilevel converter (MMC) with modified dc-system-oriented control is employed to enable smooth and secure operation under steady-state and fault conditions. The proposed SC-OWF system is quantitatively substantiated by time-domain simulations where four ac/dc fault cases are considered, and the results consolidate the feasibility of the proposed configuration and control, indicating fault resilience of the SC-OWF system. Additionally, size, weight and cost estimations of the proposed offshore substation are presented and compared to a conventional MMC offshore station, to further highlight the merits of the proposed solution.

- **James Tait**, Shuren Wang, Khaled H. Ahmed, "A DC-Based Offshore Wind Farm (OWF) Featuring Reduced Weight and Volume Requirements", *IEEE Transactions on Power Delivery* (Under Review).

  Abstract - The dc-system based offshore wind farm (OWF) is a viable alternative to conventional ac-collector based schemes. Facilitating advantageous elements from previously published schemes, this paper proposes a series-parallel architecture with high scalability and modularity for OWF applications with the aim of eliminating the detrimental effects caused by dc cable faults and minimising the offshore weight/size requirement. The proposed OWF employs a grouping scheme, where each group mainly consists of a medium-voltage dc (MVDC) link with a string of series-connected wind energy converter systems (WECSs), and a unidirectional high-gain dc-dc converter interfacing the MVDC link to the high-voltage dc (HVDC) link for transmission. Different groups are parallel connected to the HVDC link, constructing an offshore multi-terminal dc (MTDC) system. Importantly, the proposed architecture and operation enable effective containment of various faults within each group and without affecting other groups, thereby ensuring high operation security of the overall system. Topological configuration, control system, and protection strategy of the proposed OWF system are detailed, whilst operational performance in two fault cases is quantitatively

substantiated by time-domain simulation. The results consolidate the feasibility of the proposed topology and control, indicating system fault resiliency of the proposed dc-based OWF without the requirement for dc circuit breakers (DCCBs). Further assessment demonstrates that the estimated weight and volume of the proposed OWF system are significantly lower compared to centralised modular multilevel converter (MMC) based OWF systems.